RAMAN SPECTROSCOPY: A CONFORMATIONAL PROBE IN BIOCHEMISTRY*

Author: **Nai-Teng Yu**
School of Chemistry
Georgia Institute of Technology
Atlanta, Georgia

Referee: S. Krimm
Department of Physics
The University of Michigan
Ann Arbor, Michigan

INTRODUCTION

Although the Raman effect[1] was discovered in 1928, its use as an effective method for studying the structure and conformation of biological macromolecules[2-6] began in the early 1970s. During the past few years, the laser Raman technique has been successfully used to unravel some knotty problems in biochemistry and molecular biology. As a result of these applications, increasing number of researchers in the biological field are now aware of the usefulness of this technique.

The principle underlying Raman spectroscopy is simple. When light of a single frequency is focused onto or through a material, the frequency of some of the light that is scattered from the material may be shifted. These frequency shifts are equal to the frequencies of the molecular vibrations in the sample. However, the Raman effect is far more than an alternative means of observing the infrared spectrum, the factors which determine the Raman scattering intensities are quite different from those involved in the absorption of infrared radiation. The activity of a particular vibrational mode in the infrared spectrum is a function of whether there is a dipole moment change during vibration. In contrast, Raman active vibration modes are accompanied by a change in the polarizability of the molecule. This fundamental difference results in an important advantage for biological Raman spectroscopy, i.e., water is a poor Raman scatterer in contrast to its strong infrared absorption.

Unlike other physical techniques, Raman measurements can be made with ease in single crystals, powder, fibers, aqueous solution, or even intact biological specimens. The structural information derivable from Raman spectra is sometimes very specific and is often not otherwise obtainable. Most importantly, the sensitivity and selectivity of the technique can be greatly enhanced by tuning the exciting wavelength to the regions of electronic absorption of the chromophores (resonance Raman scattering).[5,6]

This review is intended primarily for biochemists who may not have extensive knowledge of Raman spectroscopy. The principles and techniques involved are treated first. Then specific applications to proteins, hemeproteins, rhodopsin,

*Dedicated to Professor Richard C. Lord on the occasion of his 65th year and his retirement.

nucleic acids, and membrane systems will be discussed. This review covers literature published from 1970 to June 1976. Reviews of various aspects of Raman studies of biological molecules have been written by pioneers in the field: Lord,[7] Peticolas,[8] Koenig,[9,10] Thomas,[11] Spiro,[12,13] Spiro and Loehr,[14] and Lewis and Spoonhower.[15]

PRINCIPLES AND TECHNIQUES

Terms and Definitions

Resonance and Nonresonance Raman

The distinction between the two processes lies in the choice of exciting wavelength relative to the electronic absorption bands. In order for resonance Raman scattering to occur, the incident photon energy ($h\nu_0$) must be approximately equal to the electron transition energy. The relative intensity of the Raman lines in a spectrum greatly depends on the exciting wavelength. The depolarization ratio (as defined below) may or may not depend on ν_0. In the nonresonance Raman process, $h\nu_0$ must be much smaller than the energy difference between the ground state ($|g,0\rangle$) and the lowest electronically excited state ($|e,0\rangle$), but much larger than the energies of vibrational quanta (Figure 1). Here the symbol $|g,0\rangle$ denotes a quantum state which has the lowest electronic energy and vibrational energy. Both relative intensity and depolarization ratio are independent of ν_0. The transition region between nonresonance and resonance Raman is frequently called preresonance Raman.

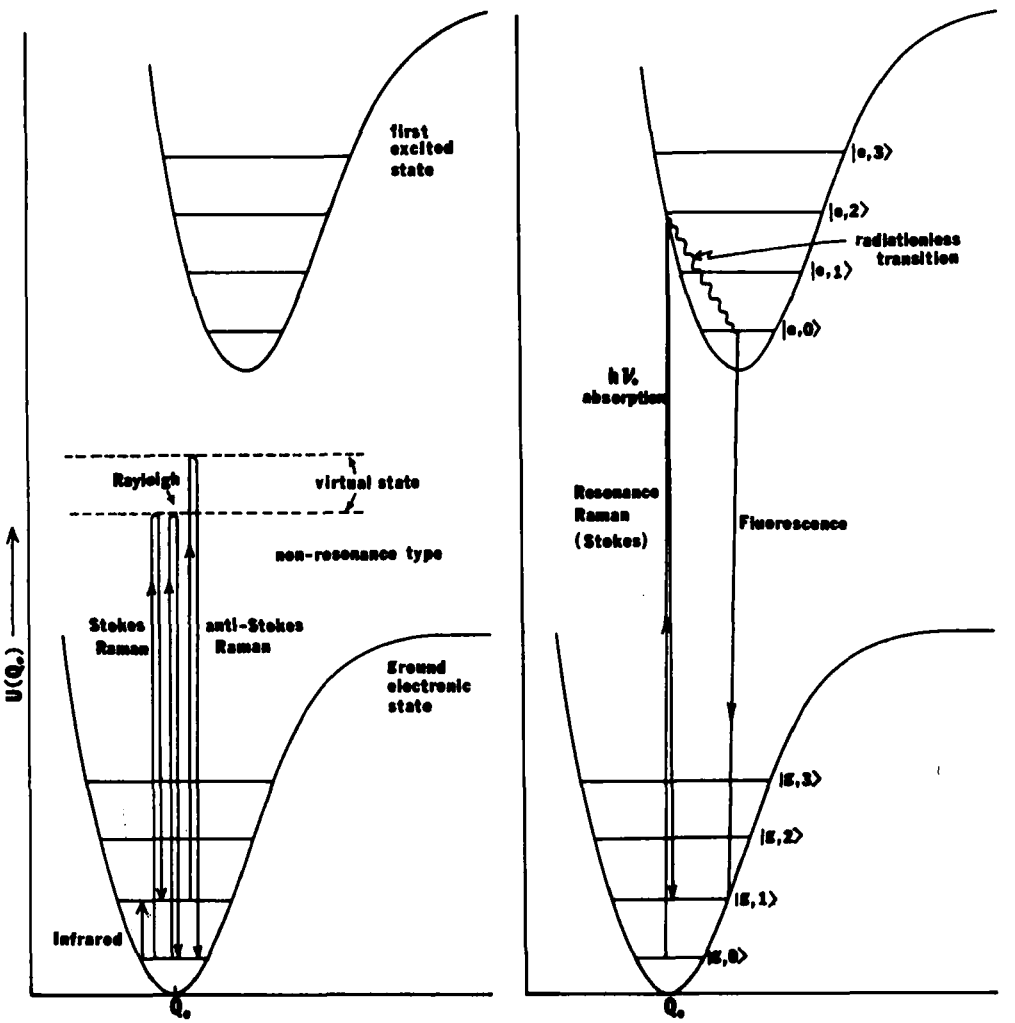

FIGURE 1. Schematic comparison of various processes: Rayleigh, Stokes Raman, anti-Stokes Raman, infrared, resonance Raman, and fluorescence.

Stokes and Anti-Stokes Lines

The inelastic scattering of monochromatic light (at ν_0) by molecules produces two kinds of lines. Lines of lower frequencies than ν_0 are called Stokes lines, whereas lines of higher frequency than ν_0 are called anti-Stokes lines. The displacements of the Raman spectral lines from ν_0 equal the differences between energy levels of the molecules producing the scattering. Since the Stokes lines are much stronger than the anti-Stokes counterparts, the spectra presented in the literature are normally of the Stokes type.

The Stokes lines originate from the $|g,0>$ state, whereas the anti-Stokes lines develop from a $|g,1>$ state. The anti-Stokes lines are weaker, as demonstrated by the relatively small number of molecules in $|g,1>$ states at room temperature. The ratio of Stokes to anti-Stokes intensities is expressed:

$$\frac{I(\text{Stokes})}{I(\text{anti-Stokes})} = \left(\frac{\nu_0 - \nu_{mn}}{\nu_0 + \nu_{mn}}\right)^4 \cdot e^{h\nu_{mn}/kT} \quad (1)$$

where

ν_{mn} = the vibrational frequency;
h = the Planck constant;
k = the Boltzmann constant.

Since the above intensity ratio of a given Raman line is a function of temperature, a Raman spectrum can provide an estimate of the temperatures of the scattering sample.

Scattering Tensor and Its Relation to Scattering Intensity

The electric field in the incident beam produces an induced dipole moment ($\vec{\mu}$) in the molecule, which is additional to any permanent dipole moment. The vector $\vec{\mu}$ is related to $\vec{E}$ by a linear relationship, $\vec{\mu} = \underset{\approx}{\alpha}\vec{E}$, provided that the electric field is not too great, as it is in the conventional Raman spectroscopy using continuous wave (CW) lasers. Here $\underset{\approx}{\alpha}$ is called polarizability tensor (or scattering tensor). The x, y, and z components of the induced dipole moment can be expressed as:

$$\mu_x = \alpha_{xx}E_x + \alpha_{xy}E_y + \alpha_{xz}E_z \quad (2)$$

$$\mu_y = \alpha_{yx}E_x + \alpha_{yy}E_y + \alpha_{yz}E_z \quad (3)$$

$$\mu_z = \alpha_{zz}E_x + \alpha_{zy}E_y + \alpha_{zz}E_z \quad (4)$$

The scattering tensor is normally written as:

$$\begin{pmatrix} \alpha_{xx} & \alpha_{xy} & \alpha_{xz} \\ \alpha_{yx} & \alpha_{yy} & \alpha_{yz} \\ \alpha_{zx} & \alpha_{zy} & \alpha_{zz} \end{pmatrix} \quad (5)$$

The symbol $(\alpha_{\rho\sigma})_{mn}$ is used to represent the $\rho\sigma$th component. Here the subscript mn denotes the Raman transition of interest from the $|m>$ to $|n>$ state, e.g., Stokes Raman transition $|g,0> \rightarrow |g,1>$. The components μ_x, μ_y, and μ_z are responsible for Raman emission in various directions. If the scattered light is observed along the z axis, μ_x and μ_y make contributions, but μ_z does not because an oscillating dipole does not emit in the direction of its axis. The intensities of the scattered light polarized in the x and y directions are proportional to $|\mu_x|^2$ and $|\mu_y|^2$, respectively. In a typical experimental configuration (Figure 2), the incident laser beam travels along the x axis with electric field polarized in the y direction (i.e., $E_y \neq 0$, $E_x = 0$, $E_z = 0$); then, $\mu_x = \alpha_{xy}E_y$, $\mu_y = \alpha_{yy}E_y$. Thus

$$I(\text{polarized along x}) \propto \alpha_{xy}^2 E_y^2 \quad (6)$$

$$I(\text{polarized along y}) \propto \alpha_{yy}^2 E_y^2 \quad (7)$$

and

$$I_T \propto (\alpha_{xy}^2 + \alpha_{yy}^2) E_y^2 \quad (8)$$

Here we have assumed that the single radiator (molecule) has a fixed orientation. To obtain the expression for a system consisting of randomly oriented molecules, the above equations must be multiplied by the number of molecules per unit volume, and the terms α_{xy}^2 and α_{yy}^2 must be averaged over all the molecular orientations relative to the fixed x, y, z coordinate system.[16] The mean square quantities $\overline{\alpha_{xy}^2}$ and $\overline{\alpha_{yy}^2}$ are expressible in terms of invariants of scattered tensor, G^o, G^s, and G^a.

$$G^o = \frac{1}{3}(\alpha_{xx} + \alpha_{yy} + \alpha_{zz})^2 = 3\bar{\alpha}^2 \quad (9)$$

$$G^s = \frac{1}{3}[(\alpha_{xx} - \alpha_{yy})^2 + (\alpha_{xx} - \alpha_{zz})^2 + (\alpha_{yy} - \alpha_{zz})^2]$$

$$+ \frac{1}{2}[(\alpha_{xy} + \alpha_{yx})^2 + (\alpha_{xz} + \alpha_{zx})^2 + (\alpha_{yz} + \alpha_{zy})^2] \quad (10)$$

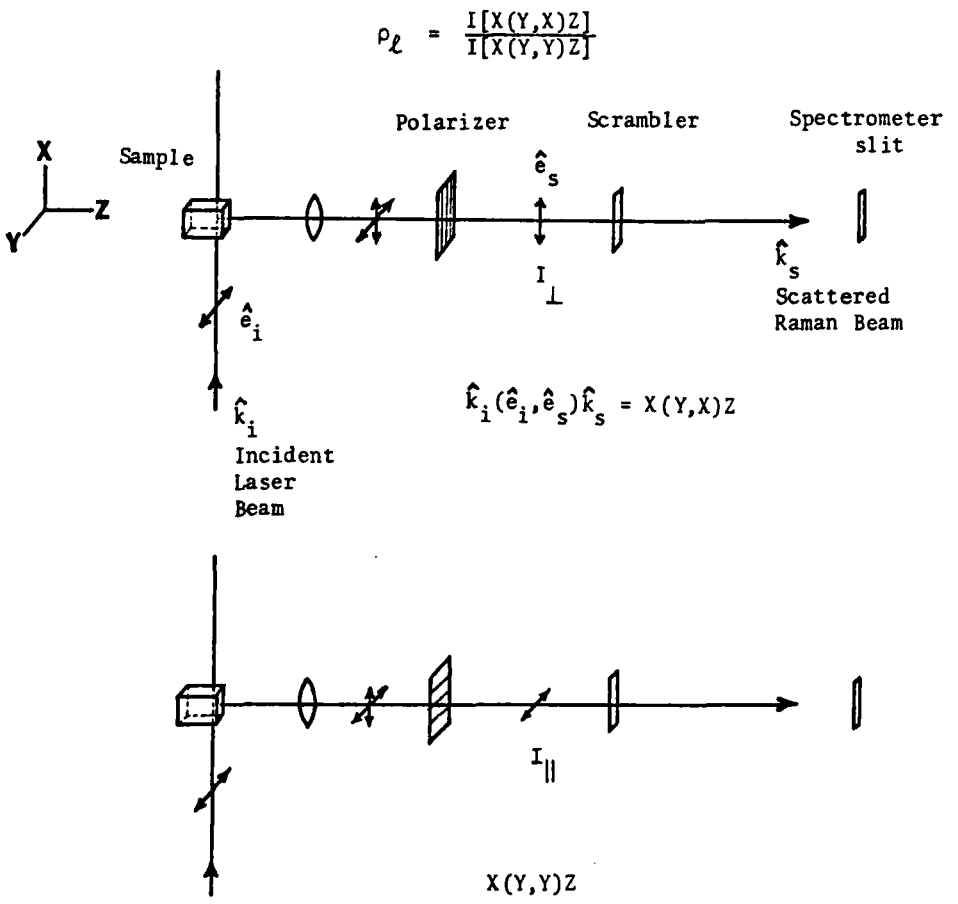

FIGURE 2. A typical 90° Raman scattering configuration.

$$G^a = \frac{1}{2}[(\alpha_{xy} - \alpha_{yx})^2 + (\alpha_{xz} - \alpha_{zx})^2 + (\alpha_{yz} - \alpha_{zy})^2] \quad (11)$$

$$\overline{\alpha^2_{xy}} \propto 3\,G^s + 5\,G^a \text{ and } \overline{\alpha^2_{yy}} \propto 10\,G^o + 4\,G^s \quad (12)$$

Therefore, the total scattering intensity of a system of randomly oriented molecules is proportional to $(7\,G^s + 5\,G^a + 10\,G^0)\,N_v I_0$, where N_v is the number of molecules per unit volume and I_0 is the intensity of the excitation source at ν_0. Scattering tensor patterns for important chemical point groups have been tabulated by McClain.[17] Examples for C_{2v} and D_{4h} are given in Equations 13 and 14, respectively.

$$A_1 = \begin{pmatrix} s_1 & 0 & 0 \\ 0 & s_2 & 0 \\ 0 & 0 & s_3 \end{pmatrix} \qquad A_2 = \begin{pmatrix} 0 & s_4 & 0 \\ s_5 & 0 & 0 \\ 0 & 0 & 0 \end{pmatrix}$$

$$B_1 = \begin{pmatrix} 0 & 0 & s_6 \\ 0 & 0 & 0 \\ s_7 & 0 & 0 \end{pmatrix} \text{ and } B_2 = \begin{pmatrix} 0 & 0 & 0 \\ 0 & 0 & s_8 \\ 0 & s_9 & 0 \end{pmatrix} \quad (13)$$

$$A_{1g} = \begin{pmatrix} s_1 & 0 & 0 \\ 0 & s_1 & 0 \\ 0 & 0 & s_2 \end{pmatrix} \qquad A_{2g} = \begin{pmatrix} 0 & s_3 & 0 \\ -s_3 & 0 & 0 \\ 0 & 0 & 0 \end{pmatrix}$$

$$B_{1g} = \begin{pmatrix} s_4 & 0 & 0 \\ 0 & -s_4 & 0 \\ 0 & 0 & 0 \end{pmatrix} \qquad B_{2g} = \begin{pmatrix} 0 & s_5 & 0 \\ s_5 & 0 & 0 \\ 0 & 0 & 0 \end{pmatrix} \text{etc.} \quad (14)$$

Scattering Plane and Depolarization Ratio

Scattering plane is defined as the plane containing the propagation directions of the incident and scattered radiation. This term has been frequently referred to when describing the experimental configuration. According to the recent recommendation by the Office of Standard Reference Data of the National Bureau of Standards (1975), the scattering geometry should be specified by a notation $\hat{k}_i\,(\hat{e}_i, \hat{e}_s)\hat{k}_s$. The vector $\hat{k}_i$ ($\hat{k}_s$) refers to the direction of propagation of the incident (scattered) light; the vector $\hat{e}_i$ ($\hat{e}_s$) refers to the direction of electric field polarization of the incident (scattered) light.

In Figure 2 the depolarization ratio is defined as:

$$\rho_l = \frac{I[X(Y,X)Z]}{I[X(Y,Y)Z]} \tag{15}$$

The subscript l indicates linearly polarized incident radiation. Two spectra are needed to determine this ratio: one with the polarizer oriented parallel to the X axis and the other with the polarizer oriented parallel to the Y axis. The scrambler between the polarizer and spectrometer slit is to eliminate the polarization dependence of the monochromator response. $I[X(Y,X)Z]$ and $I[X(Y,Y)Z]$ are often referred to as $I_\perp$ and $I_\parallel$, respectively, in the literature.

It is also possible to define P_l as the ratio of $I[X(Z,Y)Z]$ and $I[X(Y,Y)Z]$. The expressions in terms of tensor invariants are identical for the two definitions, but the latter requires the use of a half-wave plate, which rotates the electric vector of the incident light by 90°. This method of measurement is not recommended because of a large convergence error.

The depolarization ratio is related to the symmetries of normal mode vibrations. This is readily seen when one expresses ρ_l in terms of tensor invarients:

$$\rho_l = \frac{3\,G^s + 5\,G^a}{10\,G^o + 4\,G^s} \tag{16}$$

For nonresonance Raman effect, G^a is always zero. Two types of Raman lines can be classified:

1. $\rho_l = 3/4$, depolarized (dp), nontotally symmetric vibrations. The tensor patterns for these modes are such that G^0 is zero.

2. $0 < \rho_l < 3/4$ polarized (p), totally symmetric vibration. It is characterized by $G^0 \neq 0$, $G^s \neq 0$.

For resonance Raman scattering, ρ_l may take values greater than 3/4 for nontotally symmetric modes. The following additional classification can be made:

3. $3/4 < \rho < \infty$, anomalously polarized (ap).

4. $\rho \to \infty$, inversely polarized (ip), characterized by G^o and $G^s = 0$, but $G^a \neq 0$. The scattering tensors are antisymmetric (i.e., $\alpha_{\rho\sigma} = -\alpha_{\sigma\rho}$; $\alpha_{\rho\rho} = 0$).

Symmetry Properties of Normal Coordinates and Vibrational Wave Functions

In a normal mode of vibration, all of the atoms in a molecule move with the same frequency and the same phase; that is, they all pass through their equilibrium positions at the same time. Each mode can be described by a normal coordinate (Q_k) which is a linear combination of mass-weighted nuclear displacement coordinates. In terms of normal coordinates, the potential and kinetic energies can be written as the sums of squared terms: $V = 1/2 \sum_k \lambda_k Q_k^2$ and $T = 1/2 \sum_k (dQ_k/dt)^2$. For the total energy ($V + T$) to remain constant when a symmetry operation is performed, each normal coordinate must remain unchanged or, at most, change sign (i.e., $Q_k \to \pm Q_k$). In other words, for nondegenerate vibrations the normal coordinates are either symmetric or antisymmetric with respect to a symmetry operation.

In the harmonic oscillator approximation, the vibrational wave functions associated with the kth normal coordinate may be expressed as:

ground state:

$$\psi_0(Q_k) = \left(\frac{\alpha_k}{\pi}\right)^{1/4} e^{-1/2\,\alpha_k Q_k^2} \tag{17}$$

1st excited state:

$$\psi_1(Q_k) = \left(\frac{\alpha_k}{\pi}\right)^{1/4} \sqrt{2\alpha_k}\, e^{-1/2\,\alpha_k Q_k^2} \cdot Q_k \tag{18}$$

where

$\alpha_k = 4\pi^2 \nu_k / h$;
ν_k = the frequency of the kth normal mode.

Since Q_k^2 is unchanged by all symmetry operations of the molecule, the ground state vibrational wavefunction $\psi_0(Q_k)$ is always totally symmetric. However, the wavefunction $\psi_1(Q_k)$ of the first excited vibrational state has the same symmetry as Q_k.

Fermi Resonance

This vibrational perturbations was first observed by Fermi. When two vibrational states of the same symmetry species happen to have almost the same energies (accidentally degenerate), they will strongly perturb each other by shifting the

expected positions of vibrational lines as well as by affecting their intensities. Each state will lose some of its own identity and take on some of the character of the second state as a result of mixing. For example, in the case of CO_2 the state ($\nu_1 = 1$, $\nu_2 = 0$, $\nu_3 = 0$) has almost the same energy as the state ($\nu_1 = 0$, $\nu_2 = 2$, $\nu_3 = 0$), since the first normal mode (ν_1) = 1337 and the second normal mode (ν_2) = 677 cm^{-1}. Here ν_1, ν_2, and ν_3 are quantum numbers for symmetric stretching, bending, and antisymmetric stretching, respectively. Accordingly, the Raman spectrum of CO_2 shows two strong lines at 1285 and 1388 cm^{-1}, corresponding to transitions to the (0,2,0) and (1,0,0) levels from the ground level. For H_2O, the fundamental frequencies ν_1 and ν_3 are fairly close (3652 and 3756 cm^{-1}), but the corresponding vibrational states (1,0,0) and (0,0,1) cannot perturb each other since they have different symmetry species. The levels (2,0,0) and (0,0,2) both have the same symmetry species, A_1, and they interact.

Franck-Condon Factor

This is the overlap integral $\langle e,v|g,i\rangle$ between the vibration wave functions of two electronic states. In an allowed electronic absorption (electronic transition moment $M \neq 0$ by symmetry arguments), the overlap integral determines whether a transition occurs from a vibrational level of the lower state to a vibrational level of the upper state. In resonance Raman scattering, the overlap factor $\langle g,1|e,v\rangle\langle e,v|g,0\rangle$ appears in the expression for the components of scattering tensor and thus will contribute to the scattered intensities of polarized Stokes Raman lines (see Theory of Raman Intensity).

The integrand ($\psi_{e,v}^*\psi_{gi}$) must be symmetric with respect to all symmetry operations permitted by the molecule in both states, so that the overlap integral will be different from zero. If the two potential functions are exactly the same, the factor $\langle e,v|g,i\rangle$ is equal to zero, except for v = i. However, if the potential functions have different shapes but the minima are at the same positions, the overlap integral will be nonzero for totally symmetric vibrations (v-i = 0, 1, 2, 3, etc.), but zero for nontotally symmetric modes, except when v-i = 0, 2, 4, 6, etc. Since the shift (Δ) in the equilibrium position of the potential curves is generally equal to zero for nontotally symmetric modes, the factor $\langle g,1|e,v\rangle\langle e,v|g,0\rangle$ is zero for possible v values.

Normally, Δ is nonzero for totally symmetric vibrations. The overlap factor for the kth normal mode can be calculated according to the harmonic oscillator model:

$$\langle e, v_k|g,o\rangle = (v_k!)^{-\frac{1}{2}}\,\Delta^{v_k}\,e^{-\frac{1}{2}\Delta^2} \quad (19)$$

$$\langle e,v_k|g,l\rangle = (v_k!)^{-\frac{1}{2}}\,e^{-\frac{1}{2}\Delta^2}\,[v_k\,\Delta^{v_k-1} - \Delta^{v_k+1}] \quad (20)$$

The Jahn-Teller Effect

This is a type of vibration-electronic (vibronic) interaction encountered in a nonlinear molecule when the electronic state is degenerate. In 1937 Jahn and Teller[18a] showed that there is always at least one nontotally symmetric normal mode that causes a splitting of the potential curve so that the positions of the potential minima are displaced by an amount, Δ, which varies according to the vibronic interaction (Figure 3). The kinds of normal coordinates that will produce Jahn-Teller instability in degenerate electronic states have been tabulated by Herzberg.[18b]

For example, the b_{1g} and b_{2g} normal modes are Jahn-Teller active in a molecule of D_{4h} symmetry (square planar). The stable molecular geometry becomes D_{2h} type (rectangular or diamond shape). The excited state of E_u symmetry is split into B_{2u} (y-polarized) and B_{3u} (x-polarized) types. Both b_{1g} and b_{2g} normal coordinates in D_{4h} are now transformed to a_g (totally symmetric) under D_{2h} point group. Such a Jahn-Teller effect alters the Franck-Condon overlap integrals and, thus, the Raman excitation profile.

Inverse Raman Effect

When a transparent medium is irradiated simultaneously with an intense monochromatic light (ν_0) and a continuum radiation, absorption is observed in the continuum at the frequencies corresponding to both Stokes and anti-Stokes Raman lines. This phenomenon was first observed by Jones and Stoicheff[19] in 1964. The important aspect of the inverse Raman effect is that the anti-Stokes inverse Raman absorption is stronger than the Stokes counterpart. Thus, it may be used to avoid the fluorescent interference, because fluorescence is on the Stokes side. Recent studies[20,21] of the inverse Raman effect using the intracavity technique demonstrate that high-

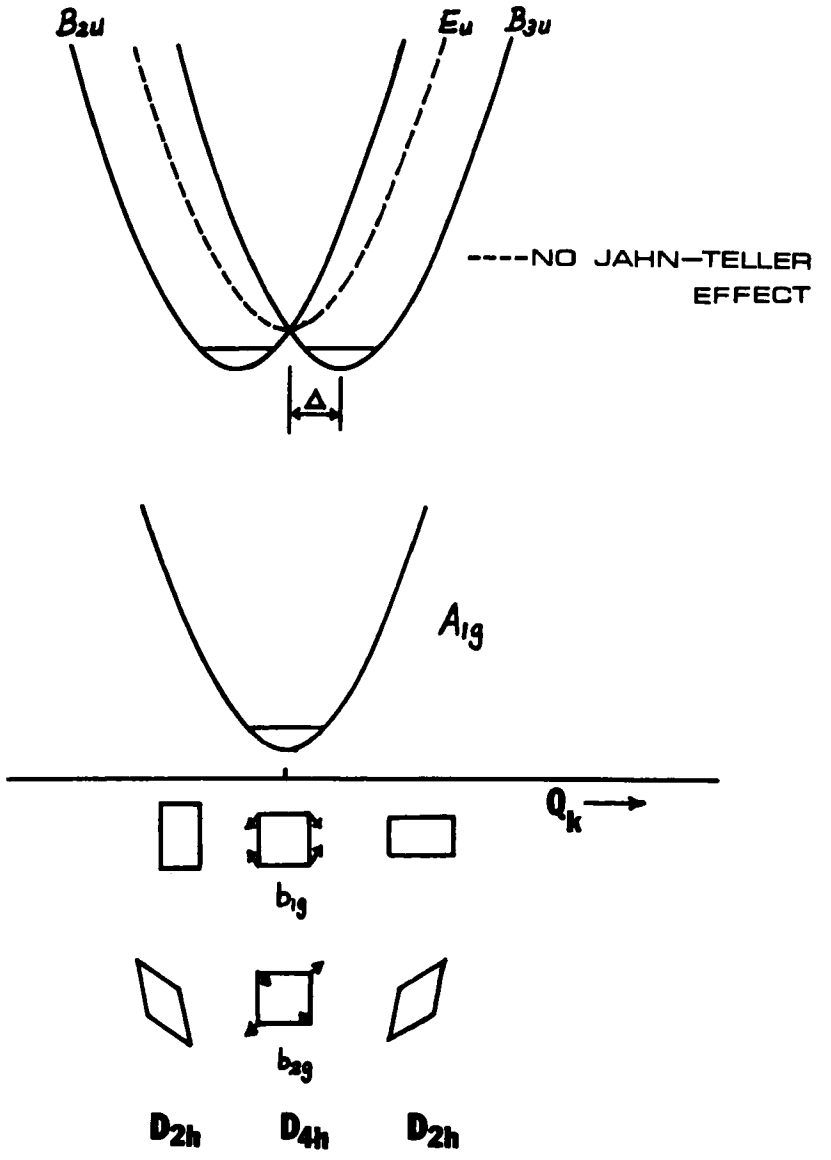

FIGURE 3. The effect of Jahn-Teller instability on potential energy curve.

quality inverse resonance Raman spectra could be obtained from highly fluorescent dyes (e.g., rhodamine 6G) at a time resolution of 30 nsec.

Coherent Anti-Stokes Raman Scattering (CARS)

This technique uses Raman-type resonance in the third order nonlinear optical polarizability. The response of a medium to an electromagnetic field is usually written

$$\vec{P} = \chi\vec{E} \qquad (21)$$

where

$\vec{P}$ = the induced electronic polarization;
$\vec{E}$ = the electric field;
χ = the electric susceptibility.

The linear relationship between polarization and electric field is valid only when the electric field is very small (as is the case in the ordinary optics). When electric field is very large, one cannot use the above equation and instead must use a power series expansion of polarization:

$$\vec{P} = \chi^{(1)}\cdot\vec{E} + \chi^{(2)}:\vec{E}\vec{E} + \chi^{(3)}:\vec{E}\,\vec{E}\,\vec{E} + \ldots \qquad (22)$$

The coefficients $\chi^{(n)}$ are tensors of rank n+1 and are called nonlinear susceptibility of n order.

When two light beams at frequencies ω_1 and ω_2 are incident on a nonlinear material, coherent emission at frequencies $\omega_3 = 2\omega_1 - \omega_2$ is generated through the third order nonlinear polarization (see Figure 4 for schematic of $[2\omega_1 - \omega_2]$ technique). The third order nonlinear susceptibility $\chi^{(3)}$ associated with this polarization is responsible for the emission. The third order nonlinear susceptibility[22] has the form:

$$\chi^{(3)} \propto \frac{1}{(\omega_1 - \omega_a)(\omega_1 - \omega_2 - \omega_R + i\Gamma_R)(2\omega_1 - \omega_2 - \omega_b)} \quad (23)$$

where

ω_a and ω_b = electronic transitions frequencies;
ω_R = the Raman vibrational frequency;
Γ_R = the half width at half maximum of the Raman signal.

$\chi^{(3)}$ shows resonance behavior as $\omega_1 - \omega_2$ approaches ω_R, producing the Raman signals.

The nonlinear Raman technique[23,24] has a greatly enhanced conversion efficiency compared to spontaneous Raman scattering; in addition, it is a coherent beam. These effects lead to a greatly enhanced signal-to-noise ratio; thus, experiments which are impossible with conventional Raman technique become feasible through the CARS technique.

In CARS spectroscopy background fluorescence is eliminated primarily by spatial filtering and by the fact that the signal is on the anti-Stokes side of the primary pump frequency while the fluorescence is on the Stokes side. High quality CARS spectra of fluorescent lens pigment, β-carboline have been obtained.[25a]

Resonance CARS spectra of ferro-cytochrome *c* in aqueous solution ($10^{-3}M$) were recently obtained by Nestor et al.[25b] With the ω_1 beam at the maximum of the α absorption peak, they observed those lines which correspond to ip and dp lines in the conventional resonance Raman spectrum of ferro-cytochrome *c*.

Description of a Modern Laser Raman Scattering System

A Raman scattering apparatus basically consists of (1) an excitation source, (2) the sample handling accessories, (3) the optics for collecting the Raman emission, (4) the spectrometer (double monochromator) and detector (photomultiplier), and (5) the photon-counting electronics and a recorder. The Raman system shown in Figure 5 is equipped with data storage and processing electronics designed by Dr. D. C. O'Shea of Georgia Tech.

The exciting radiation is normally provided by an argon-ion or krypton-ion laser. A typical power distribution among various lines is indicated in Table 1. For continuous coverage in the visible

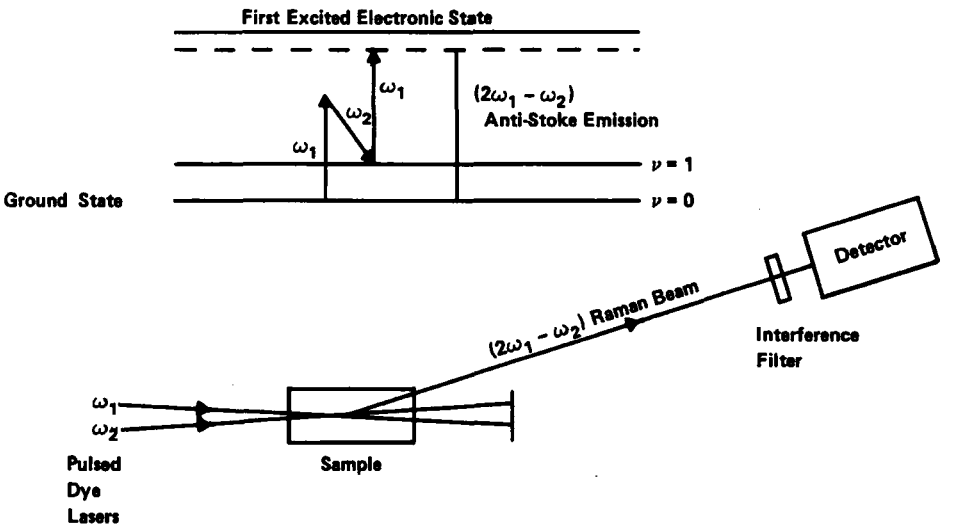

FIGURE 4. Schematic CARS $2\omega_1 - \omega_2$ technique.

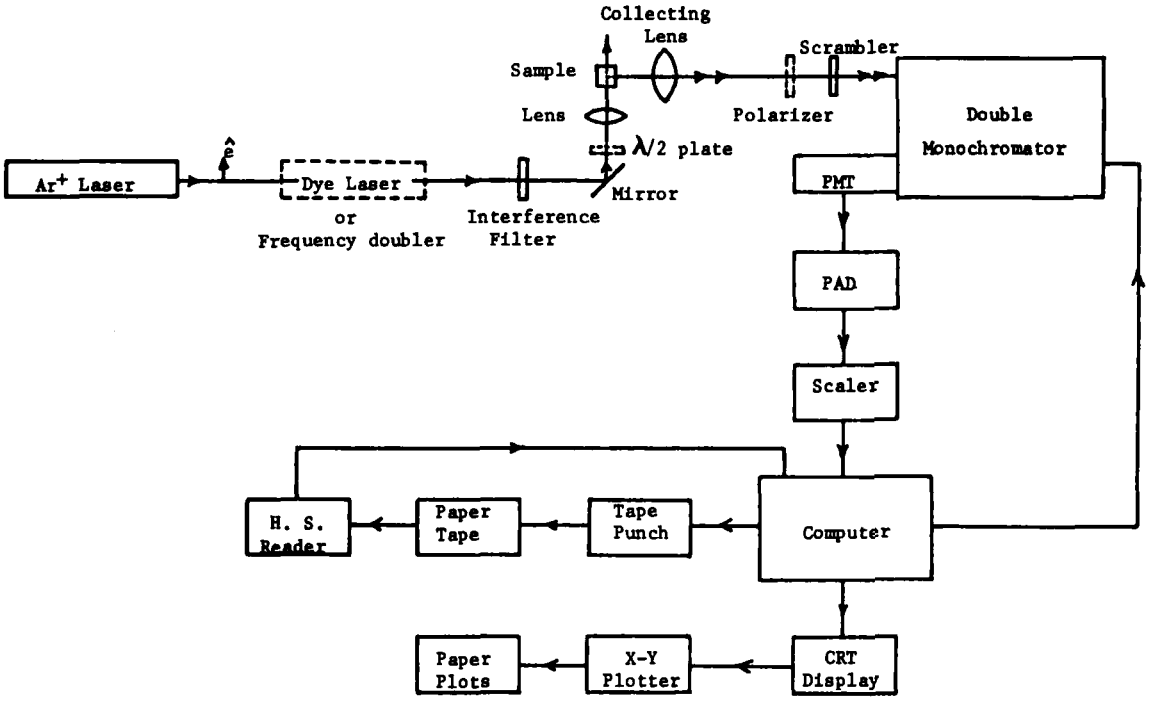

FIGURE 5. Raman scattering apparatus. (PMT) Photomultiplier tube, (PAD) preamplifier-amplifier-discriminator, (CRT) cathode ray tube, (H.S.) high speed. (From Shelnutt, J. A., Ph.D. thesis, Georgia Institute of Technology, Atlanta, 1975.)

TABLE 1

Power Outputs of Ion Lasers

Wavelength (nm)	CR-5 argon (mW)	CR 750K krypton (mW)
799.3 (IR)		45
752.5 (IR)		150
676.4 (red)		135
647.1 (red)		750
568.2 (yellow)		200
530.9 (green)		250
528.7 (green)	200	
520.8 (green)		150
514.5 (green)	2000	
501.7 (blue/green)	300	
496.5 (blue)	600	
488.0 (blue)	1500	
482.5 (blue)		75
476.5 (blue)	600	
476.2 (blue)		100
472.7 (blue)	150	
468.9 (blue)		20
465.8 (indigo)	100	
457.9 (indigo)	350	
454.5 (indigo)	125	
351.1/363.8 (UV)	250	
350.7/356.4 (UV)		250

Courtesy of Coherent Radiation.

region, a tunable dye laser is needed. Laser radiation in the 250- to 350-nm region is generated by a frequency doubling system pumped by ion lasers or dye lasers. This system consists of a properly oriented nonlinear crystal sealed in a liquid-filled oven and a proportional temperature controller. The temperature tuning method has higher conversion efficiencies than the angle tuning method.[26] The power at 2573 Å, obtained by doubling the frequency of the 514.5-nm line (~2.0 W), is approximately 15 mW.

During a Raman experiment, the laser beam first passes through a narrow band interference filter to remove plasma emissions. It is then directed upward and focused into the sample by a 60-mm focal length lens. The λ/2 plate rotates the polarization direction by 90°. A polarizer (HN-22 Polaroid sheet) is placed between the collecting lens and the scrambler to analyze Raman scattered light into its $I_{\parallel}$ and $I_{\perp}$ components. The scrambler between the polarizer and the entrance slit is a properly oriented crystalline quartz wedge which converts the plane polarized light to random, elliptically polarized light so that the response of the gratings is independent of the polarization of the scattered light.

The spectrometer is a 3/4-meter Spex Czerny-Turner double monochromator (Model 1401). The gratings have 1200 grooves/mm and are blazed at 500.0 nm. The dispersion at the exit slit of the spectrometer is 0.55 nm/mm. Typical entrance, intermediate, and exit slit widths are 250 μm; the entrance slit height is 10 mm for solution samples and 5 mm for solids samples.

Scattered light from the exit slit of the double monochromator is detected by an RCA C-31034 photomultiplier (PMT). By cooling to -20°C with a Products for Research (Model TE-104) thermoelectrically refrigerated chamber, the PMT dark count is reduced from 120 counts/sec at room temperature to ~10 counts/sec.

The system in Figure 5 is controlled by a Digital Equipment Corporation (Model PDP 8/f) computer. A spectrum is obtained by counting pulses from the PAD for specified time intervals.[27] At the end of the time interval, the number of pulses accumulated by the scaler is stored in memory and displayed on a Tektronix Model 604 oscilloscope. The computer then generates the pulses required for a stepping motor to increment the gratings, the scaler is cleared, and counting is restarted. Spectra can be stored graphically and digitally on a Metagraphics X-Y plotter interfaced to the computer.

Theory of Raman Scattering Intensities

For the standard 90° scattering geometry (Figure 2), the total intensity ($I_{\parallel} + I_{\perp}$) of a Stokes Raman line from randomly oriented molecules is:

$$I_{mn} \propto \frac{2^7 \pi^5 (\tilde{\nu}_0 - \Delta\tilde{\nu})^4 I_0 N_v}{9} (10G^0 + 7G^s + 5G^a) \quad (24)$$

where

I_0 and $\tilde{\nu}_0$ = the intensity and wave number of the exciting beam;
$\Delta\tilde{\nu}$ = the Raman frequency shift in cm^{-1};
N_v = the number of scatterers per unit volume.

The Raman transition is from the state $|m\rangle$ to $|n\rangle$. The vibrational energy difference between these two states ($E_n - E_m$) is equal to $hc\Delta\tilde{\nu}$ (in ergs). The tensor invariants G^0, G^s, and G^a are called trace scattering, quadrupole scattering, and magnetic dipole scattering, respectively; they have been defined previously. When the scattering tensor components are complex variables, it is more convenient to use the following expression:

$$I_{mn} \propto \frac{2^7 \pi^5 (\tilde{\nu}_0 - \Delta\tilde{\nu})^4 I_0 N_v}{9} (6\delta_G + \delta_F + \delta_H) \quad (25)$$

where

$G^o = 1/3\ \delta_F$;
$G^s = 1/2\ (\delta_G + \delta_H) - 1/3\ \delta_F$;
$G^a = 1/2\ (\delta_G - \delta_H)$.

The McClain[28] molecular parameters δ_F, δ_G, and δ_H are defined in terms of the scattering tensor $\alpha_{\rho\sigma}$ by:

$$\delta_F = \sum_\rho \sum_\sigma \alpha_{\rho\rho} \alpha^*_{\sigma\sigma}$$
$$\delta_G = \sum_\rho \sum_\sigma \alpha_{\rho\sigma} \alpha^*_{\rho\sigma} \quad (26)$$

and

$$\delta_H = \sum_\rho \sum_\sigma \alpha_{\rho\sigma} \alpha^*_{\sigma\rho} \quad (27)$$

where ρ, σ can be x, y, or z.

The depolarization ratio ρ_l can also be defined in terms of these parameters:

$$\rho_l = \frac{4\delta_G - \delta_F - \delta_H}{2(\delta_F + \delta_G + \delta_H)} \tag{28}$$

Based on Albrecht theory,[29] as extended by Mingardi and Siebrand,[30] the Raman scattering tensor is expressed approximately by:

$$(\alpha_{\rho\sigma})_{gi,gj} = A_{\rho\sigma} + B_{\rho\sigma} + D_{\rho\sigma} \tag{29}$$

where

$$A_{\rho\sigma} = \sum_e{}' \sum_v \frac{M^{\sigma}_{ge} M^{\rho}_{eg} \langle gi|ev\rangle\langle ev|gj\rangle}{E_{ev} - E_{gi} - h\nu_0 - i\Gamma_{ev}}; \quad B_{\rho\sigma} = \sum_e{}' \sum_{s\neq e} \sum_v \sum_k \frac{\left(h_k\right)^0_{es}}{(E^0_e - E^0_s)(E_{ev} - E_{gi} - h\nu_0 - i\Gamma_{ev})} \times \left[M^{\sigma}_{ge} M^{\rho}_{sg} \langle gj\rangle\langle ev|O_k|gi\rangle + M^{\rho}_{ge} M^{\sigma}_{sg} \langle gj|Q_k|ev\rangle\langle ev|gi\rangle\right]; \tag{30}$$

and

$$D_{\rho\sigma} = \sum_e{}' \sum_{s\neq e} \sum_v \sum_x \sum_k \frac{\left(h_k\right)^0_{es}}{(E^0_e - E^0_s)(E_{ev} - E_{gi} - h\nu_0 - i\Gamma_{ev})} \times$$

$$M^{\sigma}_{eg} M^{\rho}_{sg} \langle gj|ev\rangle\langle ev|Q_k|sx\rangle\langle sx|gi\rangle \left(\frac{h\nu^k_s}{E_{ev} - E_{sx}}\right) \{\delta_{v,x-1} - \delta_{v,x+1}\}$$

$$-M^{\rho}_{eg} M^{\sigma}_{sg} \langle gj|sx\rangle\langle sx|Q_k|ev\rangle\langle ev|gi\rangle \left(\frac{h\nu^k_e}{E_{ev} - E_{sx}}\right) \{\delta_{x,v-1} - \delta_{v,x+1}\} \tag{31}$$

where

M^{σ}_{ge} $\equiv \langle g^0|R\sigma|e^0\rangle$, the σth component of the transition dipole connecting the ground state and the eth excited state;

$\langle gi|ev\rangle$ = a Franck-Condon overlap integral between the ground state $|g,i\rangle$ and the excited state $|e,v\rangle$.

The prime in the summation indicates that the summation is over all the electronic states except the ground state. The vibronic coupling matrix element is $(h_k)^0_{es} \equiv \langle e^0|(\partial H/\partial Q_k)|s^0\rangle$, where $|e^0\rangle$ is the electronic wave function evaluated at the equilibrium positions of the normal mode coordinates. The $(\partial H/\partial Q_k)_0$ is the electronic-nuclear coupling operator for the kth normal mode Q_k and frequency ν_k. These expressions are rather complicated, but several important features and results may be extracted from them:

1. In the nonresonance region (i.e., $h\nu_0 \ll E_{ev} - E_{gi}$ for all excited states), the A term is responsible for Raleigh scattering and the B term for Raman scattering, which is independent of the exciting wavelength.

2. To determine which particular normal modes will be scattered in the non-resonance Raman effect, it is necessary to consider the symmetry properties of the term B. The following selection rule is used. A mode of vibration can be active in Raman scattering if the irreducible representation to which it can be assigned contains x^2, y^2, z^2, xy, xz, or yz.

3. As ν_0 approaches $E_{ev} - E_{gi}$, the denominators become small, giving rise to selective resonance enhancement. The A term contributes to the resonance Raman intensities of polarized Raman lines, while the terms B and D may contribute to those depolarized, anomalously polarized, and/or polarized lines, depending on the selection rule as determined by $(h_k)^0_{es}$. For example, in D_{4h} metalloporphyrins the Q (visible) and B (Soret) electronic states are both of E_u symmetry. The allowed symmetry of vibronically active modes is $E_u \times E_u = A_{1g} + B_{1g} + B_{2g} + A_{2g}$.

4. The vibrations deriving scattering intensities from the A term are called Franck-Condon modes, and those from the B term are called Herzberg-Teller modes. The term D, resulting from the first order nonadiabatic correction, is usually small and negligible. However, it was shown to be important in Mn(III)etioporphyrin.[31] The A term contribution of the scattering intensity is particularly sensitive to the intensity of the resonant electronic absorption. It depends on the square of the extinction coeffi-

cient ϵ, whereas the B term contribution depends linearly on the extinction coefficient when one state is weakly dipole allowed.[31]

5. For molecules of low symmetry where many of the vibrational modes are totally symmetric ($\rho_l < 3/4$), a useful structural information is derivable from the resonance behavior of Franck-Condon modes. Hirakawa and Tsuboi's rule[32] states that if a Raman line becomes stronger when the exciting line is brought closer to the frequency of an electronic band A ← X, then the equilibrium conformation of the molecule is distorted along the normal coordinate for the Raman line in the transition from the ground (X) to the excited state (A).

Sample Handling Techniques

The beam diameter of the Ar^+ or Kr^+ laser is ~2 mm and, after focusing, it is reduced to ~15 μ by a 60-mm focal length lens ($d = \lambda f/D$, where d is the focused beam diameter, f is the focal length of lens, D is the laser beam diameter, and λ is the wavelength of exciting light). The laser power of the sample is normally ~100 mW, which means a power density of ~10^4 W/cm^2. In order to reduce the heating of strongly absorbing samples in resonance Raman experiments, the sample cell is rotated at ~1000 rpm by a DC or AC motor (see Figure 6). Further cooling can be achieved by blowing cold nitrogen gas at the rotating cell. The cell shown in Figure 6 requires only ~0.2 ml of liquid sample. For photolabile molecules such as rhodopsin, a rapid-flow (jet-stream) technique,[33,34] requiring a ~250-ml sample, has been developed.

For nonresonance Raman studies, the so-called axial/transverse and transverse/transverse methods are commonly employed. Since small glass capillary cells (0.5- to 1.0-mm bore) are used, the sample volume is now reduced to 5 to 20 μl. In the axial/transverse method, the laser beam enters along the axis of a capillary, and the scattered light is collected at 90° to the capillary wall. The capillary with a fire-polished flat end is held vertically so that its axis is parallel with the entrance slit of the spectrometer. However, in the transverse/transverse arrangement, the incident beam is perpendicular to the cell axis. Standard melting point capillary tubes of approximately 1.0-mm bore have been found to work satisfactorily. The ends of the capillary tube may be sealed to prevent evaporation or air oxidation. To enhance nonresonance Raman signals (~400 times or greater), a slitless optical fiber laser Raman technique[35] has been developed. Variations of sample temperature in the -15 to 100°C range may be conveniently achieved by employing a thermostat[36] designed for the transverse/transverse capillary system. The temperature can also be set in the -196 to 200°C range by a Harney-Miller variable temperature assembly, which is commercially available from Spex Industries, Inc.

Solid samples (amorphous or crystalline) can be packed into the capillary; the transverse/transverse method can be used to obtain Raman spectra. However, the weak fluorescence and Raman scattering from glass may interfere with the measurements. A simpler and better method for handling solid powder is to pack the sample into a conical depression at the end of an 1/8-in. stainless steel rod which is held horizontally. The laser beam is then directed upward and focused onto the sample at the grazing angle so that the scattering column is a strip on the powder surface, 1/8 in. long and approximately 20 μm wide. When the control of relative humidity is required, the sample rod can be fastened inside a thermovac flask equipped with a rubber "O" ring and a vacuum-tight stopcock.[37] Since the sample is not rotating, the laser power should be kept at a minimal level (<50 mW) or an unfocused beam should be used in order to avoid the dehydration of the molecules. For protein single crystals,[38] the sample should be immersed in the mother liquid. The laser beam is then sent through the crystal, and the scattered light directly from the scattering column inside the crystal is collected and analyzed by the spectrometer. Studies of an intact ocular lens[39] can be performed in a similar fashion in a culture medium which keeps the organ in the living state.

For colored solid samples (e.g., metalloporphyrins), KBr pellets (0.5 mg of porphyrin per 200 mg of KBr) or crystalline powder affixed to transparent tape may be used to obtain Raman spectra. To prevent photodecomposition, the pellet or tape is held in place on a rotating aluminum platform (3/4 in. diameter) by applying parafilm over the outer edge of the sample. The platform is oriented so that the incident beam and the surface of the pellet form a 10° angle.[40]

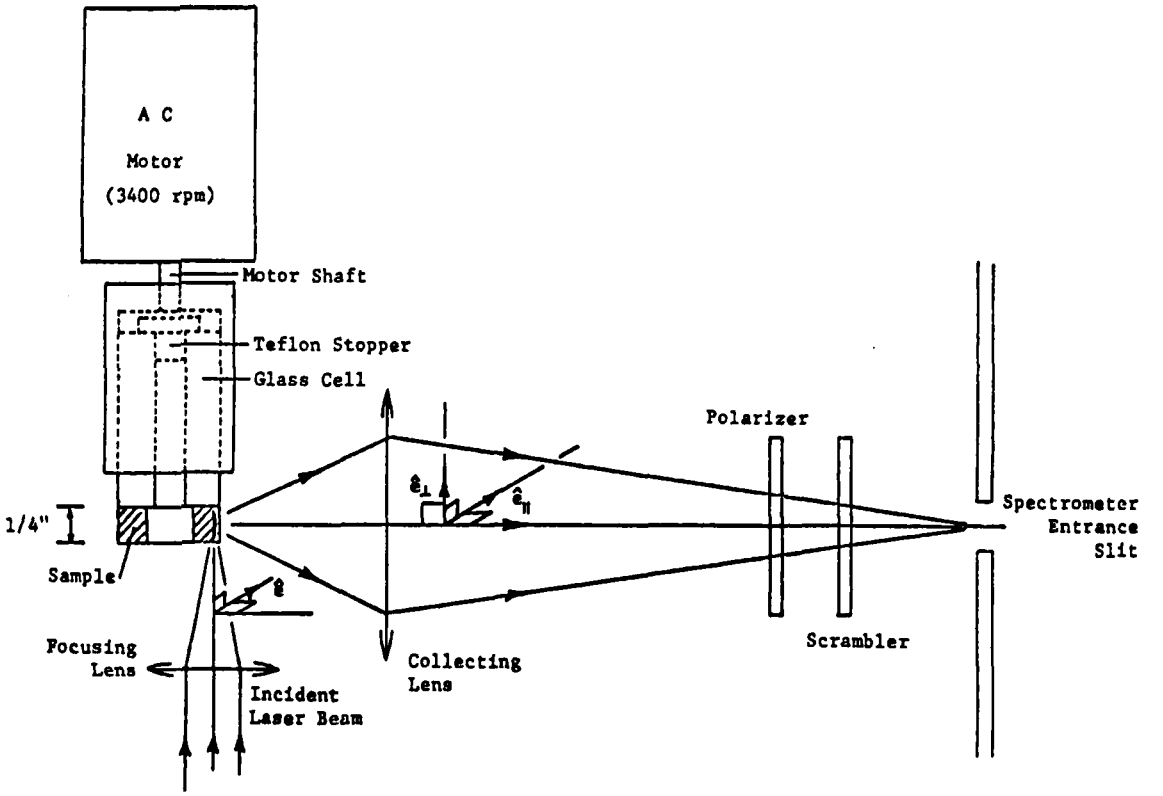

FIGURE 6. Standard Raman scattering arrangement: 90° scattering geometry. (Rotating cell is shown.) (From Shelnutt, J. A., Ph.D. thesis, Georgia Institute of Technology, Atlanta, 1975.)

Methods for Eliminating Fluorescence Background

The most serious problem in Raman spectroscopy is the interference due to fluorescence, which can be caused by either fluorescent impurities or the sample itself. The impurities can usually be removed by modern purification methods. Methods are available to suppress or avoid fluorescence background. 1. Long exposure to laser beam,[2] particularly biopolymer solid and solution. 2. Collision quenching by adding potassium iodide to solution. 3. Phase detection with rotating polarizer.[41] 4. Pulsed laser excitation with a gate detection electronics.[42] 5. Inverse Raman effect.[19-21] 6. CARS $2\omega_1 - \omega_2$ technique.[23,24] 7. Foster resonance transfer.[43] The first method is time consuming and may work only in limited cases. The second method is often undesirable because of the high concentration of KI required, or it becomes ineffective because the fluorescent moieties may become "buried." The third method requires that fluorescent molecules may be rapidly rotating. In addition, only polarized and anomalously polarized Raman lines can be detected by this technique. The fourth method requires relatively long-lived emitting electronic states. Since the laser pulse duration (N_2 laser) is $\gtrsim$10 nsec, this method would fail if the fluorescent lifetime of the pigments is in the same order of magnitude. The principles involved in methods 5 and 6 have been discussed previously. These two methods appear promising and currently under active development. The last method involves resonance energy transfer of the excited singlet state to an acceptor which does not emit, emits with long lifetime, or emits far in the red (so that the fluorescent background does not interfere with Raman signals). The most efficient resonance transfer occurs when the acceptor is attached to the macromolecule, properly oriented, and near the fluorescent sites.

Dependence of Amide Modes on Conformation: Theoretical Considerations

The use of vibrational spectra for conformational diagnoses of polypeptides and proteins depends on characteristic amide group frequencies. Nine frequencies are associated with the peptide group motion of the model compound *N*-methylacetamide: 3280 (amide A), 3090 (amide B), 1653 (amide I), 1567 (amide II), 1299 (amide III), 627 (amide IV), 725 (amide V), 600 (amide VI), and 206 (amide VII). Among these modes, amides I, II, and III are more useful in the conformational studies and have been the subject of extensive investigations using both infrared[44-49] and Raman spectroscopy.[2,50-53] The atomic displacement in each mode is shown in Figure 7. The amide I vibration is primarly C=O stretching (~70%) and C–N stretching (~16%). The amide II and III frequencies are both coupled vibrations of C–N stretching and the N–H in-plane bending. The amide II band is strong in infrared absorption, but virtually unseen in the nonresonance Raman effect. However, it becomes enhanced when the exciting wavelength (at 2573 Å) lies close to the π_1-π^* transition of the peptide chromophore near 190 nm. Additionally, amides I and III are also greatly enhanced. This is not surprising since the $\pi_1 \rightarrow \pi^*$ transition causes the contraction of the C–N distance.[54] In Figure 8 the ultraviolet absorption spectra of poly-L-lysine is shown in three different conformations. The hypochromic effect of the α helix and the hyperchromic effect of the β structure of proteins should be greatly manifested in the resonance Raman effect, since the intensities of amide modes should increase according to the square of the extinction coefficients (Albrecht's A term).

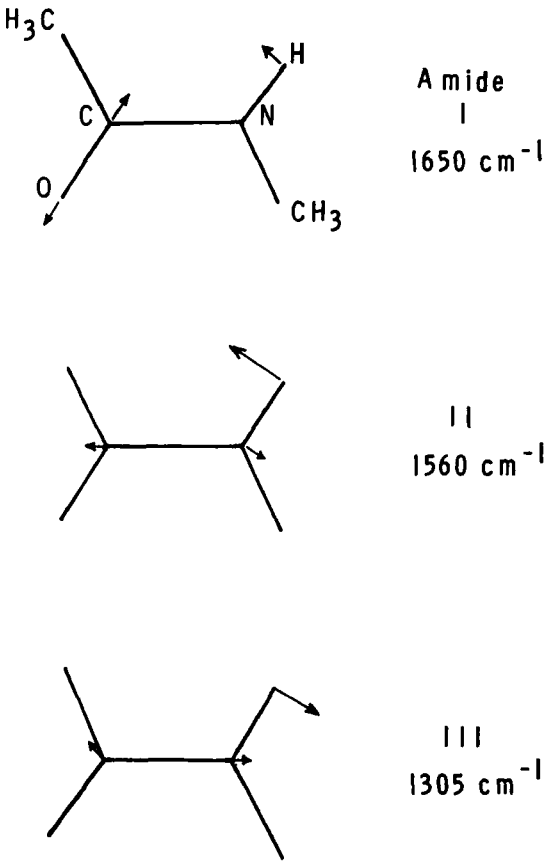

FIGURE 7. Atomic displacements of characteristic in-plane vibrations of the CONH group.

The important factors in determining the amide I, II, and III frequencies in a polypeptide chain are ϕ and ψ dihedral angles, H-bonding, and interaction effects. The effect of ϕ and ψ angles on the vibrations of amide I and III was recently studied by Hsu et al.,[53] using *N*-acetyl-L-alanine-*N*-methylamide $CH_3CONHCH(CH_3)CONHCH_3$ as a model. The geometries of this dipeptide varied from the potential minima associated with the α-helical structure and the antiparallel chain pleated β-sheet. The amide I frequency distribution for α-helical conformations is very narrow; for extended conformations it is only about 2 cm^{-1}. However, the difference between the amide I frequencies of these two regions is large (i.e., 1653.5 → 1664 cm^{-1}). The line-width associated with the unordered structure is expected to be larger than a regular structure because of a wider distribution in ϕ and ψ angles. In the amide III region, the normal vibration calculations indicate that the frequencies are more sensitive to small changes in ϕ and ψ. In the α-helical region, a change of 10° in ϕ causes a shift of 11 cm^{-1}; a 10° variation of ψ and ϕ in the β region causes a change of 6 cm^{-1}. This result indicates that the amide III band is very sensitive to the conformation of the polypeptide chain.

The effect of H-bonding is to decrease the C=O stretching frequency (amide I), but to increase the NH bending frequencies (amide II and III). For example using methyl phenylacetamidoacetate, the amide I mode decreases by about 30 cm^{-1} and the amide II increases by ~40 cm^{-1} as it changes

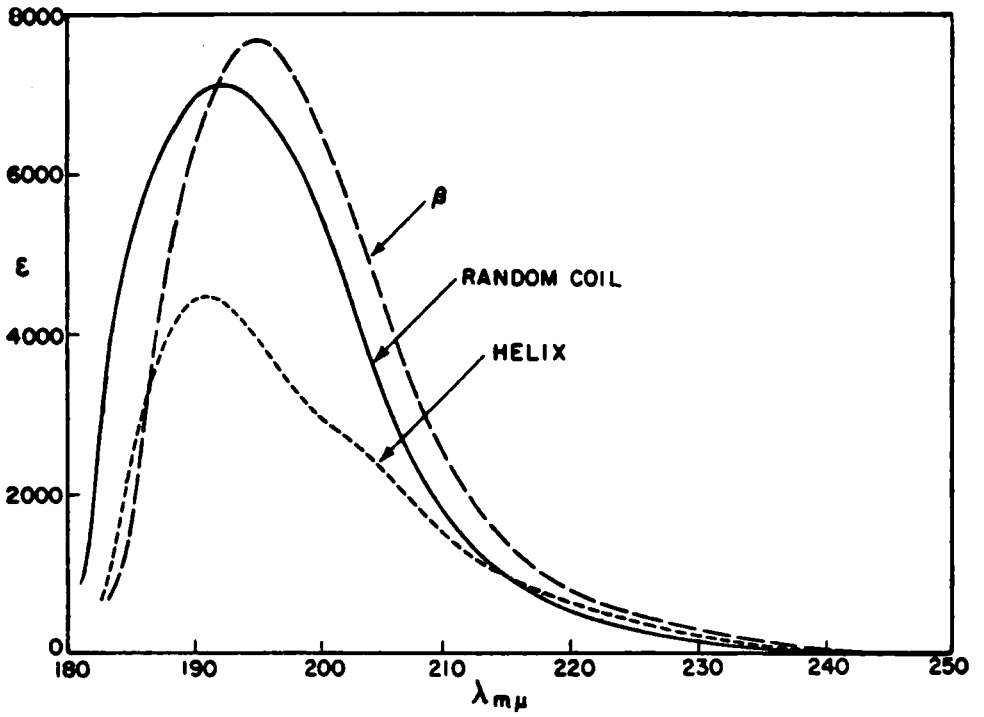

FIGURE 8. Ultraviolet absorption spectra of poly (L-lysine) in aqueous solution: random coil, pH 6.0, 25°; α-helix, pH 10.8, 25° C; β-conformation, pH 10.8, 52° C. (From Rosenheck, K. and Doty, P., *Proc. Natl. Acad. Sci. U.S.A.*, 47, 1775, 1961. With permission.)

from chloroform solution (weakly H-bonded) to a solid (strongly H-bonded).[55a] For *N*-methylacetamide, the frequency shifts from gaseous phase (non-H-bonded) to liquid phase (H-bonded) are as follows: amide I (1715 → 1650 cm^{-1}), amide II (1494 → 1563 cm^{-1}) and amide III (1263 → 1300 cm^{-1}).[55b] These data indicate that amide frequencies are sensitive to H-bonding.

The vibration interactions among intra- and interchain peptide units were first considered by Miyazawa.[45] In his well-known perturbation theory, a localized amide frequency is given by:

$$\nu(\delta,\delta') = \nu_0 + \sum_i (D_i \cos i\delta + D_i' \cos \delta') \qquad (32)$$

where

- ν_0 = the unperturbed peptide group frequency;
- D_i = the interaction constant between ith neighbors in the chain;
- D_i' = the interaction constant between the peptide groups connected by the interchain hydrogen bond;
- δ and δ' = the phase angles between the vibrations in the appropriate peptide groups (see Figure 9).

For the antiparallel β-pleated sheet structure, only D_1 and D_1' are assumed to be important.[46] Thus the above equation takes the following form:

$$\nu(\delta,\delta') = \nu_0 + D_1 \cos \delta + D_1' \cos \delta' \qquad (33)$$

According to the symmetry properties of the two-dimensional unit cell of the antiparallel β-pleated sheet structure, four different phase combinations are possible:

$$\begin{aligned} \nu(0,0) &= \nu_0 + D_1 + D_1' && A_1 \text{ symmetry} \\ \nu(0,\pi) &= \nu_0 + D_1 - D_1' && B_1 \text{ symmetry} \\ \nu(\pi,0) &= \nu_0 - D_1 + D_1' && B_2 \text{ symmetry} \\ \nu(\pi,\pi) &= \nu_0 - D_1 - D_1' && B_3 \text{ symmetry} \end{aligned} \qquad (34)$$

Although all four vibrations are Raman active, the totally symmetric mode $\nu(0,0)$ of A species is expected to be the most intense in the Raman effect (nonresonance). Among the four species, only B_1, B_2, and B_3 are infrared active.

Recently the Raman intense $\nu(0,0)$ mode was observed[56] at 1674 cm^{-1} in polyglycine I, which

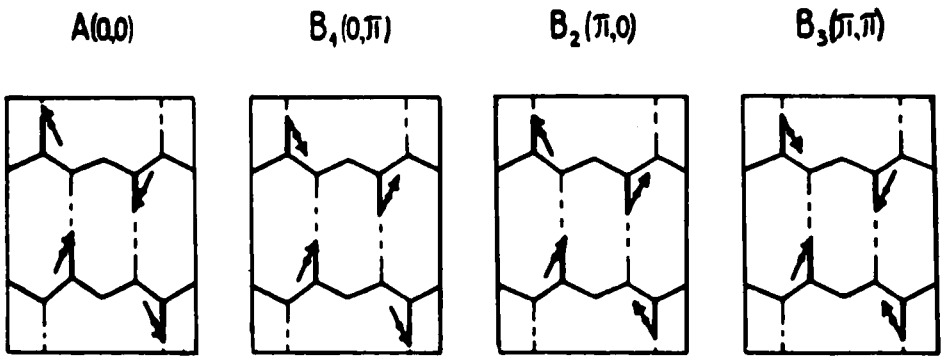

FIGURE 9. Transition dipoles of the amide I vibration in the unit cell of the antiparallel chain pleated sheet for the vibrations of different symmetry type. (From Chirgadze, Y. N. and Nevskaya, N. A., *Bipolymers*, 15, 607, 1976. With permission.)

had caused considerable difficulties in the quantitative application of the perturbation theory. To achieve a more consistent understanding, Krimm and Abe[48] modified the perturbation expression by adding the transition dipole coupling term D_{11}. The new equation is expressed by:

$$\nu(\delta,\delta') = \nu_0 + D_1 \cos\delta + D_1' \cos\delta' + D_{11} \cos\delta \cos\delta'$$

By assuming $D_1 = 0$, they obtained the following expressions:

$$\begin{aligned}
\nu(0,0) &= 1674 = \nu_0 + D_1' + D_{11} \\
\nu(0,\pi) &= 1685 = \nu_0 - D_1' - D_{11} \\
\nu(\pi,0) &= 1636 = \nu_0 + D_1' - D_{11} \\
\nu(\pi,\pi) &= [1723] = \nu_0 - D_1' + D_{11}
\end{aligned} \qquad (35)$$

The value $\nu(\pi,\pi) = 1723$ was predicted on the basis of $\nu_0 = 1679.5$, $D_1' = -24.5$, and $D_{11} = 19\ cm^{-1}$, which were obtained by solving the first three equations. The observed frequencies for poly-L-alanine in β-structure, are $\nu(0,0) = 1669$, $\nu(0,\pi) = 1695$, and $\nu(\pi,0) = 1630\ cm^{-1}$; the constants are[57] $\nu_0 = 1682.0$, $D_1' = -32.5$ and $D_{11} = 19.5\ cm^{-1}$. The differences in the structure of these two β polypeptides are reflected in the similarities and differences between these parameters.

For the parallel chain pleated sheet, the transition dipole orientations are such that D_{11} is essentially zero.[48] The equations for the two optically active amide I modes are given by:

$$\nu(0,0) = \nu_0 + D_1 + D_1' \qquad (36)$$

$$\nu(\pi,0) = \nu_0 - D_1 + D_1' \qquad (37)$$

The constants were estimated by Moore and Krimm.[57] For (a) polyglycine, $\nu_0 = 1676.0$, $D_1 = 3.2$, and $D_1' = -22.9\ cm^{-1}$; for (b) poly-L-alanine, $\nu_0 = 1682.4\ cm^{-1}$, $D_1 = 3.5$, and $D_1' = -25.7\ cm^{-1}$. The frequencies of the parallel chain pleated sheet have not been observed individually, but the predicted amide I vibrations are (a) polyglycine, $\nu(0,0) = 1656.3$ and $\nu(\pi,0) = 1649.9\ cm^{-1}$; (b) poly-L-alanine, $\nu(0,0) = 1660.2$ and $\nu(\pi,0) = 1653.2\ cm^{-1}$.

If a polypeptide chain assumes the α-helical conformation, the interchain interactions may be neglected. Since the intrachain hydrogen bonds are formed between third neighbors, the D_3 terms should be included in the expression:

$$\nu(\delta) = \nu_0 + D_1 \cos\delta + D_3 \cos 3\delta \qquad (38)$$

For the amide I vibration of the α helix, the components $\nu(0)$ and $\nu(\theta)$, which are parallel and perpendicular, respectively, in the infrared dichroism, have nearly the same frequency.[58]

Nonresonance Raman of Some Polypeptides as Conformational Models

Poly(L-glutamic acid)

The vibrations of a polypeptide backbone are not isolated from the motions of the side chain. To examine the effects of conformational changes on Raman spectra without uncertainties due to differences in side chains, one needs a model homopolypeptide which is capable of assuming a variety of conformations. Poly-(glu) is unique in this respect because it is known to exist in random-coil, α-helix, and two different antiparallel chain pleated sheet β structures.[59] The so-called β_1 form prepared by heating at temperatures between 40 and 85°C has an X-ray diffraction

pattern similar to that of an ordinary antiparallel pleated sheet structure. However, β_2 form produced by heating above 85°C gives diffraction lines sharper than those for the β_1 form, indicating that the crystallinity (or the degree of order) of the β_2 form is higher than that of the β_1 form. It was concluded[59] that the main differences between the two β forms are in the intersheet spacing (β_1, 9.03 Å, β_2, 7.82 Å) and the orientation of the carboxyl side groups. In the β_1 form, the planes of the carboxyl groups lie almost parallel to the chain axis, and hydrogen bonds are formed between carboxyl groups belonging to different neighboring sheets. However, the carboxyl groups in the β_2 form, lie in planes normal to the chain axis, and hydrogen bonds are formed within the same sheets.

Raman spectra of poly-(Glu) in α helix and β_1 and β_2 form were investigated by Fasman et al.[60] The important spectral features and implications may be summarized as follows.

The amide I mode in the Raman spectrum has shifted from 1652 (α helix) to 1672 (β_1 structure) and to 1647 and 1666 cm^{-1} (β_2 structure). The splitting observed in the β_2 form is unusual. The values for the α helix and β_1 form (ordinary antiparallel β structure) are typical for these two conformations. It is interesting to note that the amide I frequencies from Raman and infrared are nearly the same for the α helix (Raman, 1652; infrared, 1656 cm^{-1}), but quite different for the β_1 structure (Raman, 1672; infrared, 1625 and 1680 [?]) and β_2 structure (Raman, 1647 and 1666 cm^{-1}; infrared 1601 cm^{-1}). Based on Miyazawa's perturbation theory, as extended by Krimm and Abe, the splittings are due to the strong interchain interactions, which are virtually absent in the α-helical conformation. In the case of the β_2 form, the intersheet interactions may be important as well. The Raman 1672 cm^{-1} line can be assigned to the $\nu(0,0)$ mode, while the infrared 1680 and 1625 cm^{-1} bands are assigned to the $\nu(0,\pi)$ and $\nu(\pi,0)$ components, respectively. However, the assignment of the amide I modes for the β_2 form have not been made.

Normally, the amide II vibrations are quite weak in the nonresonance Raman effect, but they are considerably strong in the spectra of poly-(Glu). Differences between Raman and infrared data in the amide II frequencies were found in the β_1 and β_2 forms.

Both frequencies and intensities of the amide III vibrations are sensitive to conformation. The amide III frequency for the α helix (~1295 cm^{-1}) is higher than both random-coil (~1248 cm^{-1}) and antiparallel β structures (β_1, 1236 cm^{-1}; β_2, 1230 cm^{-1}). The amide III intensity for the α helix is intrinsically weak and contributes only about one third of the observed intensity at ~1295 cm^{-1}, as evidenced by deuteration experiments.[60,61] The remaining two thirds is due to the CH_2 deformation. The variations of the amide III intensities (α helix < random coil < β structure) are probably related to the hypochromic or hyperchromic effects[62] in the $\pi_1 \rightarrow \pi^*$ transitions near 190 nm.

The differences in side-chain conformation between the two β forms are manifested in the 800- to 1200-cm^{-1} region, as well as in the C=O stretching region at ~1730 cm^{-1}. In the β_1 form, the carbonyl frequency of the γ-COOH groups appears as a weak broad band near 1726, while in the β_2 form it shows up as a sharp and strong line at 1732 cm^{-1}. It was concluded[61] that the intrasheet hydrogen bonding of the γ-COOH groups in β_2 is weaker than the intersheet hydrogen bonding in β_1.

Alpha (α)-helical conformation has a characteristic line near 900 to 950 cm^{-1} due to a C–C symmetric stretching mode of the backbone skeleton coupled with its side-chain C–C stretching. This line is strong and characteristic and has been readily identified in various α-helical polypeptides and proteins. It is at 924 cm^{-1} in poly-(Glu),[61] 945 cm^{-1} in poly-L-lysine,[52] 940 cm^{-1} in δ-crystallin of bird lens,[63] and ~945 cm^{-1} in α-helical Pfl and fd coat proteins of filamentous bacterial viruses.[64] The corresponding C–C stretching lines characteristic of β structures are often difficult to identify.

Poly-L-lysine

Poly-L-lysine exists in aqueous solution as a random coil at low pH, α helix at high pH and low temperature, and the antiparallel chain pleated sheet structure at high pH and high temperature.[65] Raman spectra have been reported for all three conformations in aqueous solution.[52]

The conversion of α helix to β structure causes the following frequency shifts: 1645 → 1670 (amide I), 1311 → 1240 cm^{-1} (amide III), and 945 → 1002 cm^{-1} (C–C stretching) (Figure 10). The amide I frequency at 1645 cm^{-1} is unusually low for α helix since it is normally observed at 1650 to

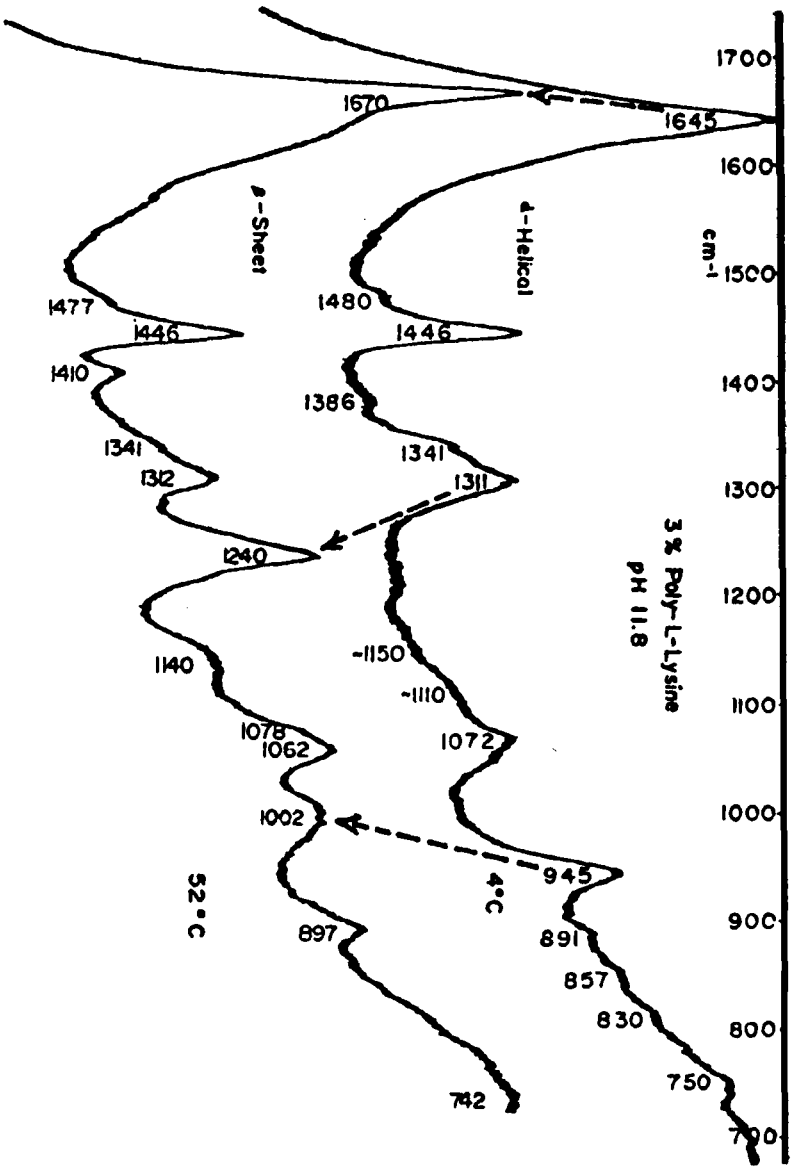

FIGURE 10. Raman spectra of (top) α-helical poly-L-lysine, 3% in H_2O, pH 11.8, T = 4° C and (bottom) β-sheet poly-L-lysine, 3% in H_2O, pH 11.8, T = 52° C. (From Yu, T. J., Lippert, J. L., and Peticolas, W. L., *Biopolymers*, 12, 2161, 1973. With permission.)

1660 cm^{-1}, e.g., poly-L-glutamic acid (1652 cm^{-1}), poly-γ-benzyl-L-glutamate (1650 cm^{-1}), poly-L-leucine (1652 cm^{-1}), poly-L-alanine (1655 cm^{-1}), and glucagon (1658 cm^{-1}). The amide III at 1311 cm^{-1} in α-helical poly-L-lysine is rather high in comparison with the other α-helical polypeptides (1265 to 1300 cm^{-1}). The observed intensity at 1311 cm^{-1} is not completely due to the amide III mode. As discussed earlier, the amide III intensity of α helix in the nonresonance Raman effect is intrinsically weak. Chen and Lord[51] were able to observe the splittings of the amide III modes in the α-helical poly-L-alanine. The triplet observed at 1265, 1275, and 1283 cm^{-1} was assigned to A, E_1, and E_2 species, respectively. Such splittings have not been observed in α-helical poly-L-lysine.

The Raman spectrum (not shown) of the ionized form (at pH 9) of poly-L-lysine exhibits the amide III line at 1243 cm^{-1} and the C–C stretch at 958 cm^{-1}, which is between the corresponding lines of α helix (945 cm^{-1}) and β

structure (1002 cm^{-1}). The amide I mode was not observed because it is weak and masked by a water band near 1645 cm^{-1}. The ionized form of poly-L-lysine is thought to be either random coil[65] or "extended helix."[66] The term "extended helix" refers to a local conformation. Unlike CD spectra, Raman spectra are not sensitive to the existence of an "extended helix" conformation in the ionized state.[52] The CD curves show a change in the ionized form as a function of temperature, but no change was found in the Raman spectrum of the ionized form between 40 and 60°C. It was concluded[52] that Raman spectroscopy may not be able to uncover the difference between the extended helix state and the totally unordered state.

Glucagon

Glucagon is a polypeptide hormone of 29 amino acid residues whose sequence is known. It exists in ~75% α helix in crystals and in a random coiled form in freshly prepared acidic solution. After standing at 26°C, this acidic solution is gradually converted into a gel, which is predominantly an antiparallel β structure. Raman spectra in the 1120 to 1700 cm^{-1} region of glucagon have been reported.[67]

Figure 11 shows the Raman spectra of glucagon in crystals, freshly prepared aqueous solution (pH 2.25), and gels. These spectra show a stepwise decrease in frequency of the amide III lines from 1266 (α helix) to 1248 (random coil) and then to 1232 cm^{-1} (antiparallel β). These frequencies are very similar to those of α-helical poly-L-alanine, random-coiled poly-L-glutamic acid, and antiparallel β polyglycine I, respectively. In the 1630- to 1700-cm^{-1} region, the amide I line of crystalline glucagon is seen at 1658 cm^{-1}. In the middle spectrum, the strong water line near 1640 cm^{-1} has obscured the amide I frequency of glucagon in freshly prepared aqueous solution. However, upon gel formation the amide I line sharpens considerably and shows up in the spectrum as an intense sharp line at 1672 cm^{-1} on the sloping background of water.

Intensity Variation of Tyrosine Doublet at 850 and 830 cm^{-1}

Tyrosyl residues in proteins give rise to two Raman lines[68] at 850 and 830 cm^{-1}. Yu and co-workers[37] first noticed a change in the intensity ratio of these two lines when ribonuclease (lyophilized powder) was dissolved in water. They suggested that this might be caused by the change in the local environment of the three tyrosines (i.e., Try-25, -92, and -97) with an abnormally high pKa value. Subsequent studies[69,70] of cobramine B and neurotoxin α

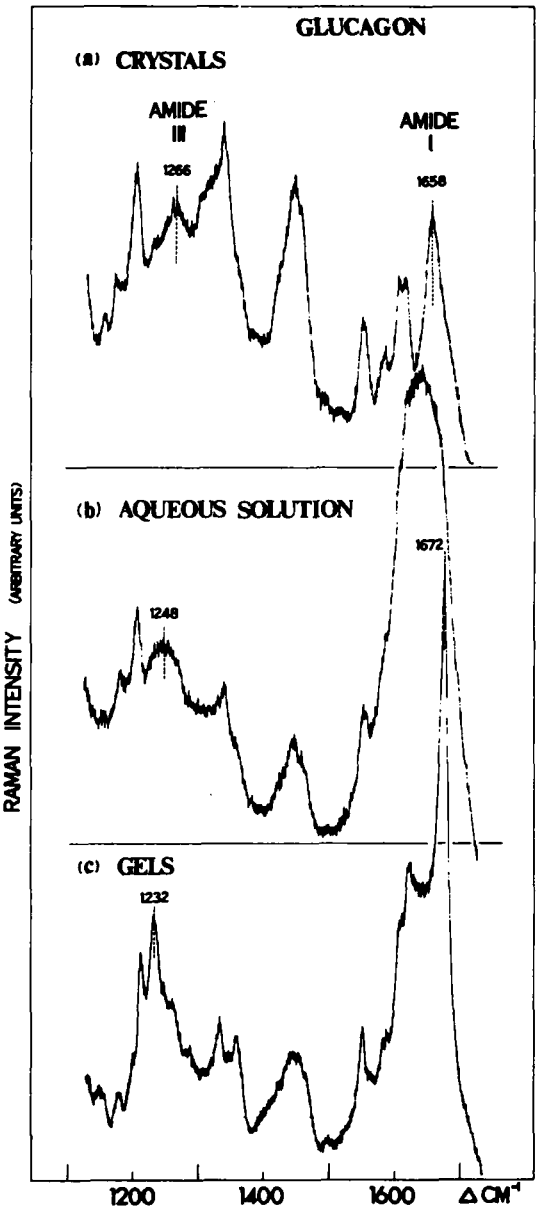

FIGURE 11. Raman spectra of glucagon in various states of aggregation. (a) Spectrum of crystalline glucagon (powder form); (b) spectrum of freshly prepared aqueous glucagon; (c) spectrum of gels formed from (b) on standing (~40 hr at 26°). (From Yu, N. T. and Liu, C. S., *J. Am. Chem. Soc.*, 94, 5127, 1972. Copyright by the American Chemical Society. With permission.)

indicated that the intensity ratio, I(850)/(830), depended on protein conformation and possibly the strong hydrogen bonds between phenolic hydroxyl groups in the "buried" environment which is not accessible to water.

Earlier Bellocq et al.[71] noted the significant difference between the frequencies of these two lines in bovine serum albumin (820 and 852 cm^{-1}) and β-lactoglobulin (832 and 860 cm^{-1}); they attributed these to differences in the hydrogen bonding of the phenolic hydroxyl group. Siamwiza et al.[72] showed that the doublets at 850 and 830 cm^{-1} are due to Fermi resonance between the ring-breathing vibration and the overtone of an out-of-plane ring-bending vibration of the para-substituted benzene. Further examination of the effects of pH and solvents on the Fermi doublet and of crystallographic data revealed that the intensity ratio of the two lines depends on changes in the relative frequencies of the vibrations. These frequencies were found to be sensitive to the nature of the hydrogen bonding of the phenolic hydroxyl group or its ionization. The reported Raman intensities of the doublets observed in several proteins have been interpreted on the basis of the relative intensities of the doublet in model systems in which the phenolic hydroxyl group is known to be strongly hydrogen bonded, weakly hydrogen bonded, free, or ionized.[72]

Dependence of ν(S–S) and ν(C–S) on Local Geometry

Raman spectra of compounds containing disulfide bonds show well-defined lines in the 500 to 730 cm^{-1} region; these lines arise from S–S and C–S stretching modes. The behavior of these Raman lines as a function of structural parameters has been investigated extensively using model compounds.[73-77] A linear relationship was found by vanWart et al.[74] between the S–S frequency and the CS–SC dihedral angle for compounds with similar CC–SS dihedral angles. However, Sugeta et al.[75] argued cogently that the S–S frequency did not depend on the CS–SC dihedral angle, but rather on the torsional angles about the C–S bonds in the C–C–S–S–C–C group. Assuming that the dihedral angle around the S–S bond is fixed at ~90° (gauche), the S–S frequency depends on whether the two torsional angles about the C–S bonds are both gauche, one gauche, and one trans, or both trans. The ν(S–S) frequencies are 510 cm^{-1} (GGG), 525 cm^{-1} (GGT), and 540 cm^{-1} (TGT). A diagram showing this correlation is presented in Figure 12.

The C–S frequency of the primary disulfide $X-\overset{|}{\underset{|}{C}}-CH_2S-S-$ depends on the nature of the atom X at the trans site with respect to the closer sulfur atom. When X is a hydrogen atom (denoted as P_H), the C–S stretching vibration lies at 630 to 670 cm^{-1}. It is at 720 cm^{-1} if X is a carbon atom

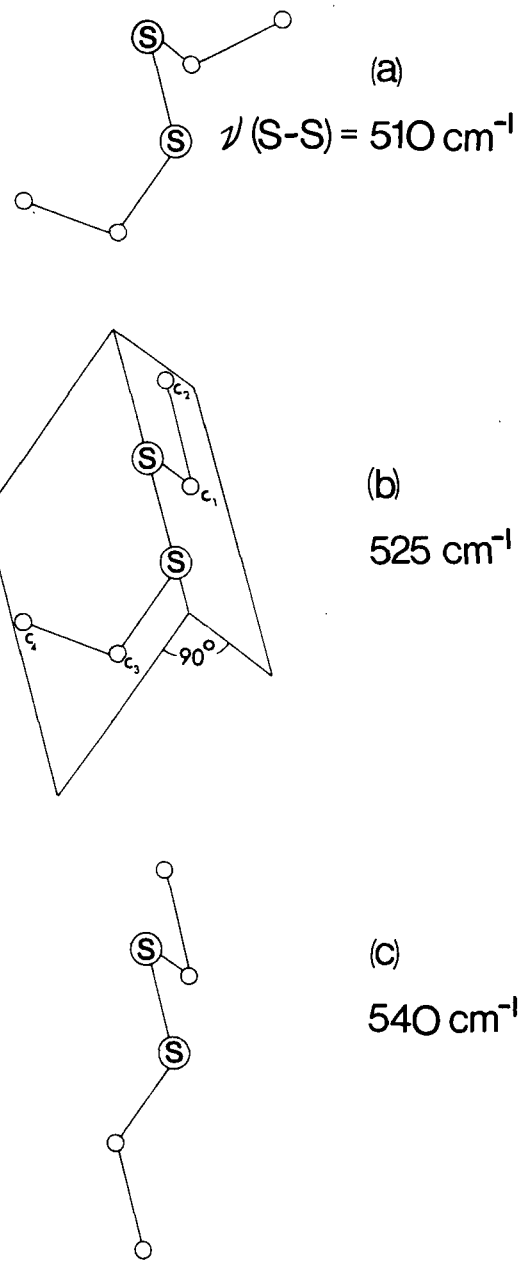

FIGURE 12. Correlation between the C–C–S–S–C–C geometry and ν(S–S) frequency. (From Chang, R. C. C., Ph.D. thesis, Georgia Institute of Technology, 1976.)

(P_C) and at 700 cm^{-1} if X is a nitrogen atom (P_N). Various conformations of the half-cystine group are shown in Figure 13.

The C–S stretching modes from methionine residue are also expected to appear near the 700 cm^{-1} region. The correlation between the C–S stretching frequency and internal rotation angles surrounding the C–C and C–S bonds was made by Nogami et al.[77] Two C–S frequencies are expected at 760 and 719 cm^{-1} for the trans-trans form, at 746 and 697 cm^{-1} for the trans-gauche form, at 667 cm^{-1} for the gauche-trans form, and at 723 and 645 cm^{-1} for the gauche-gauche form.

The above correlations have been directly applied to the Raman data of lysozyme,[78] ribonuclease,[79] α-lactalbumin,[80] and lens crystallins.[81]

Comparison of Protein Structure in Crystals, in Lyophilized State and in Solution

X-ray diffraction studies of protein structure are restricted to crystals, whereas CD and ORD methods are applicable only in solution. Laser Raman spectroscopy is a technique which can provide structural information from a variety of phases. It provides new insight into the local geometry of the disulfide cross-links, the specific H-bonding of "buried" tyrosine residues, the secondary structure of protein backbone (i.e., α helix, antiparallel β, parallel β structure, H-bonded or non-H-bonded random coil, etc.), the presence and environment of the sulfhydryl groups, the configuration of the methionine side chains, the specific interaction of tryptophan, and the skeletal stretching and bending vibrational characteristics in proteins.

The effects of crystallization and lyophilization on the structures of lysozyme,[82] ribonuclease,[70] insulin,[32,82] and α-lactalbumin[83] have been investigated. Important results may be summarized as follows.

1. Crystallization of lysozyme, ribonuclease A, and α-lactalbumin does not produce any significant effect on the environment of the peptide backbone, as shown by the amide III region.

2. The secondary structure of insulin crystals grown at pH 6.0 is significantly different from that of insulin solution at pH 2.75. Since insulin is not soluble at pH 6.0, it is not clear whether the spectral differences observed are caused by a pH change from 6.0 to 2.75 or by crystallization.

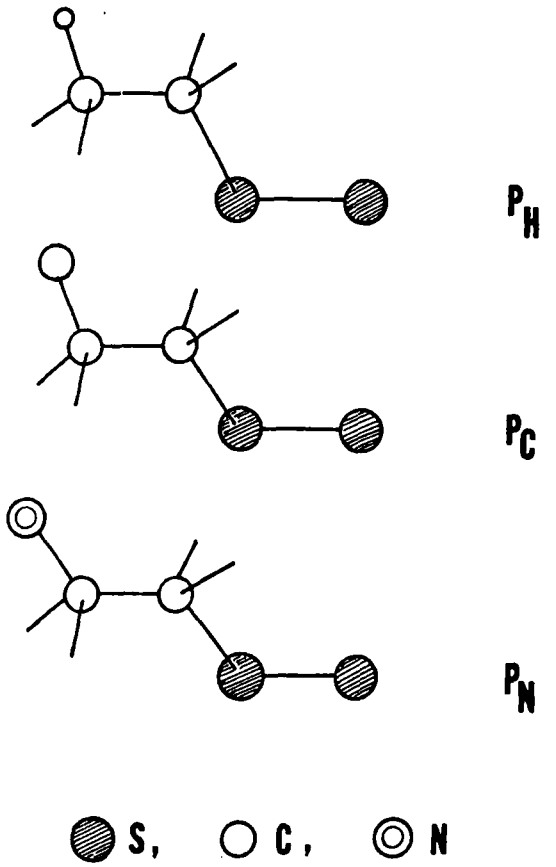

FIGURE 13. Various conformations of half-cystine group. (From Jo, B. H., Ph.D. thesis, Georgia Institute of Technology, 1975.)

3. In the 500- to 700-cm^{-1} region, where the S–S and C–S stretching and the tyrosyl ring vibrations appear, the spectral features of a single crystal of RNase A are different from those of lyophilized powder and solution. The Raman spectra of a single crystal of RNase A and its mother liquid are shown in Figure 14. A comparison of Raman spectra from three different phases is shown in Figure 15.

4. Lyophilization altered the Raman spectra of the four proteins examined, indicating considerable changes in protein main-chain and side-chain conformation. However, this may not be true for other proteins. For example, the predominantly antiparallel β structure of lens crystallins[84] is not appreciably affected by the lyophilization process.

Structural Studies of Intact Ocular Lenses

The living lens is an exquisite collection of a single type of cells, without blood vessels and nerves (Figure 16). The concentration of protein is

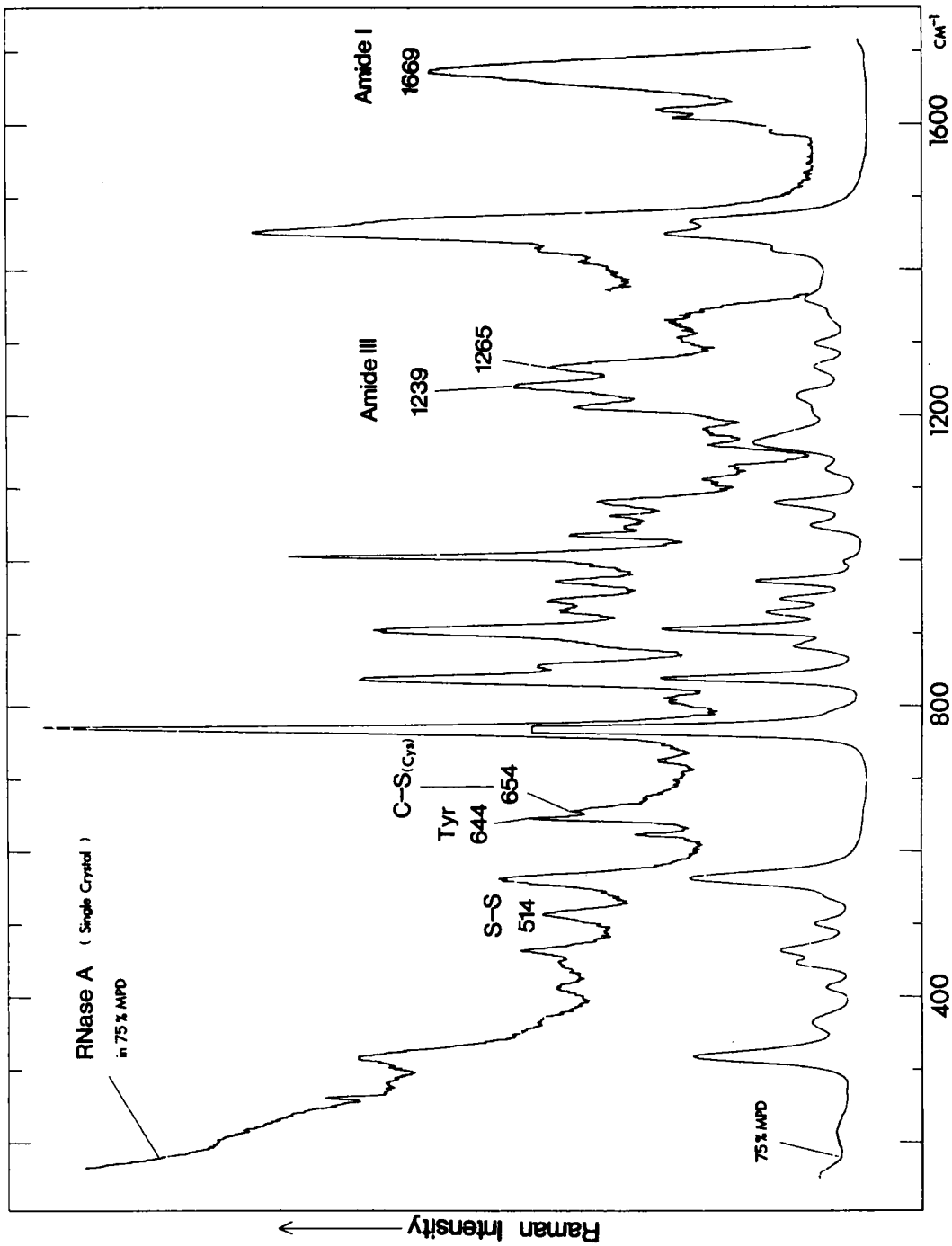

FIGURE 14. Raman spectra of a single crystal of RNase A (upper) and 75% MPD (2-methyl-2,4-pentanediol) (lower). (From Yu, N. T. and Jo, B. H., *J. Am. Chem. Soc.*, 95, 5033, 1973. Copyright by the American Chemical Society. With permission.)

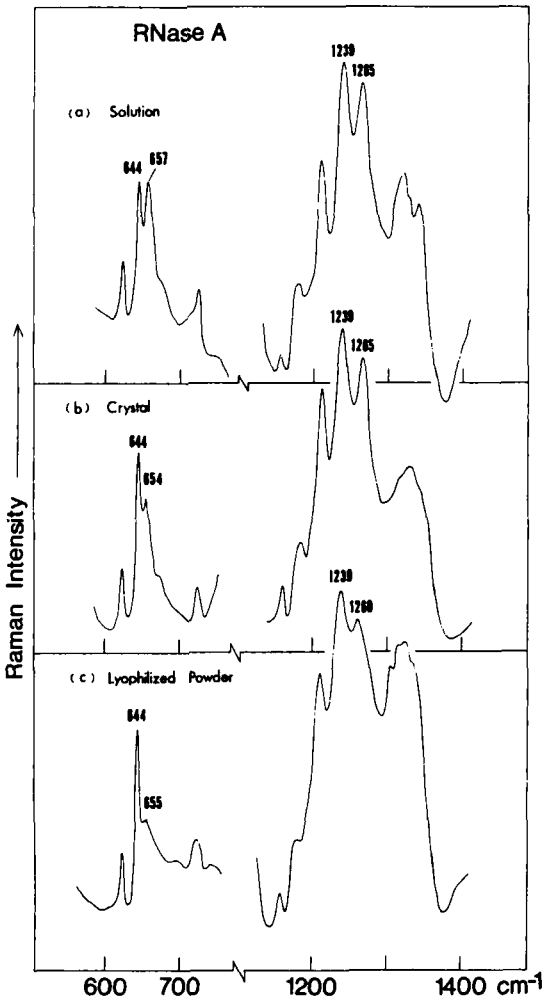

FIGURE 15. A comparison of the Raman spectra of solution, single crystal, and lyophilized RNase A in the 600- to 750- and the 1180- to 1400-cm^{-1} regions. (From Yu, N. T. and Jo, B. H., *J. Am. Chem. Soc.*, 95, 5033, 1973. Copyright by the American Chemical Society. With permission.)

rather high (~30 to 70% by weight). The lens is completely encapsulated and contains a single layer of more or less cuboidal epithelial cells at the front (anterior side), which transform into lens fibers. Each fiber is approximately 10 μm wide with a hexagonal cross section and extends from anterior suture to posterior suture. There is a continuous growth of lens fibers throughout life, although the rate decreases with age. As one proceeds from the cortex (outer portion) to the nucleus (center), one passes from recently synthesized protein to protein which was produced during early life.

Generally, the protein in a mammalian lens is composed of three water-soluble fractions (α-, β-, and γ-crystallin) and an insoluble albuminoid. These lens proteins are believed to be globular and arranged in a certain regular fashion. They maintain the transparency of the normal lens remarkably well. However, the clear lens can be converted into a cloudy or opaque "cataract" by a number of influences, such as the aging process, ultraviolet and X-ray irradiation, diabetes mellitus, and galactosemia. The mechanisms which result in loss of normal lens transparency have been the subject of numerous experimental studies and speculations.[85]

Laser Raman scattering is a noninvasive, sensitive, and selective probe of lens structures at the molecular level. In contrast to most biochemical methods requiring classical isolation procedures, it is employed to extract structural and conformational information directly from a living intact lens, thus avoiding possible aerobic oxidation of the sulfhydryl groups. The sulfhydryl groups which may play a role in the function of some lenses can be readily detected and measured quantitatively in the Raman effect.[84] Recent studies[86] on aging effects indicate that the rate of SH → S–S conversion was species dependent and linked to the metabolic process. The precipitous drop of SH peak intensity at 2580 cm^{-1} with a concomitant increase of the S–S peak at 508 cm^{-1} provides unequivocal evidence that the S–S bonds form in vivo during the aging process.

Conformational studies of crystallins in intact bovine lens have been reported.[38,84] α-, β-, and γ-crystallin exist in an antiparallel β structure (with a small amount ~15% of unordered form) in an intact lens, as well as in the isolated state. Schachar and Solin[87] also performed Raman studies of bovine lens; they agree with Yu et al.'s[38] conclusion that lens proteins have a predominantly antiparallel β structure. However, based on their polarized data (which are of doubtful validity), they proposed that lens proteins were fibrillar with the hydrogen-bonded linear CONH groups of the antiparallel β-pleated sheet preferentially oriented in directions orthogonal to the optic axis of the lens. Because of the similarity between the hexagonal cross section of lens fibers and the hexagonal arrangement of atoms in the antiparallel β-pleated structure, they argued that the relationship between the fiber macrostructure and protein microstructure was causal. However, a recent finding[63] that bird lens protein is chiefly α helical

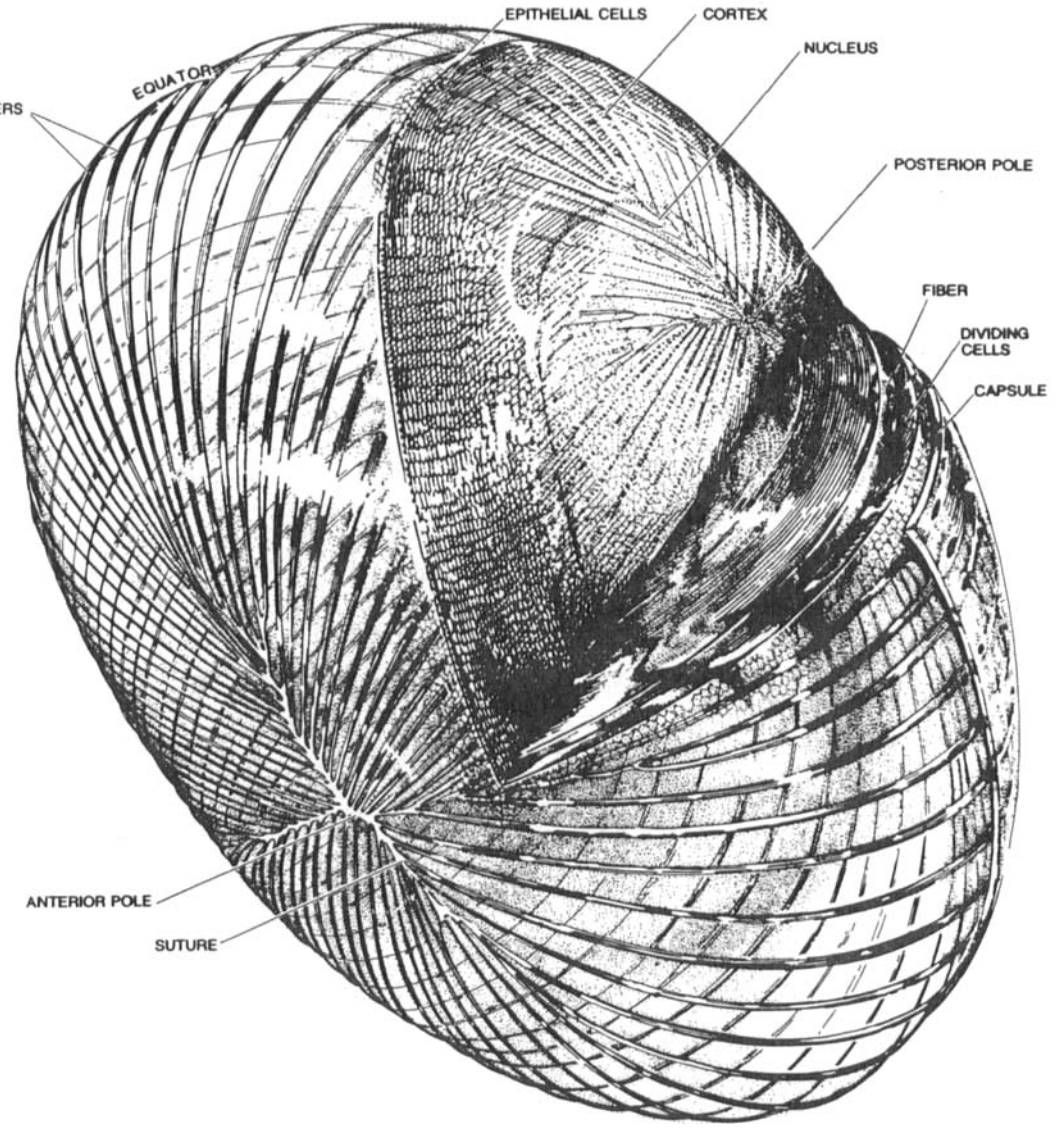

FIGURE 16. Structure of human lens. (From van Heyningen, R., What Happens to the Human Lens in Cataract, *Sci. Am.*, p. 77, 1975. Copyright © by Scientific American, Inc. All rights reserved. With permission.)

appears to contradict the suggestion of Schachar and Solin.[87] The cross section of avian lens fibers is also hexagonal,[88] suggesting no dependence on the protein secondary structure.

A unique feature of lenses of birds is the protein called δ-crystallin. Raman spectra of purified δ-crystallin from chick indicate that it exists chiefly in the α-helical conformation; this finding is in agreement with the results of CD studies.[81] The use of Raman spectroscopy with chick lenses clearly shows that δ-crystallin is also predominantly α-helical in the intact state (Figure 17). The spectral features close to 524, 940, 1240, 1670, and 2582 cm^{-1} between the spectra of cows and chicks are dramatically different. The Raman spectra of mature hen lens[81] indicate that the proteins in the nuclear region are very different from the proteins in the cortical region in both amino acid composition and conformation (Figure 18).

Denaturation of Proteins

The sensitivity of Raman spectroscopy to protein conformation is best illustrated by comparing the spectra of native and denatured protein. This is shown in Figure 19 using the insulin protein

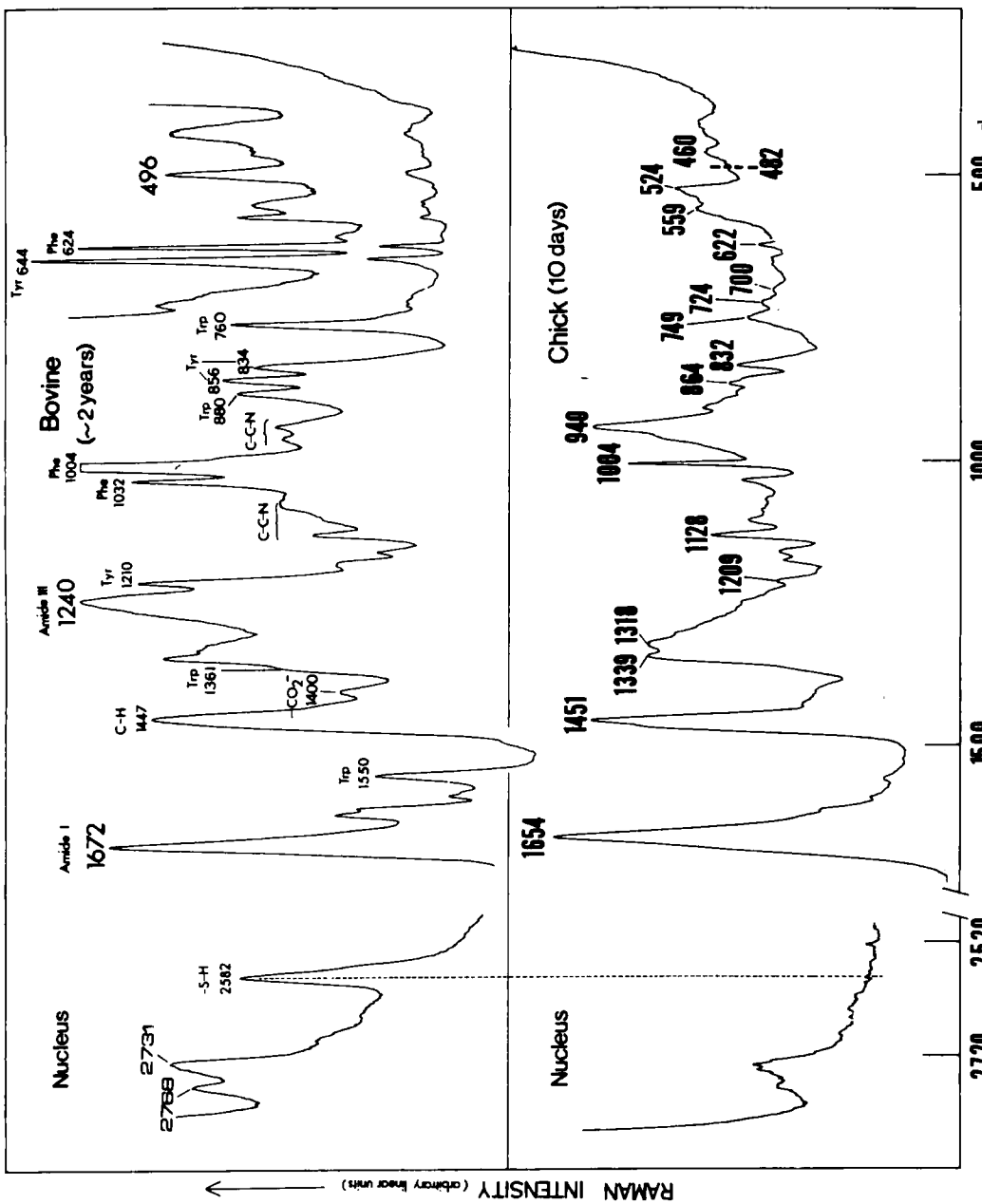

FIGURE 17. Comparison of the Raman Spectra of bovine and chick lenses. The spectra were obtained with the 514.5-nm line excitation. (From Kuck, J. F. R., Jr., East, E. J., and Yu, N. T., *Exp. Eye Res.*, 23, 9, 1976. With permission.)

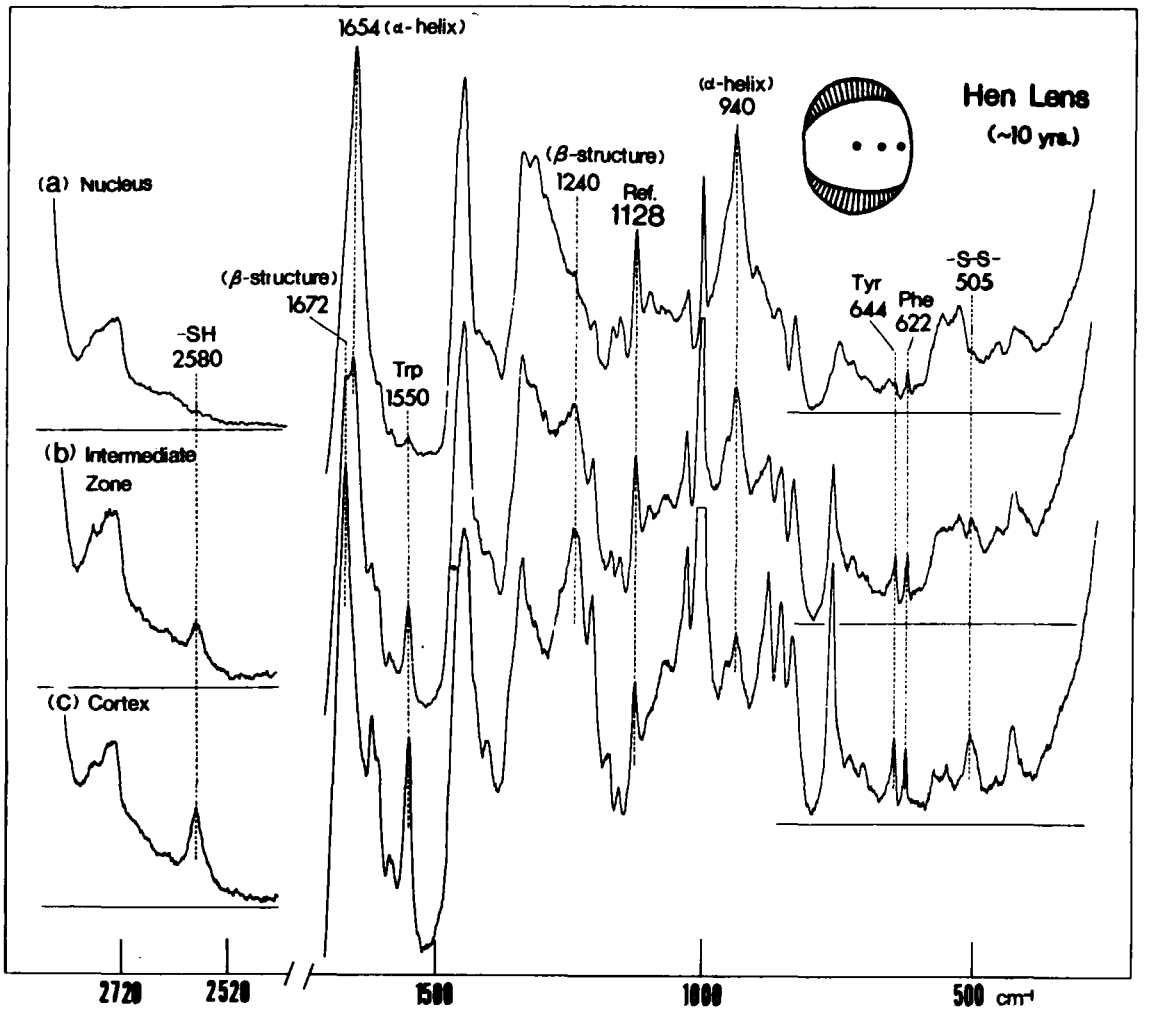

FIGURE 18. Variation of protein conformation from α helix (nucleus) to β structure (cortex) in a 10-year-old hen lens. (From Chang, R. C. C., Ph.D. thesis, Georgia Institute of Technology, 1976.)

molecule as an example. The vibrational frequencies with assignments for both native and denatured forms are tabulated in Table 2.

Insulin undergoes an interesting reversible globular-fibrous transformation in dilute HCl solution when heated with a concomitant loss in its activity. This transformation can also be brought about by seeding with preformed fibrous insulin at 0°C. This process can be reversed, yielding active, crystallizable insulin. Because of this reversibility, Waugh[89] suggested that the fibrils were arrays of only slightly distorted globular insulin molecules. This view is shared by other investigators.[90-92] However, Raman spectroscopic studies[50] provided useful information pertaining to the nature of this globular-fibrous transformation. The local geometry of the disulfide linkages has been distorted and the backbone conformation has undergone extensive unfolding in the conversion from native to denatured insulin. Further investigation led Yu et al.[50] to conclude that the denatured insulin exists in a predominantly antiparallel pleated sheet structure (the so-called cross-β conformation), in agreement with the proposals of Ambrose and Elliott[44] and Burke and Rougvie.[93]

The reversible thermal denaturation of ribonuclease A at pH 5 in the 32 to 70°C range was recently investigated by means of Raman spectroscopy.[79] By examining intensity changes in the amide I and III regions, it was learned that substantial amounts of ordered conformations (helical and pleated sheet) remained at 70°C. The intensity ratio of the doublet at 830 and 850 cm^{-1} was used to reveal changes in the strength of hydrogen bonding of "buried" tyrosyl residues.

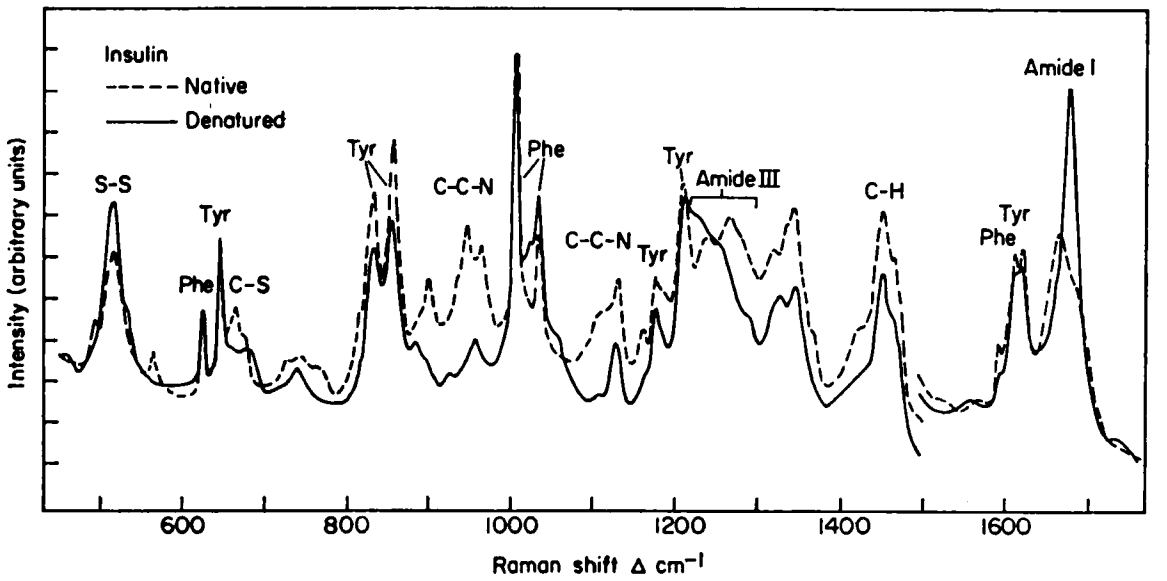

FIGURE 19. Superimposed comparison between the spectra of native and denatured insulin. The line at 624 cm^{-1} due to the in-plane ring vibration of phenylalanine residues is conformation independent and used as an internal reference. (From Yu, N. T., Liu, C. S., and O'Shea, D. C., *J. Mol. Biol.*, 70, 117, 1972. With permission.)

TABLE 2

Raman Spectra of Insulin (Bovine) (200 to 1800 cm^{-1})

Frequencies (cm^{-1})		
Native (crystals)	Denatured (solid)	Tentative assignments
	265 (0.9)	Skeletal bending
333 (0.9)	325 (0.8)	Skeletal bending
410 (0.8)	420 (0.5)	Skeletal bending
467 (0.8)	460 (0.4)	Skeletal bending
495 (1.2)	480 (0.3)	Skeletal bending
515 (3.2)	513 (4.4)	ν(S–S)
	532 (1.5sh)	Skeletal bending
563 (1.0)		
624 (2.0S)	624 (2.0S)	Phe
644 (3.6S)	644 (3.6S)	Tyr
668 (2.0)	657 (1.1)	ν(C–S) of the C–S–S–C group
678 (1.0sh)	680 (1.3)	ν(C–S) of the C–S–S–C group
725 (0.8T)		Skeletal bending
747 (0.8T)	737 (0.9B)	Skeletal bending
770 (0.8T)		Skeletal bending
814 (1.4sh)		
832 (4.4D)	830 (3.9D)	Tyr
854 (5.5D)	853 (4.5D)	Tyr
900 (2.0)	882 (1.5)	ν(C–C)
934 (2.0sh)	922 (0.8)	ν(C–C)
946 (3.2D)		ν(C–C)
963 (2.9D)	956 (1.6B)	ν(C–C)
1004 (10.0S)	1004 (10.0S)	Phe
	1020 (2.5)	ν(C–N)
1032 (3.3S)	1032 (3.3S)	Phe
	1057 (1.3sh)	ν(C–N)
1112 (1.5sh)		ν(C–N)
1128 (1.8)	1127 (1.7)	ν(C–N)

TABLE 2 (continued)

Raman Spectra of Insulin (Bovine) (200 to 1800 cm^{-1})

Frequencies (cm^{-1})		
Native (crystals)	Denatured (solid)	Tentative assignments
1162 (0.9)	1161 (0.5sh)	ν(C–N)
1177 (2.4)	1175 (2.4)	Tyr
1212 (4.6S)	1214 (4.9)	Tyr and Phe
	1227 (4.3)	Amide III (β-structure)
	1252 (4.0sh)	Amide III (β-structure)
1239 (5.0sh)		Amide III (random-coil)
1270 (5.3)		Amide III (α-helical)
1288 (4.7sh)		Amide III (α-helical)
1322 (2.0sh)	1327 (2.0D)	CH deformation
1344 (4.0)	1343 (3.1D)	CH deformation
1367 (1.6sh)		CH deformation
	1407 (0.4sh)	
1425 (2.5sh)	1422 (1.1sh)	Symmetrical CO_2-stretching
1450 (5.0)	1450 (3.8)	CH_2 deformation
1462 (4.6sh)	1462 (3.1sh)	CH_2 deformation
1587 (1.3)	1587 (1.0sh)	Phe
1607 (3.6D)	1607 (3.5D)	Phe and Tyr
1615 (3.6D)	1615 (3.5D)	Tyr
1662 (4.6)		Amide I (α-helical structure)
	1673 (8.6S)	Amide I (β-structure)
1685 (4.0sh)		Amide I (random-coil)
	1735 (0.4B)	–COOH

Taken from Yu, N. T., Liu, C. S., and O'Shea, D. C., *J. Mol. Biol.*, 70, 117, 1972. With permission.

The Raman lines due to S–S and C–S bonds in cystines and methionines were employed to monitor configurational changes in these residues. The Raman data were found quantitatively consistent with the six-state scheme of unfolding proposed by Burgess and Scheraga.[94]

Polarized Raman Spectra of Oriented Polypeptide Chain Structures

Like infrared dichroism, polarized Raman scattering may be employed to determine whether polypeptide chains are uniquely oriented and, if so, in what direction. It is also possible to utilize Raman data to make quantitative estimates of the orientation angles of certain groups in a helical biopolymer.[95]

Wilser and Fitchen's work[95] on α-helical poly-γ-benzyl-L-glutamate will be presented here to illustrate the principles involved in this polarized Raman technique. Figure 20 shows three scattering geometries; the first two were employed by Wilser and Fitchen. The third geometry may be more convenient for certain biological specimens. A combination of these scattering geometries permits one to determine the following polarization components: (Z,Z), (X,X), (X,Z), (Z,X), (Y,X), (X,Y), (Y,Z), and (Z,Y). The components (Z,Z) and (X,X) are of particular interest because they should be identical for randomly oriented molecules, but quite different in a well-oriented system. This has been demonstrated in the case of α-helical poly-γ-benzyl-L-glutamate (Figure 21). The (Z,Z) and (X,X) spectra in Figure 21 were obtained by the 180° scattering geometry and labeled as $Y(Z,Z)\bar{Y}$ and $Y(X,X)\bar{Y}$, respectively. They may also be obtained by the 90° scattering technique: X(Z,Z)Y and Z(X,X)Y. In the (Z,Z) measurements, the polarization direction of the incident and scattered light is nearly parallel to the C=O and N–H bonds. However, in the (X,X) measurements, both the incident and scattered polarization are perpendicular to the C=O and N–H bonds. Since the induced polarizability change along a bond may be quite different from that perpendicular to the bond, there should be relatively different Raman scattering intensities.[53]

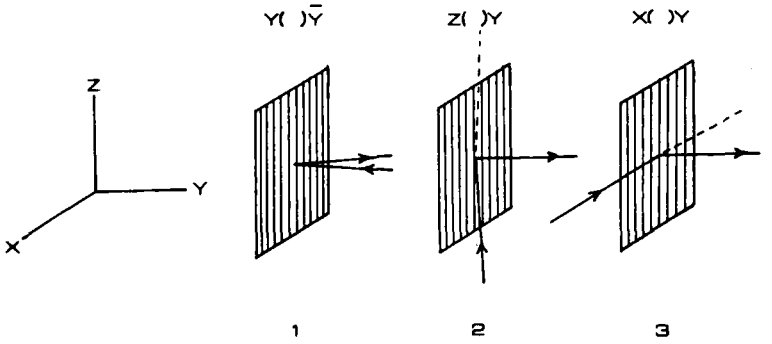

FIGURE 20. Three scattering geometries for oriented polypeptides.

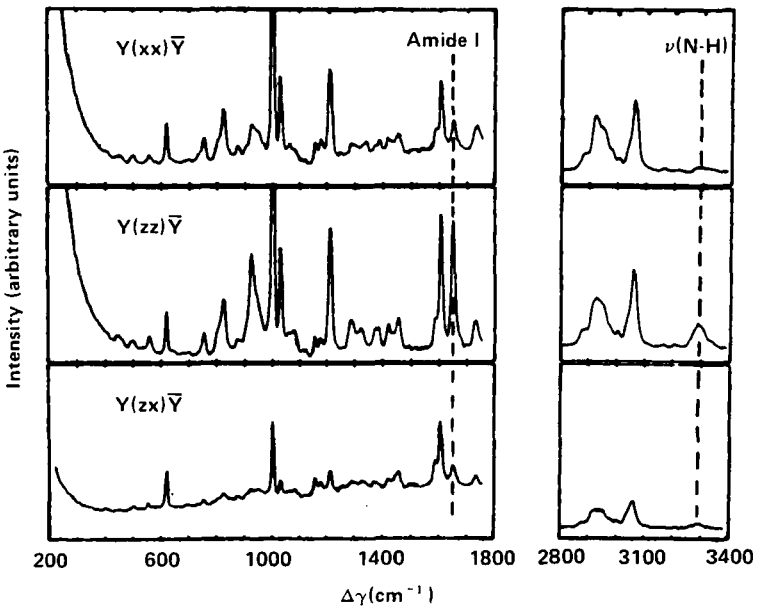

FIGURE 21. Polarized Raman spectra for an oriented film of poly-γ-benzyl-L-glutamate (PBLG) in the backscattering geometry. The intensity scale in the 2800- to 3400-cm^{-1} range is reduced by a factor of 3.6. (From Wilser, W. T. and Fitchen, D. B., *J. Chem. Phys.*, 62, 720, 1975. With permission.)

Figure 21 clearly shows that the amide I (mainly C=O stretching vibration) at 1651 cm^{-1} and the N–H stretching mode at 3290 cm^{-1} are greatly enhanced in the Y(Z,Z)$\bar{Y}$ spectrum relative to the Y(X,X)$\bar{Y}$ spectrum. The intensity ratios for amide I, I(Z,Z)/I(X,X), and N–H stretch were reported[95] as 3.7 ± 0.5, and 10 ± 3, respectively. Detailed analysis of Raman data led to these estimations of orientation angles (ϕ): 39° ± 2° (amide I) and 28° ± 3° (ν(N–H)), in agreement with data obtained by infrared dichroism.[96]

Hsu et al.[53] used the polarized Raman scattering method to help determine assignments in the amide I region of feather keratin. There were two component bands at 1640 and 1670 cm^{-1} in the Raman spectrum of feather keratin. Two Raman spectra were obtained with incident polarization perpendicular and parallel to the quill axis. Presumably, the C=O bonds involved in the β structure were perpendicular to the quill axis. A comparison of the two spectra revealed that the 1640-cm^{-1} component has approximately the same intensity for both polarizations, whereas the 1670-cm^{-1} component had a greater intensity when incident polarization was paralleled to the C=O bond (i.e., perpendicular to the quill axis) than when it was perpendicular to this bond.[53] As a result, the two amide I bands at 1640 and 1670 cm^{-1} were attributed to unordered structure and β sheet, respectively.

RESONANCE RAMAN OF HEMEPROTEINS OXIDATION STATE MARKER AND STRUCTURAL IMPLICATIONS (CORE-EXPANSION MODEL VS. DOMING MECHANISM)

The resonance Raman technique provides a selective structural probe of the prosthetic group of hemeproteins. The vibrational normal modes of the heme can be observed in aqueous solution at high dilution (10^{-3} to 10^{-5} *M*) without interference from the modes of the protein. This was first demonstrated by Strekas and Spiro[97] and by Brunner et al.[6] When excitation occurs in the Q bands region (500 to 600 nm), porphyrin in-plane skeletal modes are greatly enhanced. Vibrations of a bound ligand may be enhanced via resonance with a charge-transfer transition.[98] New information can be extracted from Raman data on heme geometry and on the nature of the excited electronic state via excitation profiles.[99-101]

Earlier investigations of hemeproteins attempted to find structural correlations among different derivatives. Brunner et al.[6] first suggested that the polarized Raman line at ~1370 cm^{-1} could be correlated with the out-of-plane movement of the iron atom because it shifts from 1378 to 1355 cm^{-1} between in-plane oxy- and out-of-plane deoxyhemoglobin. This correlation appears to be incorrect in view of the fact that the line appears at 1375 cm^{-1} in Fe(III) horseradish peroxidase (high-spin, out-of-plane), 1362 cm^{-1} in Fe(II) cytochrome c (low spin, in-plane), and 1376 cm^{-1} in Fe(III) octaethylporphyrin chloride (high-spin, out-of-plane).[100] However, several investigators considered this polarized line at ~1370 cm^{-1} as an oxidation state marker.[102-104] The frequency for ferric hemeproteins (1370 to 1380 cm^{-1}) is normally higher than that for ferrous states (1355 to 1365 cm^{-1}). On the basis of this correlation, it was concluded that oxyhemoglobin contained an Fe(III) (low-spin) O_2^- complex.[102,103] However, the reliability of this correlation was questioned by other investigators.[100,105] Recently, Spiro and Burke[98] studied a variety of mesoporphyrin (IX) complexes; they felt that the porphyrin modes may not be able to tell the oxidation state of the O_2-heme complex. Perhaps the polarized line at ~1370 cm^{-1} indicates the extent of π back donation, but not the total charge on the iron.[98] It should be noted that this line was found to be relatively insensitive for a wide variety of metals (such as VOEtio, ZnOEP, MgOEP, MnOEPCl, CuOEP, and (NiOEP), despite the anticipated large differences in charge density migration from the various metal ions to the porphyrin ring.[100]

Improved interpretations of resonance Raman data require an understanding of the nature of the Raman active normal modes (a_{1g}, a_{2g}, b_{1g}, and b_{2g} under D_{4h} point group). Several investigators[106-109] have undertaken the normal coordinate analysis of model metalloporphyrins. Earlier analysis[110] of metalloporphyrins was confined to infrared active modes, yielding information difficult to correlate with resonance Raman spectra of hemeproteins. Important internal coordinates contributing to the potential energy of normal modes above 1500 cm^{-1} in NiOEP(D_{4h}) are indicated in Table 3. Rimai[109]

TABLE 3

Important Internal Coordinates Contributing to the Potential Energy of Normal Modes above 1500 cm^{-1} in NiOEP D_{4h}

Symmetry	Observed (CH_2Cl_2)	Internal coordinates
b_{1g}	1654	$\nu(C_a-C_m) >> \nu(C_a-C_b) \sim \delta(C_bC_aN) > \nu(C_b-C_b)$
a_{2g}	1603	$\nu(C_a-C_m) >> \nu(C_a-N)$
a_{1g}	1600	$\nu(C_b-C_b) >> \nu(C_a-C_m) \sim \delta(C_bC_aN)$
b_{1g}	1575	$\nu(C_a-N) > \nu(C_a-C_m)$
a_{1g}	1519	$\nu(C_a-N) > \nu(C_a-C_m)$

From Spaulding, L. D., Chang, R. C. C., Yu, N. T., and Felton, R. H., *J. Am. Chem. Soc.*, 97, 2517, 1975. Copyright by the American Chemical Society. With permission.

and Abe et al.[108] have studied atomic displacements for these modes. The a_{2g} vibration at ~1590 cm^{-1} (at 1603 cm^{-1} in NiOEP) is of particular interest because it involves the stretching and contraction of the chemical bonds in the inner 16-membered ring (Figure 22). A vibration of this kind is likely to reflect the properties of the porphinato core. Spaulding et al.[100] found that the *ap* line at ~1590 cm^{-1} in a series of metalloporphyrins with known structures correlated remarkably well with d(Ct-N), the distance between the center of the porphyrin core and the pyrrole nitrogen (Figure 23 and Table 4). This distance is equivalent to the size of the core. An increase in d(Ct-N) corresponds to a decrease in the a_{2g} frequency. Changes in the force constants of the C_a–C_m and C_a–N bonds associated with the core expansion are probably responsible for the observed frequency shifts.[100]

This "core expansion" correlation indicates that assessment of the out-of-plane displacement of the metal is possible if the metal-to-pyrrole nitrogen distance, d(M–N), can be estimated. In oxyhemoglobin, d(Fe–N) = 2.00Å in a low-spin iron(II) complex. The anomalously polarized line of oxyhemoglobin[103] appears at 1585 cm^{-1}, implying a d(Ct-N) distance of ~2.00Å. It is therefore concluded that oxyhemoglobin contains in-plane iron (a well-known fact). The assessment of iron displacement in deoxyhemoglobin is of more interest. The out-of-plane displacement of the high-spin Fe(II) was estimated[100] at about 0.40Å, which is considerably smaller than Perutz's[111] estimate of 0.75Å. It is interesting to note that recent refinement of the X-ray diffraction data from deoxyhemoglobin crystals[112] has reduced his estimate to 0.60Å. Eicher et

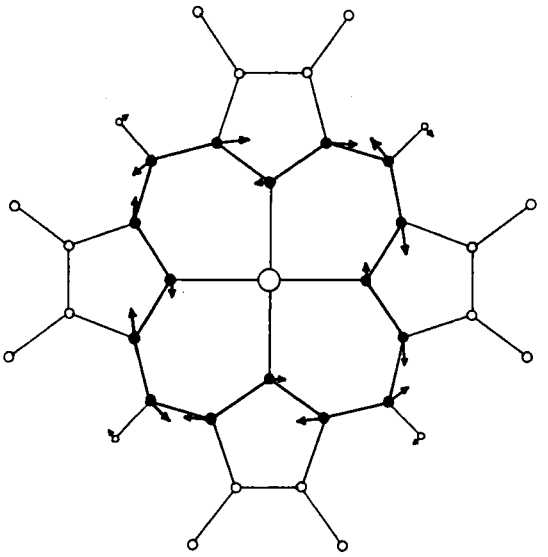

FIGURE 22. Atomic displacement of the a_{2g} normal mode at ~1590 cm^{-1} in a metalloporphyrin (D_{4h}). (From Rimai, L., unpublished results.)

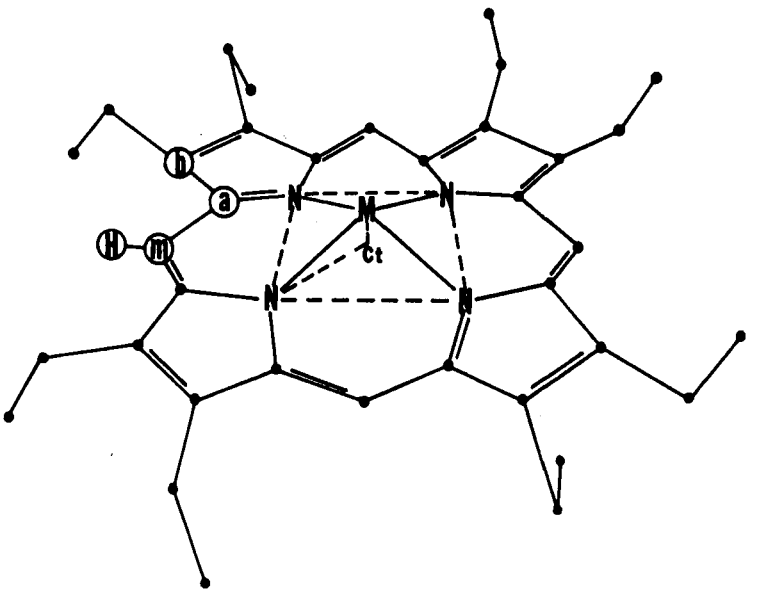

FIGURE 23. Labelling scheme for porphinato moiety. (From Spaulding, L. D., Chang, R. C. C., Yu., N. T., and Felton, R. H., *J. Am. Chem. Soc.*, 97, 2517, 1975. Copyright by the American Chemical Society. With permission.)

TABLE 4

Correlation of the Anomalously Polarized Frequency with Ct–N Distance

Compound	$\bar{\nu}$, cm^{-1}	Ct–N, Å	Structure
$SnOEPCl_2$	1545	2.082 (2)	$SnOEPCl_2$
AgOEP	1550	~2.08	AgTPP
MgOEP	1558	2.055 (6)	$MgTPP(H_20)$
ZnOEP	1565	2.047 (2)	PyZnTPyP
RhEtio $(DMA)_2Cl$	1578	2.038 (6)	RhEtio $(DMA)_2Cl$
$(FeOEP)_2O$	1570	2.027	$(FeTPP)_2O$
FeOEPCl	1568	2.019 (3)	Average hemin
FeProtoDMECl	1575	2.007 (5)	FeProtoCl
VOEtio	1574	2.01 (4)	VODPEP
PdOEP	1585	2.009 (9)	PdTPP
$Fe^{II}Etio(Py)_2$	1587	2.004 (4)	$Fe^{II}TPP(Im)_2$
CuOEP	1585	2.000 (5)	CuTPrP
$Fe^{III}OEP(Im)_2Cl$	1590	1.989 (5)	$Fe^{III}TPP(Im)_2Cl$
FeOEP(NO)	1593	1.990	FeTPP(NO)
MnOEPCl	1591	1.99	MnTPPCl
CuOEP	1605	1.981 (7)	CuTPP
CoOEP(NO)	1605	1.976 (3)	CoTPP(NO)
NiOEP (D_{4h})	1609	1.958 (2)	NiOEP
NiOEP (D_{2d})	1590	1.929 (3)	NiOEP

Note: (Py) pyridine, (Im) imidazole, (TPyP) tetra (4-pyridyl)porphinato, (DMA) dimethylamine, (Proto) protoporphyrin IX,(DPDP) deoxyphylloerythroetioporphinato, (TPrP) tetra (*n*-propyl)porphinato, (DME) dimethoxy ester.

al.'s[113] estimate of 0.5 ± 0.1 Å for the Fe(II) out-of-plane displacement in deoxyHb on the basis of Mossbauer experiments agrees well with the estimate obtained from the resonance Raman method.

Earlier Spiro and Strekas[103] had labeled the *ap* line at ~1590 cm^{-1} as a spin state marker. Conversion of iron from low to high spin without change in oxidation state causes this *ap* line to shift to a lower wave number. They suggested that "doming" of the porphyrin ring accompanying out-of-plane displacement of the iron is responsible for the observed shifts. However, normal coordinate calculations on domed octamethylporphyrin cannot produce large frequency shift without simultaneously adjusting the bond stretching force constants. Since adjustments of the bond force constants imply changes in bond lengths and thus the size of the porphyrin core, the "doming" model of Stein et al.[106] is not completely incompatible with the "core expansion" mechanism of Spaulding et al.[100] It should be noted that there is no clear evidence that heme structure is considerably "domed" in deoxyhemoglobin or other high-spin hemeproteins.

The structural implication of the two interpretations differs when the anomalously polarized line is lower than ~1580 cm^{-1}. At pH 7, native horseradish peroxidase has an *ap* line at 1576 cm^{-1} (Figure 24); the "doming" model would predict a more planar porphyrin core and smaller out-of-plane iron displacement to the native enzyme than horseradish peroxidase fluoride with the *ap* line at 1555 cm^{-1}. However, the 1576-cm^{-1} value is characteristic of model high-spin ferric complexes, e.g., Fe(III)OEPCl; the "core expansion" correlation suggested[100] the metal displacement was ~0.5Å, which is greater than that for horseradish peroxidase fluoride. A lower *ap* line frequency (1555 vs. 1576 cm^{-1}) means a larger d(Ct-N) value for the fluoride complex and, since d(Fe-N) is presumably invariant in the two high-spin complexes, there is a smaller Ct-Fe distance in horseradish peroxide fluoride.

A comparative resonance Raman study of

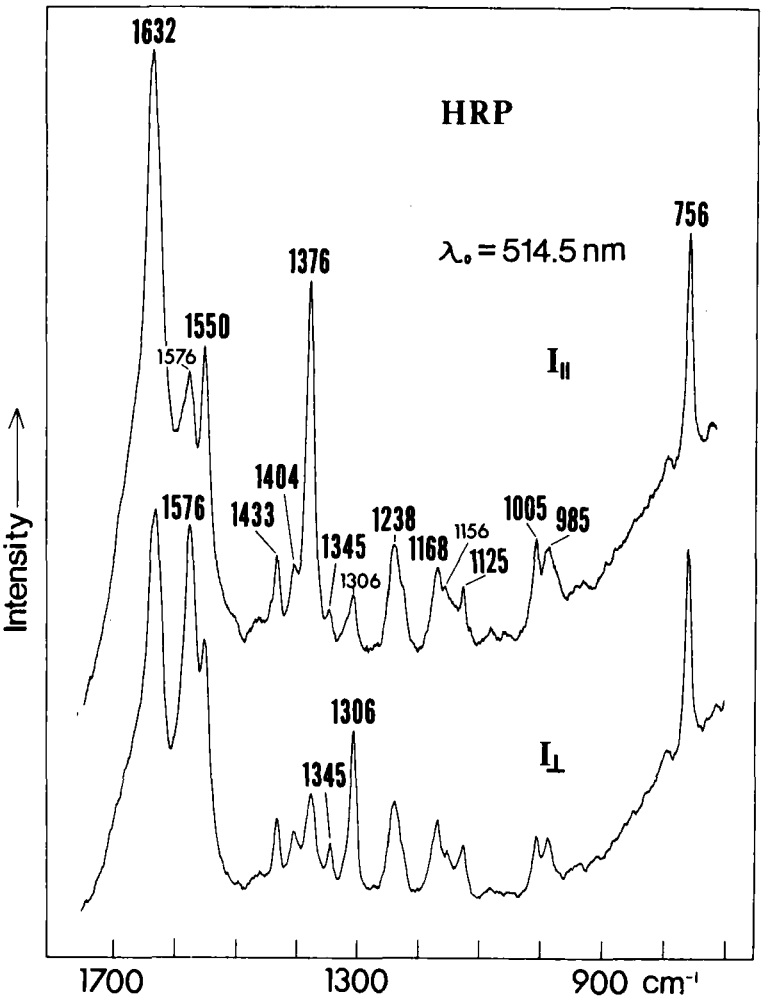

FIGURE 24. Resonance Raman spectra of horseradish peroxidase solution. (From Felton, R. H., Romans, A. Y., Yu, N. T., and Schonbaum, G. R., *Biochim. Biophys. Acta*, 434, 82, 1976. With permission.)

oxidized hydroperoxidases (horseradish peroxidase, horse blood catalase, and cytochrome c peroxidase) was performed by Felton et al.[114] In compound II of horseradish peroxidase and horse blood catalase and in the enzyme-substrate complex of cytochrome c peroxidase, the *ap* line appears at 1587 to 1590 cm^{-1}, indicating in-plane iron. This conclusion is consistent with both the "core expansion" correlation and Spiro's "doming" model. Movement of the iron atom into the porphyrin plane in the oxidized enzymes is consistent with but not proof of a six-coordinate metal. The functional consequences of iron movement are not obvious. However, it is conceivable that d_π-p_π interactions between metal and porphyrin in compound II of hydroperoxidases are enhanced by the in-plane metal, with resultant facilitation of electron transfer to the iron via the porphyrin ring. Additionally, weak Raman scattering[114] found in horseradish peroxidase I is consistent with a porphyrin π-cation radical formulation.

RESONANCE RAMAN OF ENZYME/SUBSTRATE AND ENZYME/INHIBITOR INTERACTIONS

Carey and Schneider[115,116] and Carey et al.[117] performed prototype experiments utilizing the resonance Raman labelling technique to study the catalytic mechanisms of enzymes. A chromophoric substrate, 4-amino-3-nitrocinnamic acid methyl ester, was introduced into the active site of α-chymotrypsin to form a stable acylenzyme at pH 3.0. They were able to obtain resonance Raman

spectra of protein-bound substrate without interference from protein Raman spectra (nonresonance) in the concentration range 10^{-4} to 10^{-5} *M*. The Raman line at 1625 cm^{-1}, assigned to the –C=C– stretch in the acryloyl residue, was used to monitor changes at the catalytic site (near the ester linkage). As pH was raised to values between 5.7 and 7.0 (at which the acyl enzyme became active), a large intensity reduction (by ~65%) at 1625 cm^{-1} was observed during the mixing and observation period of 10 to 15 sec. Supporting data from deacylation kinetics indicates that the spectral change preceded and was independent of the rate-determining step in deacylation. Although they proposed three possible explanations of the intensity reduction (at 1625 cm^{-1}), Carey and Schneider felt that substrate geometric deformation seemed most likely.[116]

Evidence of substrate reorganization in the active site of papain[117] was recently obtained by means of resonance Raman spectroscopy. The chromophoric substrate methyl-4-dimethylamino-3-nitro-(α-benzamido)-cinnamate (see Figure 25 for chemical structure) was used to form an acyl-enzyme intermediate linking the thiol group pf papain with the acyl residue of the substrate. Upon binding with papain, the absorption band of the substrate at 350 nm is considerably red-shifted to 412 nm. Resonance Raman spectra of the acyl enzyme and the free substrate obtained with 441.6-nm excitation are shown in Figure 26. The acyl-enzyme spectrum differs mainly in the absence of the intense 1636-, 1611-, and 1353-cm^{-1} lines and the presence of a new strong feature at 1570 cm^{-1}. On the basis of accumulated spectral data and arguments, Carey et al.[117] were able to propose a plausible chemical structure (Figure 25) for the substrate in the acyl-enzyme intermediate.

Resonance Raman studies of enzyme inhibitor interactions were recently reported by Kumar et al.[118] Resonance Raman spectra of 4-sulfonamido-4′-dimethylaminoazobenzene, 4-sulfonamido-4′-hydroxyazobenzene, and 4-sulfonamido-4′-aminoazobenzene bound to various isoenzymes of carbonic anhydrase were obtained by exciting into the sulfonamide absorption bands in the 400- to 500-nm region. A new Raman line appeared in the spectra of the enzyme inhibitor complexes and was interpreted in terms of a change in geometry near the sulfonamido sulfur atom. It was suggested

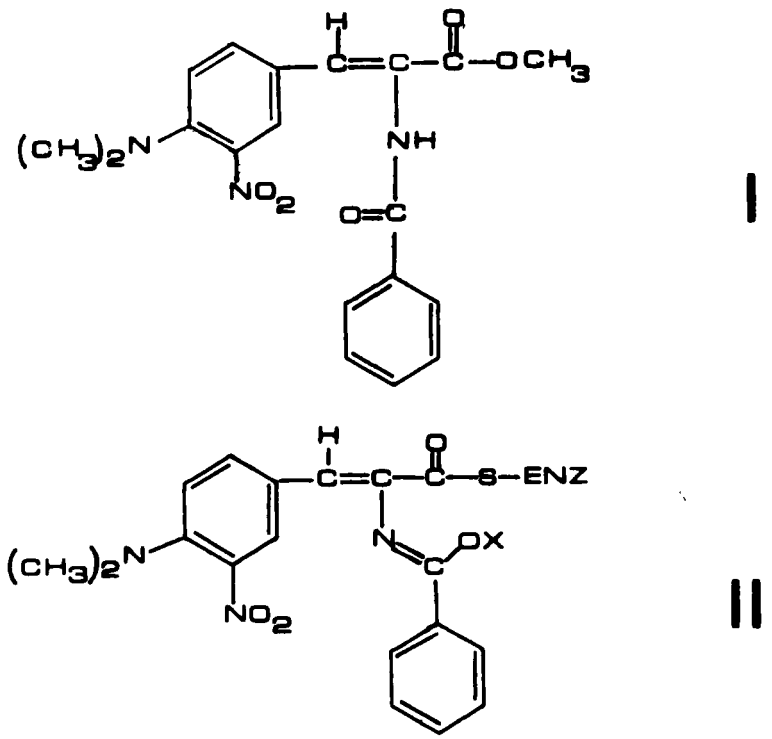

FIGURE 25. Chemical structures of the papain substrate and its acyl intermediate.

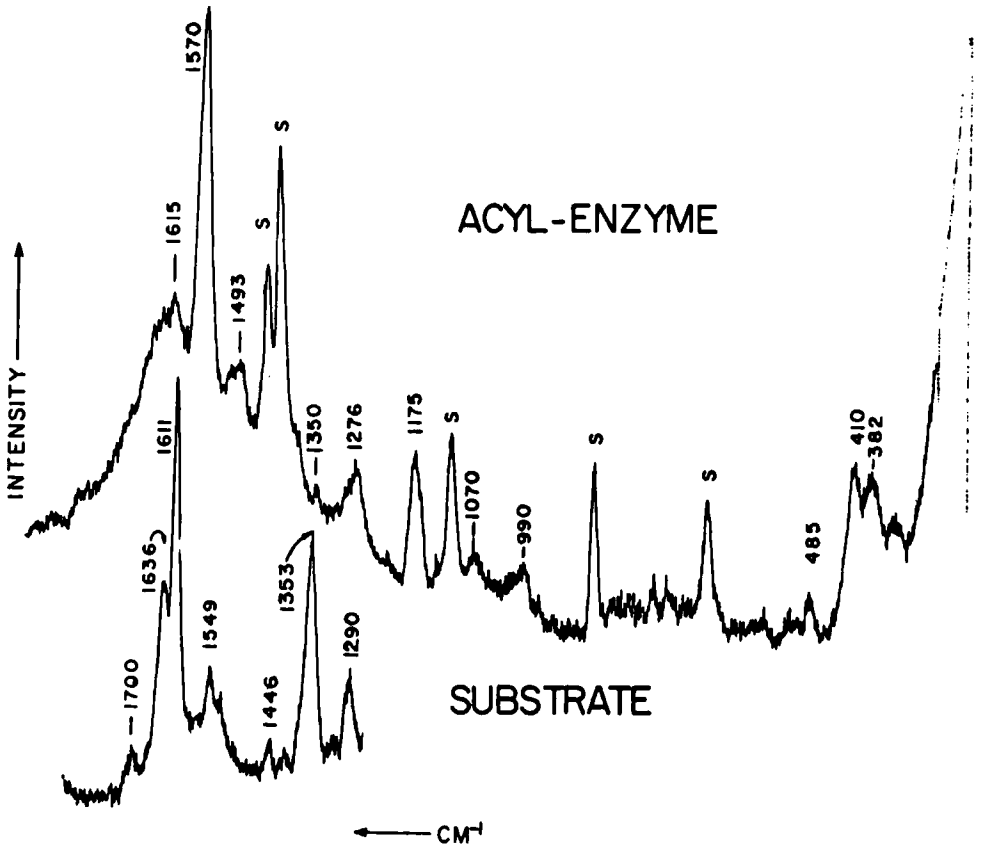

FIGURE 26. Resonance Raman spectra of 4-dimethylamino-3-nitro (α-benzamido) cinnamoyl-papain (commercial crystallized): intermediate (top) and the substrate (α BA) alone (bottom). The substrate spectrum below 1290 cm^{-1} contains only weak features which are obscured by solvent bands. S = solvent bands, resulting from dimethylformamide moving with the acyl enzyme during chromatography. (From Carey, P. R., Carriere, R. G., Lynn, K. R., and Schneider, H., *Biochemistry*, 15, 2387, 1976. Copyright by the American Chemical Society. With permission.)

that the bound sulfonamide group closely mimics the transition state of the reactants in the reversible hydration of CO_2.

RHODOPSIN AND BACTERIORHODOPSIN

Vertebrate rhodopsin is a protein molecule responsible for light energy reception in the retinal rod cells. Its prosthetic group (11-*cis*-retinal) is attached to the protein (opsin) by a Schiff-base linkage. Upon absorption of a photon, 11-*cis*-retinal is rapidly converted to all *trans*-retinal following a series of conformational changes, resulting in the hydrolysis of the Schiff-base linkage.[119] The intermediates in the bleaching sequence have been identified as prelumirhodopsin (or bathorhodopsin; 543 nm), lumirhodopsin (497 nm), metarhodopsin I (480 nm), and metarhodopsin II (380 nm).

Rhodopsin-like protein is also found in halophilic bacteria (e.g., *Halobacterium halobium* or *H. cutirubrum*), but it apparently has a different biological role in these organisms. The bacteriorhodopsin enables the cells to utilize photon energy to generate a proton gradient across the membrane, providing for ATP synthesis.[120] The nature of the opsin binding site in bacteriorhodopsin is different from that in vertebrate rhodopsin. The latter accommodates 11-*cis*, 9-*cis*, and 9,13-di-*cis* isomers,[121] while the former accommodates 13-*cis* and all *trans*-retinal isomers.[122]

Although a great deal is known about the visible and near ultraviolet spectroscopic properties of rhodopsin and related compounds and their photochemistry, little is understood about the conformation of retinal chromophores in the opsin matrix and the retinal-opsin interactions responsible for the bathochromic shift in the absorption spectra. Resonance Raman spectros-

copy appears to be capable of yielding important information pertaining to the *in situ* conformation of retinal.

Resonance Raman spectra of unphotolyzed bovine rhodopsin and isorhodopsin (containing 9-*cis*-retinal) were recently studied[33,34] and are shown in Figure 27. These spectra were obtained by a jet-stream flow technique to avoid photoisomerization. The rhodopsin spectrum reported earlier by Lewis et al.[123] (using a stationary sample) probably represents a partially modified sample. The spectra of 11-*cis*, 9-*cis*, 13-*cis*, and all *trans*-retinal in carbon tetrachloride solution and in a crystalline state have been reported.[34,124,125] The general conclusion is that frequencies and intensities of Raman lines due to skeletal vibrations are sensitive to conformation in the so-called fingerprint region (900 to 1450 cm^{-1}). Specific structural information is difficult to extract at present because these modes are highly mixed (C–C stretching, C–H bending, C–H out-of-plane bending, etc.) and no information is available on the potential energy distribution of each mode among various internal coordinates.

The question of whether Schiff base nitrogen is protonated is important to theories concerned with the origin of bathochromic shift.[126,127] Researchers generally agree that retinal and opsin are joined by a protonated Schiff base in both rhodopsin and bacteriorhodopsin.[33,34,123,128] The assignments of the lines at 1654 and 1622 cm^{-1} to ν(C=N) in the protonated and unprotonated form, respectively, seem convincing. Earlier, Mendelsohn[129] incorrectly identified the –C=N– stretching mode at 1622 cm^{-1} in *H. halobium* bacteriorhodopsin (λ_{max} = 570 nm). Lewis et al.[130] clearly showed that the 1622-cm^{-1} line was due to the 412-nm intermediate (converted from the 570-nm complex by laser light) present in Mendelsohn's sample.

In principle, there are at least four C=C stretching modes in 11-*cis*-retinal,[131] but in practice only a very strong line is observed in rhodopsin (1545 cm^{-1}) and 11-*cis*-retinal (1582 cm^{-1}). This presumably corresponds to the C=C stretching mode with the largest Franck-Condon overlap.

Since the ν(C=C) mode is strongly polarized ($0 < \rho < 0.3$), the scattering intensity should be derived from Albrecht's A term, as is the case in β-carotene.[132] It was found that an inverse linear correlation exists between the ν(C=C) frequency and the position of the absorption maximum of a particular species. A plot of λ_{max} vs. ν(C=C) in retinal-containing proteins is shown in Figure 28.

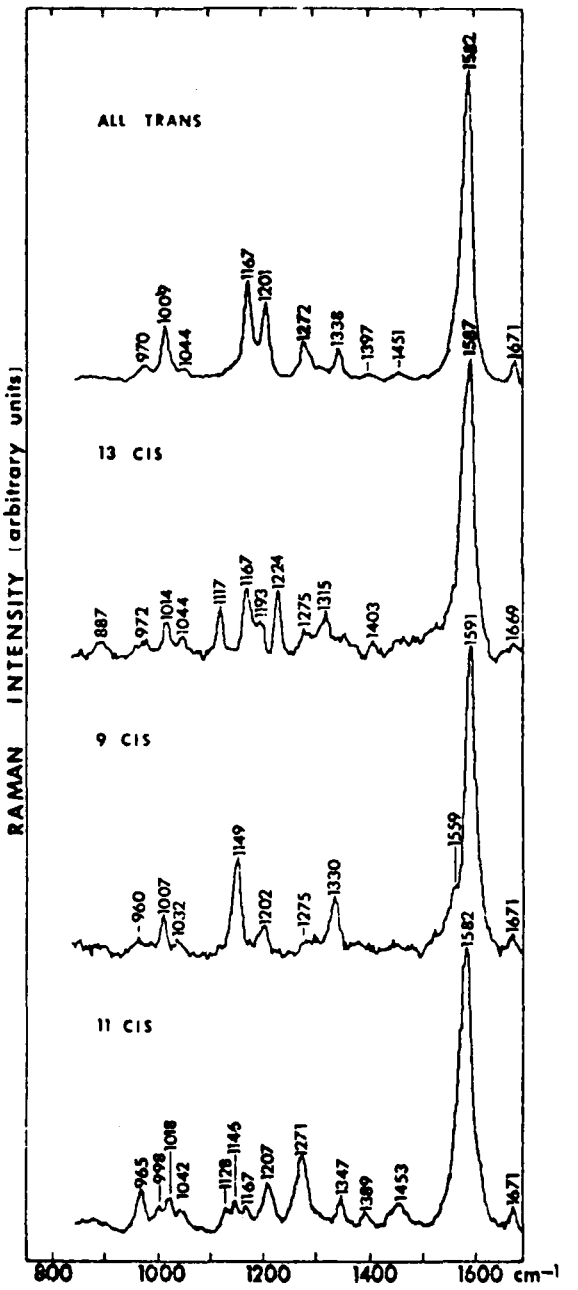

FIGURE 27. Resonance Raman spectra of bovine rhodopsin and isorhodopsin taken with 568.2-nm laser irradiation at a resolution of 10 cm^{-1}. The spectra of 11-*cis*-and 9-*cis*-retinal in CCl_4 solution are shown for comparison purposes. (From Callender, R. H., Doukas, A., Crouch, R., and Nakanishi, K., *Biochemistry*, 15, 1621, 1976. Copyright by the American Chemical Society. With permission.)

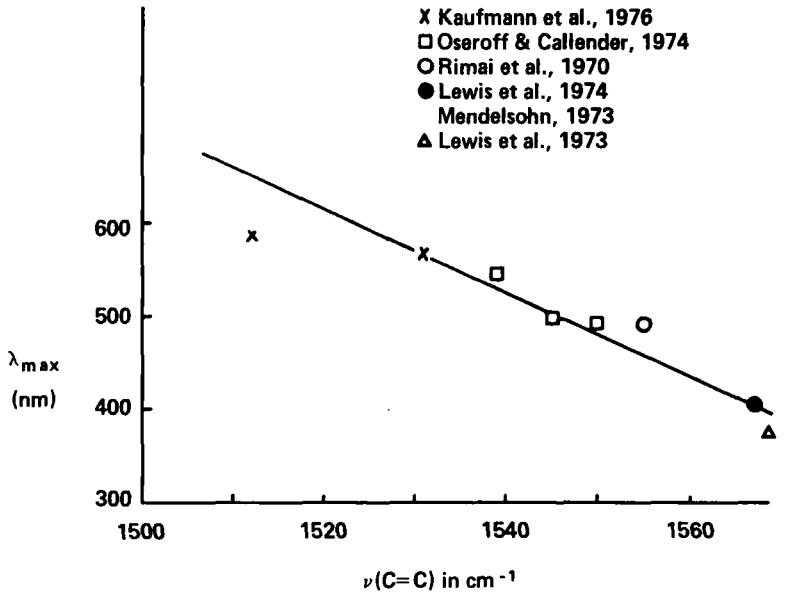

FIGURE 28. Inverse linear correlation between λ_{max} and ν(C=C) in retinal-containing proteins.

This correlation can be understood by considering that bathochromic shift is caused by an increased delocalization of the electrons of the polyene chain, which decreases the force constants of the C=C bonds.[34] This correlation is not expected to hold for cyclic polyene models.

Some theories claim that the position of a negative charge on the protein controls the bathochromic shifts of rhodopsin formation. A molecular orbital study, based on the Pariser-Parr-Pople method, was recently carried out by Waleh and Ingraham.[126] The results show that when the charge is moved closer to the protonated Schiff base, the λ_{max} shows a blue shift to 440 nm; a red shift to about 556 nm is obtained when the charge is moved to the opposite end of the molecule. However, based on studies of resonance Raman spectrum of partially photolyzed rhodopsin, Lewis et al.[123] proposed that the bathochromic shift was caused by the intimate contact between the π orbitals of aromatic rings and the π orbital of 11-*cis*-retinylidenelysine. The mechanism of this π-electron delocalization is not clear. The validity of their assignments of Raman lines between 600 and 840 cm^{-1} to Phe, Tyr, and Trp is now in doubt. These low-frequency aromatic ring vibrations have not been observed in bacteriorhodopsin (bR_{560}) with excitation in the visible absorption of the retinal chromophore.[133-134]

Normal Coordinate Analysis of Polyene Chains

Resonance Raman spectra of polyene molecules display strong lines at 1540 cm^{-1} (ν_1) and 1100 cm^{-1} (ν_2); this is largely caused by C=C and C–C stretching vibrations. To explain chain-length dependence and the effect of deuteration, Inagaki et al.[135] carried out detailed normal mode calculations using poly (acetylene) and β-carotene as models.

In the case of β-carotene, the ν_1 and ν_2 modes contain appreciable C–H bending motion. The atomic displacements of these two modes and the one at ~1290 cm^{-1} are shown in Figure 29. Since the excited state equilibrium conformation in the $\pi \rightarrow \pi^*$ transition is distorted along the ν_1 and ν_2 normal coordinates, Hirakawa and Tsuboi's rule predict that these two modes should be strongly resonance enhanced. On the other hand, the normal mode at ~1291 cm^{-1} is nearly orthogonal to the direction of geometry change and thus is not expected to be resonance enhanced, since the product of overlap integrals of Albrecht's A term vanishes. Hirakawa and Tsuboi's rule is only valid when the Raman lines are polarized and derive resonance Raman intensities primarily from the A term, as is the case in the ν_1 and ν_2 vibrations of β-carotene.[132]

Nonresonance Raman of Opsin Membranes

When excitation occurs in the visible region, Raman spectra of intact photoreceptor membranes are dominated by the resonance-enhanced Raman signals from the retinylidene chromophore. Recently, Rothschild et al.[136] were able to

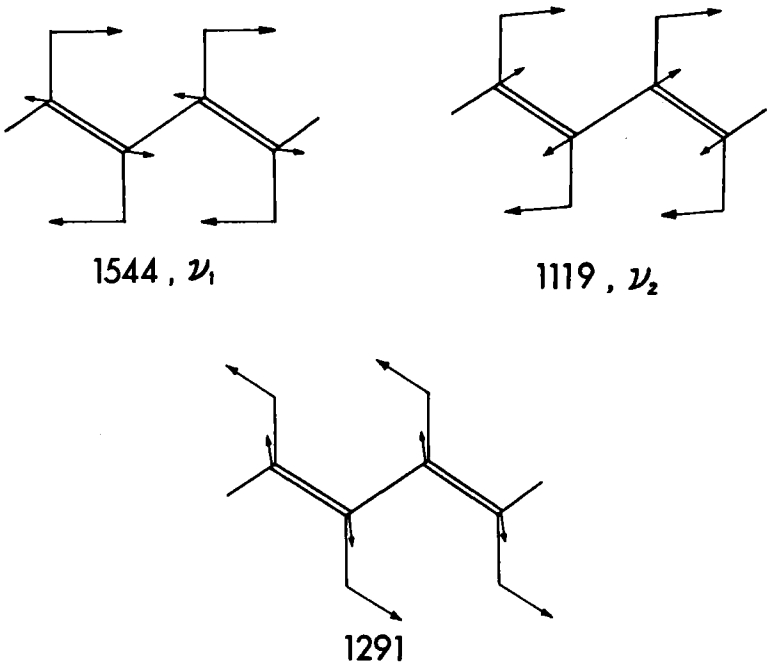

FIGURE 29. Atomic displacement of the normal modes at 1544, 1119, and 1291 cm^{-1} in a linear polyene chain. (Adapted from Inagaki, F., Tasumi, M., and Miyazawa, T., *J. Raman Spectrosc.*, 3, 335, 1975.)

observe relatively weak normal Raman scattering from opsin membranes after removal of the chromophore.

The major conclusions drawn from their studies are:

1. The protein opsin contains large fractions of α-helical form, but little β structure. This is consistent with X-ray diffraction data about purple membrane, which indicates that seven closely packed α-helical segments are perpendicular to the plane of the membrane.[137]
2. The intensity ratio of the tyrosine doublet at 850 and 831 cm^{-1} suggests that some "buried" tyrosines are involved in strong H-bonding.
3. The two disulfide bonds do not have the usual gauche-gauche-gauche configuration.
4. The relative intensities at 1082 cm^{-1} (gauche) and 1068 cm^{-1} (trans) indicate that the membrane lipids are in a fluid state at room temperature.

CONFORMATIONAL STUDIES OF NUCLEIC ACIDS AND VIRUSES

Sugar-phosphate Backbone Conformation

Raman spectra of nucleic acids contain information about the conformation of the backbone chain. Erfurth et al.[138] first showed that the sugar-phosphate vibrations in the 750- to 850-cm^{-1} region are sensitive to the conformation of DNA. Raman spectra of DNA fibers prepared in the A, B, and C forms are reproduced in Figures 30 and 31.

Earlier, Yu[139] observed a similar line at 814 cm^{-1} in the spectra of polyriboadenylic acid (poly A) and assigned it to the symmetric –O–P–O– diester stretch on the basis of normal coordinate calculations of dimethyl phosphate by Shimanouchi et al.[140] However, recent normal coordinate studies by Brown and Peticolas[141] indicated that this diester stretch is coupled to vibrations of the ribose ring. Thus the sugar-phosphate backbone vibration of interest involves the $-C_3'-C_4'-C_5'-O-P-O-C_3-C_4-C_5-$ group along the chain. They claim that the frequency shift from 807 cm^{-1} (A-DNA) to 787 cm^{-1} (B-DNA) is caused by a change in ribose conformation from C_3'-endo (A-form) to C_3'-exo (B-form). Therefore, the 814-cm^{-1} line is characteristic of the A form of RNA. The corresponding line in the spectrum of C-DNA may have overlapped with the ring modes of cytosine and thymine at 784 cm^{-1}. The weak Raman line at ~835 cm^{-1} in both the A- and B-forms of DNA

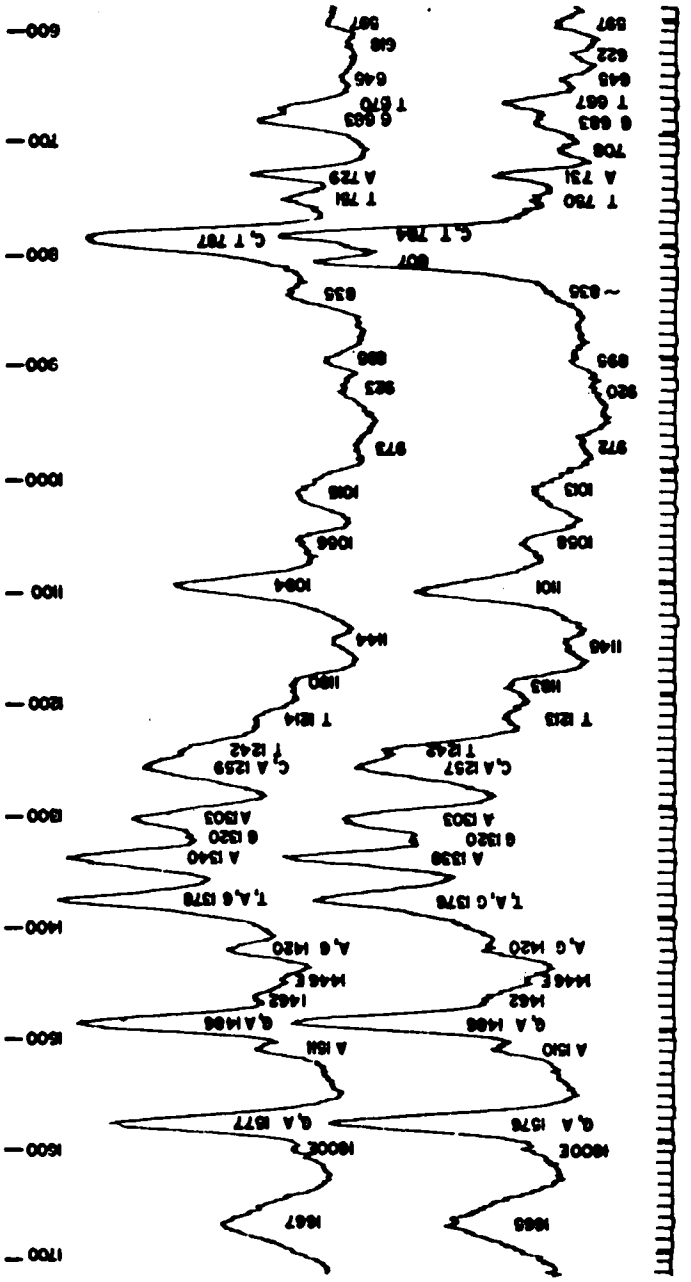

FIGURE 30. Raman Spectra of a fiber of the sodium salt of calf thymus DNA at 98 (upper) and 75% (lower) relative humidity; the spectra are completely reversible with changing humidity. (From Erfurth, S. C., Kiser, E. J., and Peticolas, W. L., *Proc. Natl. Acad. Sci. U.S.A.*, 69, 938, 1972.)

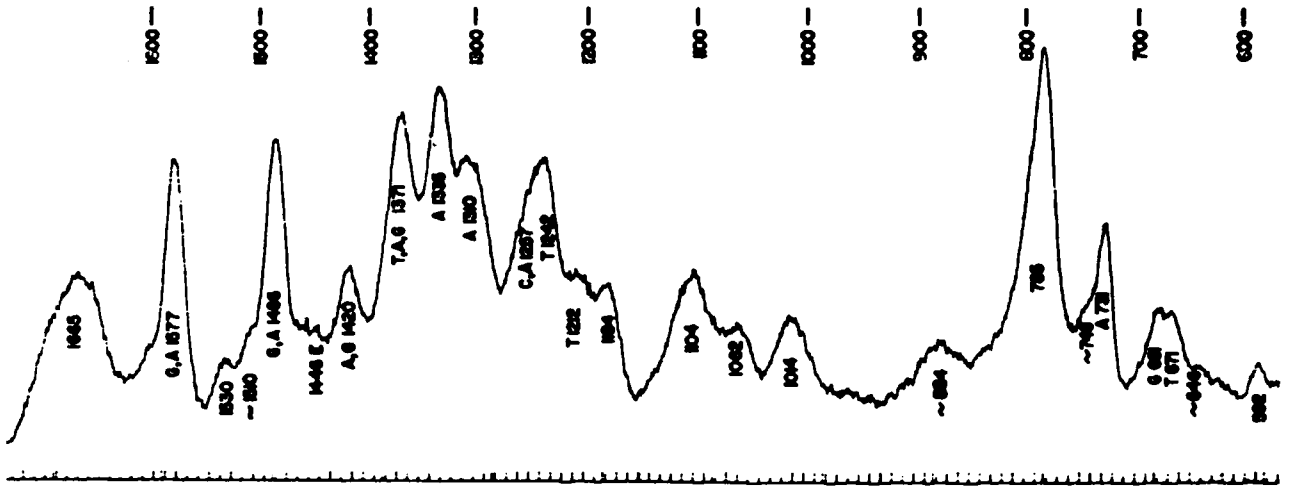

FIGURE 31. Raman spectrum of a fiber of the lithium salt of calf thymus DNA at 32% relative humidity. (From Erfurth, S. C., Kiser, E. J., and Peticolas, W. L., *Proc. Natl. Acad. Sci. U.S.A.*, 69, 938, 1972.)

was assigned[141] to the anti-symmetric diester –O–P–O– stretch.

Symmetric PO_2^- dioxy stretch[138,139,142] appears at ~1100 cm^{-1}; its intensity is independent of conformation and has been used as an internal standard. Thomas and Hartman[143] have used the intensity ratio, I(814)/I(1100), as a measure of order in RNA. The PO_2^--dioxy stretching frequency is slightly sensitive to conformation and dehydration.[138] It appears at 1101 cm^{-1} in A-DNA and at 1094 cm^{-1} in B-DNA and shifts to 1109 cm^{-1} upon extensive drying over P_2O_5.

Base-Pairing and Base-Stacking Interactions: Raman Hypo- and Hyperchromism

The intense lines of the Raman spectra of polynucleotides and nucleic acids are due to the in-plane vibrations of the purine and pyrimidine bases. The Raman intensities (nonresonance) of these ring modes are sensitive to base-pairing and base-stacking interactions. However, the effects of these two types of interactions are difficult to separate.

To illustrate the spectra changes associated with the formation of a double helix, Raman spectra of poly A·poly U at 32 and 85°C are compared in Figure 32. Several lines caused by the ring vibrations of A or U undergo large intensity decreases with helix formation, particularly the uracil line at 1231 cm^{-1} (Raman hypochromism).[144] On the other hand, certain lines (e.g., 1490 and 1570 cm^{-1}) gain intensities following complex formation (Raman hyperchromism). Hyperchromicity is also observed for a guanine ring mode at 670 cm^{-1} (Figure 33). Pezolet et al.[145] showed that Raman and UV hypochromisms are related. They claimed that the Raman lines of adenine which decreased in intensity upon base stacking derived their intensities from the UV absorption band at 2600 Å, while the uracil line at 1231 cm^{-1} derived its intensity from the hypochromic UV band at 2050 Å.

Studies of the melting behavior of nucleic acids by Raman spectroscopy[146] provide more specific information than UV absorption, since the events in each base or sugar-phosphate backbone can be separately monitored. Figure 33 shows Raman spectra of $tRNA^{Phe}$ recorded at 25 and 60°C. The thermal transition curves monitored by the line at 670 (guanine), 725 (adenine), 785 (cytosine and uracil), and 814 cm^{-1} (backbone chain) are presented in Figure 34. The vibrations specific for adenine indicate a slightly lower melting temperature, while those specific for guanine have a slightly higher melting temperature than that of the ribophosphate backbone.[146]

Viruses

The first successful attempt to utilize Raman spectroscopy to determine structural features of intact viruses was made by Hartman et al.[147] They compared Raman spectra of the RNA viruses R17 (a bacteriophage) and protein-free RNA in solution. They observed Raman lines due to vibrations of both RNA and protein capsomers. The reduction in intensity at 1480 cm^{-1} (~70% contribution from G base) while changing from protein-free RNA to phage RNA was interpreted as reflecting a change in RNA secondary structure imposed by the viral proteins.

Ideally, one hopes to investigate the structural parameters such as the percent of AU (or AT) and GC base pairing in the double-stranded regions; the percent of each RNA or DNA base in the single-stranded regions which exhibit base stacking; the percent of sugar-phosphate groups which exist in an ordered configuration; the conformation of the ribose-phosphate linkages (A-, B-, or C-form), the fraction of the total bases which are in double stranded regions; and the relative amounts of α-helix, β-pleated sheet, and unordered configuration in the intact capsomer protein. However, these data are not often obtainable from the nonresonance Raman spectra because of the serious line overlapping. Selective enhancement of vibrations due to protein or nucleic acid may be obtained by resonance Raman spectroscopy using UV lasers, but no such studies have been reported so far.

Recently, Thomas and Murphy[148] selected a good model system for nonresonance Raman studies of viruses. Filamentous bacterial Pfl and fd viruses consist of linear assemblies of coat protein subunits encapsulating single-stranded, circular DNA.[149] The virions contain more than 88% (by weight) protein; thus, Raman spectra display predominant lines due to protein vibrations (Figure 35). The major coat protein in these two strains has a molecular weight of about 5000 and is largely α helical, according to Chou and Fasman.[150] The only two regions of four or more residues with average P_α less than 1.00 are residues 1 to 6 and 22 to 25 for Pfl and residues 1 to 5 and

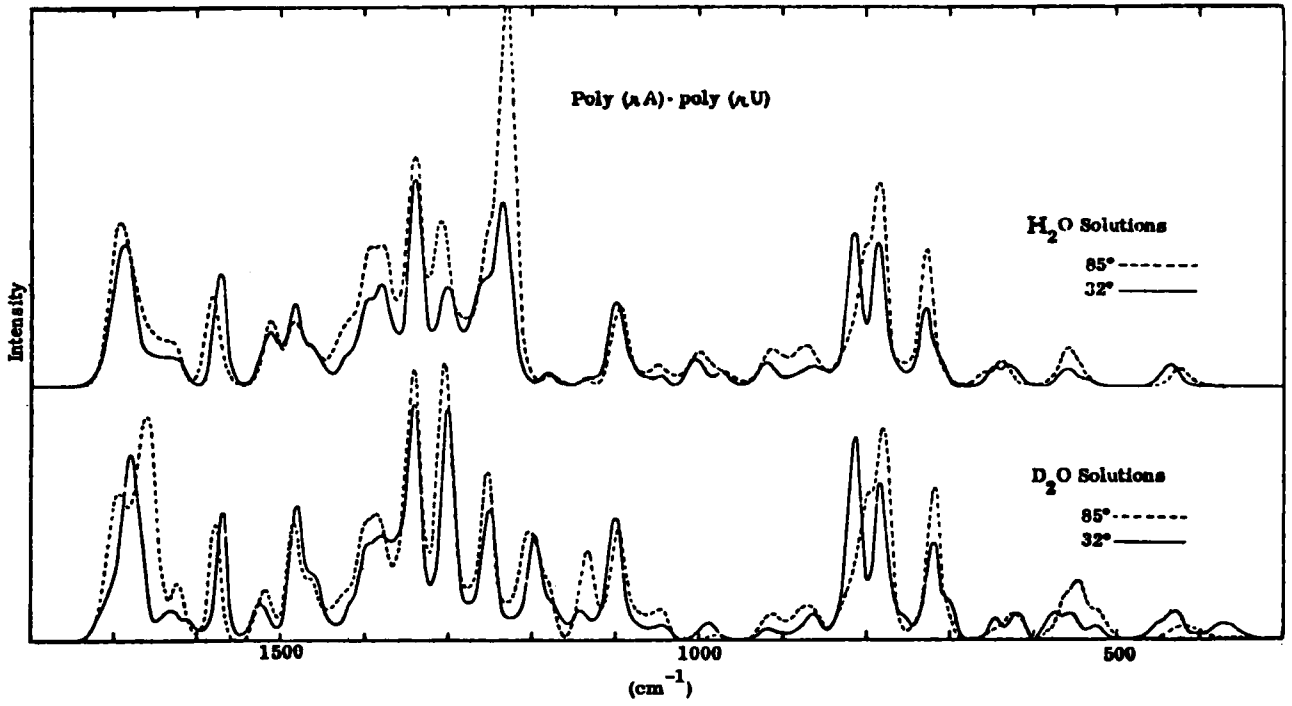

FIGURE 32. Raman spectra of H_2O and D_2O solutions of poly (rA) poly (rU) at 32 and 85°C. (From Lafleur, L., Rice, J., and Thomas, G. J., Jr., *Biopolymers*, 11, 2423, 1972. With permission.)

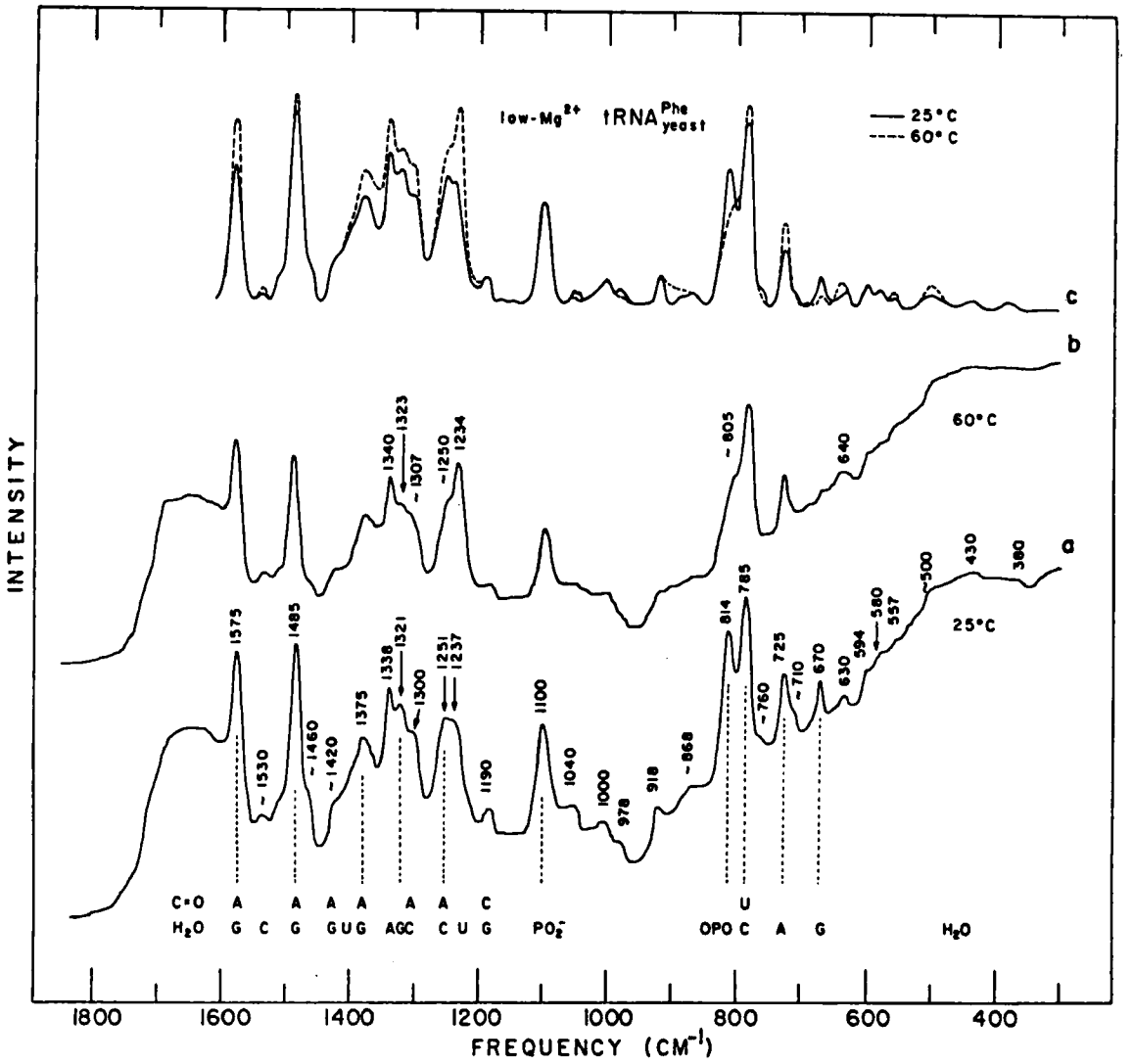

FIGURE 33. Original recording of Raman spectra of low Mg^{2+}-RNA^{Phe} : (a) 25°, (b) 60°, (c) superposition of spectra a and b after correction for the water background and normalization to give the same intensity at 1100 cm^{-1}. (From Chen, M. C., Giege, R., Lord, R. C., and Rich, A., *Biochemistry*, 14, 4385, 1975. Copyright by the American Chemical Society. With permission.)

21 to 24 for fd. The prevalence of α helix in the intact capsomer proteins is reflected in the spectral features of the amide I and III regions, which are very similar to those of α-helical δ-crystallin in intact chick lens (Figure 17). An indication of α helix also appears at 945 and 527 cm^{-1}, corresponding to 940 and 524 cm^{-1} in δ-crystallin. Circular dichroism measurements of Pfl and fd show that more than 90% of the residues in the coat protein are in the α-helix conformation.[151] In addition to strong protein lines, weak Raman scattering from DNA is also seen in Figure 35. The pyrimidine line at 785 cm^{-1} is clearly identified. Normally, A-DNA produces a Raman line at 810 cm^{-1} with an intensity equal to that of the pyrimidine line at 785 cm^{-1}. The apparent absence of the 810-cm^{-1} line indicates that virial DNA backbones do not exhibit the A-type geometry. However, whether the DNA is in the B- or C-form cannot be determined.

Raman studies of MS2 phage and its isolated components were reported by Thomas et al.[152] The coat protein in the native phage was found to have ~60% β-sheet and ~40% unordered structures. The RNA within the virion contains ~85% of the bases in a paired and/or stacked state in which the backbone assumes a geometry of the A-type. Raman intensity profiles as a function of

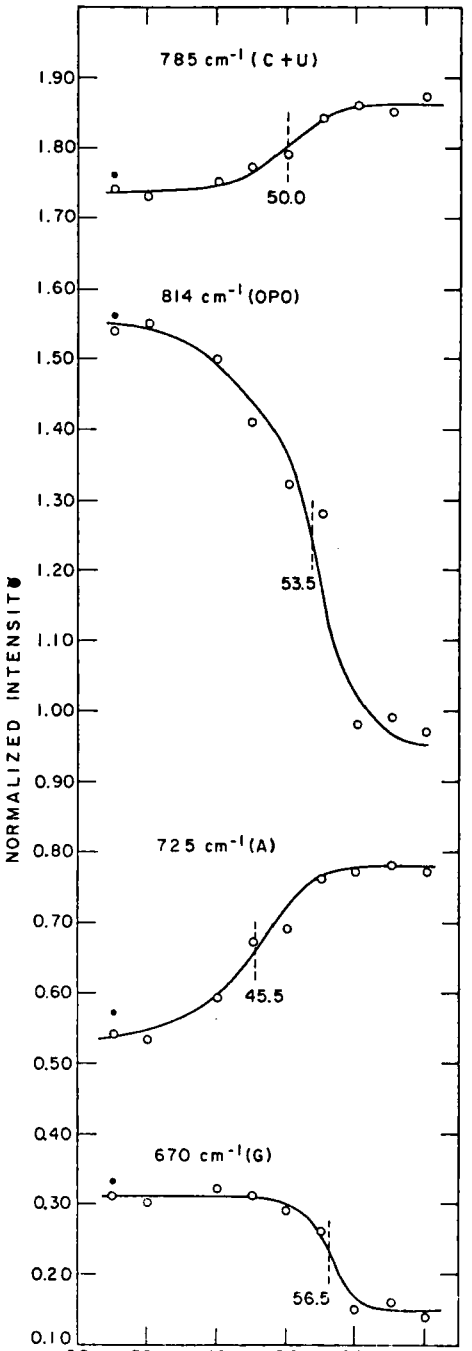

FIGURE 34. Thermal transition curves of low Mg^{2+}-$tRNA^{Phe}$ as monitored by the lines at 670, 725, 785, and 814 cm^{-1}. The melting temperatures of transitions are also indicated. Solid symbols represent measurements after solution from 70° to 25° over a period of approximately 3 hr. Letters in parentheses denote the origin of the Raman line in question. (From Chen, M. C., Giege, R., Lord, R., and Rich, A., *Biochemistry*, 14, 4385, 1975. Copyright by the American Chemical Society. With permission.)

temperature show that disordering of the MS2 RNA backbone and rupture of H-bonding are noncooperative. However, the unstacking of purine and pyrimidine bases is a more cooperative phenomenon occurring above 55°C.

NONRESONANCE RAMAN OF PHOSPHOLIPIDS AND MEMBRANES

General Features of the Raman Spectra of Phospholipids

Raman spectra of phospholipids are dominated by vibrations of the fatty acyl chains, particularly the skeletal C–C stretching modes (1000 to 1150 cm^{-1}),[153,154] CH_2 twist (~1296 cm^{-1}), CH_2 bend (~1450 cm^{-1}), and symmetric and antisymmetric CH_2 stretching vibrations[155] at 2849 and 2884 cm^{-1}. Vibrations of the head group appear at ~720 cm^{-1} (symmetric C–N stretch)[154] and at ~1100 cm^{-1} (symmetric PO_2^- dioxy stretch, overlapped with the C–C modes of hydrocarbon rotamers).[154,155]

The region between 1000 and 1150 cm^{-1} is particularly sensitive to the configurational state of the hydrocarbon chains. The two Raman lines near 1065 and 1130 cm^{-1} are characteristic of all *trans*-chain configuration (assigned[155] to the B_{1g} and A_g modes, respectively), whereas the broad line at ~1100 cm^{-1} is characteristic of random gauche configuration.[153] The ratio of either of the *trans* lines (1065 cm. or 1130 cm^{-1}) to the gauche line (~1100 cm^{-1}) may be used as a measure of the relative amount of *trans* order of the hydrocarbon chains in phospholipids.[155] Raman spectra of DL-dipalmitoyllecithin sonicates in the 1000- to 1150-cm^{-1} region as a function of temperature are shown in Figure 36.

The sensitivity of the C–H stretching modes (2800 to 2900 cm^{-1}) to the environment and packing of the hydrocarbon chains of lipids has been demonstrated.[156–158] Disruption of regular chain packing results in a reduction in the relative intensity of the 2890-cm^{-1} line to the line at 2850 cm^{-1}. This intensity effect may be caused[155] by Fermi resonance[159] between the first overtone of the CH_2 bending modes near 1450 cm^{-1} and the symmetric CH_2 stretching modes.

Quantitative Interpretation of the C–C and C–H Stretching Modes

Substantial progress in the interpretation of phospholipid Raman spectra was recently made by Gaber and Peticolas,[155] who proposed the use of

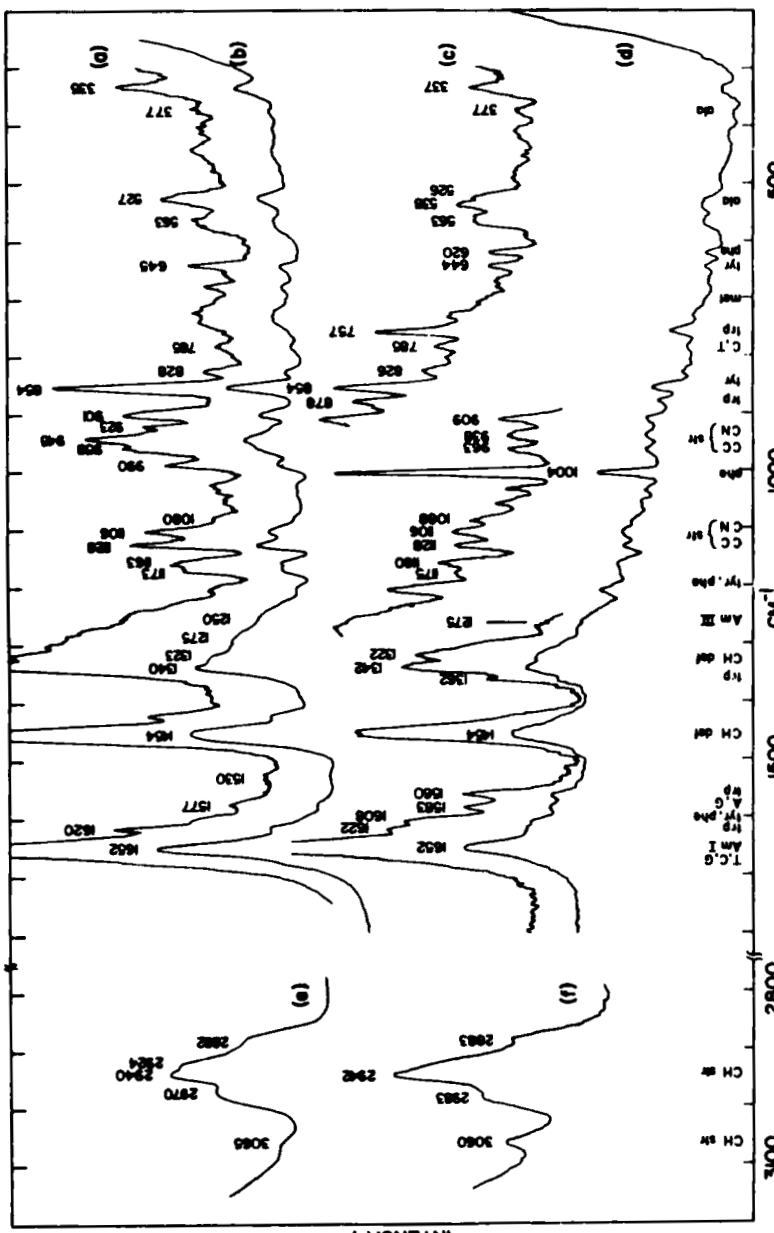

FIGURE 35. Raman spectra of filamentous bacterial (FB) viruses in 0.05 *M* NaCl at 32° C and pH 9. Curves (a), (b), and (e): pfl strain; curves (c), (d), and (f): fd strain. The spectra were obtained with a 488.0-nm line excitation. (Str) Stretching, (def) deformation, (CH) carbon–hydrogen bond, (C–C) carbon–carbon bond; (CN) carbon–nitrogen bond. A, T, C, G, ala, met, Phe, etc. are standard abbreviations for nucleic acid bases and amino acid residues. (From Thomas, G. J., Jr. and Murphy, P., *Science*, 188, 1205, 1975. Copyright © 1975 by the American Association for the Advancement of Science. With permission.)

two quantitative order parameters, S_{trans} and $S_{lateral}$. The first parameter provides a measure of the fraction of all *trans* bonds in the hydrocarbon chains while the second is a measure of the lateral crystal-like order between the chains. The *trans* parameter is defined as:

$$S_T = \frac{(I_{1133}/I_{ref})\ \text{observed}}{(I_{1133}/I_{ref})\text{DPPC solid}} \quad (39)$$

The C–N stretch at 722 cm^{-1} is taken as the reference because it is insensitive to conformation. Solid DPPC (dipalmitoyl phosphatidyl choline) is a suitable all-*trans* standard as indicated by the presence of the longitudinal acoustical mode (at ~154 cm^{-1}), which is observed only when a very high degree of all-*trans* order is present in the chain. On the other hand, the order parameter for the lateral interaction is more difficult to define because the change in the intensity of the 2890-cm^{-1} line is due to a decrease in vibrational coupling and phonon dispersion broadening. However, by assuming that about half of the observed intensity decrease at 2890 cm^{-1} is due to each of the two effects, the order parameter may be defined as follows:

$$S_L = \frac{[I_{CH_2}\ (\text{sample}) - I_{CH_2}\ (\text{liq. hexadecane})] \div 2}{I_{CH_2}\ (\text{crystalline hexadecane}) - I_{CH_2}\ (\text{matrix isolated hexadecane})} \quad (40)$$

where

$$I_{CH_2} = I_{2890}/I_{2850}$$

The parameters defined above have been applied to the study of differences between vesicles and dispersions of dipalmitoyl phosphotidyl choline (DPPC), dimyristoyl choline, and egg lecithin. The vesicles of DPPC were found to be less ordered than the dispersions. For example, at 30°C, vesicles are characterized by $S_T = 0.54$ and $S_L = 0.23$; dispersions are characterized by $S_T = 0.76$ and $S_L = 0.44$.

The melting behavior of phospholipid dispersions and vesicles was also studied by Gaber and Peticolas.[155] A plot of I_{133}/I_{722} vs. temperature shows that dispersions of DPPC have two melting phenomena: the main melting transition at 41.5°C and a premelting event at 34.2°C. However, vesicles of DPPC melt with a single broad transition at 37°C.

Biological Membranes

The biological membranes which have been examined using the laser Raman technique include hemoglobin-free human erythrocytes,[160–162] thymocyte membranes,[163] sarcoplasmic reticulum membranes,[164] and opsin membranes.[136] Raman studies of opsin membranes were discussed earlier in connection with rhodopsin and bacteriorhodopsin.

In erythrocyte ghosts, Lippert et al.[161] were able to identify Raman lines caused by the protein and membrane components. The protein fraction in the amide III region (1240 to 1267 cm^{-1}) in water and the amide I′ region (1630 to 1670 cm^{-1}) in D_2O was estimated to have 40 to 55% α helix with little β structure. The relative intensities of the three C=C stretch lines at 1062, 1082, and 1128 cm^{-1} suggested a 55 to 65% all-*trans* configuration in the fatty acyl chains of the phospholipid component.

Verma et al.[163] observed the effect of melittin (an amphipathic polypeptide) on the intensity ratios (I_{2890}/I_{2850}) of dipalmitoyl lecithin and dipalmitoyl phosphatidyl ethanolamine. The appreciable increase in these ratios following the addition of melittin reflects an enhancement in acyl chain lateral interactions (according to Gaber and Peticolas[155]) or the increased restriction of acyl chain mobility.[163]

ACKNOWLEDGMENTS

The author is indebted to the National Institutes of Health (N.I.H.) for a Career Development Award (EY 00073). The portions of the author's research described here were supported by grants from N.I.H. (GM 18894 and EY 01746) and Research Corporation.

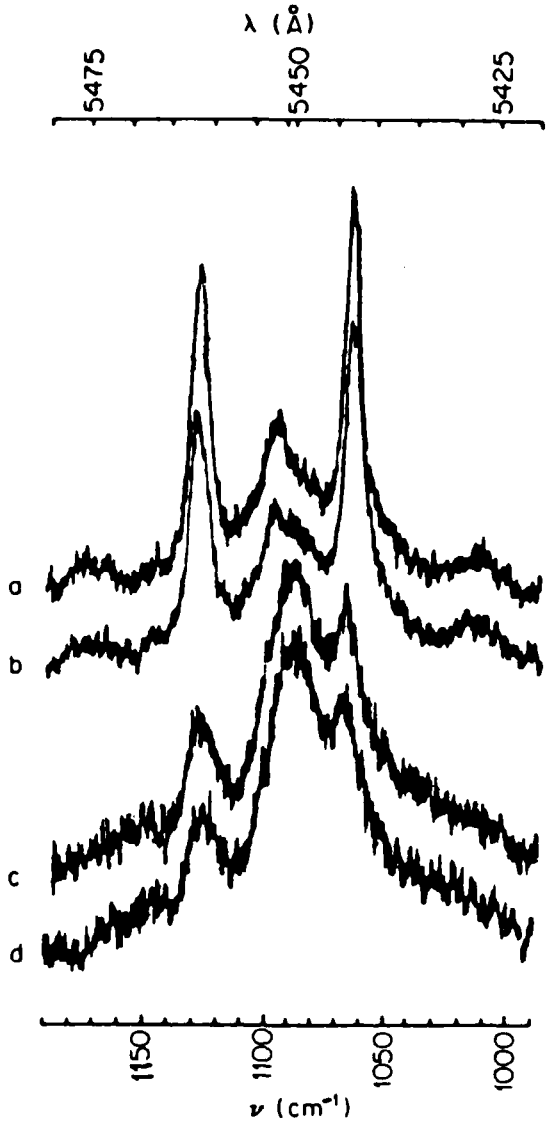

FIGURE 36. Raman spectra of the 1100-cm^{-1} region of 20% (by weight) DL-dipalmitoyllecithin sonicates in water at (a) 20, (b) 30, (c) 40, and (d) 50° C. (From Lippert, J. L. and Peticolas, W. L., *Proc. Natl. Acad. Sci. U.S.A.*, 68, 1572, 1971.)

REFERENCES

1. Raman, C. V. and Krishnan, K. S., A new type of secondary radiation, *Nature*, 121, 501, 1928.
2. Lord, R. C. and Yu, N. T., Laser-excited Raman spectroscopy of biomolecules. I. Native lysozyme and its constituent amino acid, *J. Mol. Biol.*, 50, 509, 1970.
3. Small, E. W. and Peticolas, W. L., Conformational dependence of the Raman scattering intensities from polynucleotides, *Biopolymers*, 10, 69, 1971.
4. Thomas, G. J., Jr., Medeiros, G. C., and Hartman, K. A., Raman spectral studies of nucleic acids. V. The dependence of Raman scattering on the conformation of ribosomal RNA, *Biochem. Biophys. Res. Commun.*, 44, 587, 1971.

5. Spiro, T. G. and Strekas, T. C., Resonance Raman spectra of hemoglobin and cytochrome c: Inverse polarization and vibronic scattering, *Proc. Natl. Acad. Sci. U.S.A.*, 69, 2622, 1972.
6. Brunner, H., Mayer, A., and Sussner, H., Resonance Raman scattering on the heme group of oxy- and deoxyhemoglobin, *J. Mol. Biol.*, 70, 153, 1972.
7. Lord, R. C., Laser Raman spectroscopy of biological macromolecules, *Pure Appl. Chem.*, Suppl., 7, 179, 1971.
8. Peticolas, W. L., Raman spectroscopy of polynucleotides and nucleic acids, in *Procedures in Nucleic Acid Research*, Vol. 2, Cantoni, G. L. and Davis, D. R., Eds., Harper and Row, New York, 1971, 94.
9. Koenig, J. L., Raman spectroscopy of biological molecules: a review, *J. Polym. Sci. Macromol. Rev.*, 6, 59, 1972.
10. Koenig, J. L. and Frushour, B. G., Raman spectroscopy of proteins, in *Advances in Infrared and Raman Spectroscopy*, Vol. 1, Clark, R. J. H. and Hester, R. E. Eds., Heyden and Sons, London, 1975, chap. 2.
11. Thomas, G. J., Jr., Raman spectroscopy of biopolymers, in *Vibrational Spectra and Structure*, Vol. 3, Durig, J. R., Ed., Marcel Dekker, New York, 1975, 239.
12. Spiro, T. G., Raman spectra of biological materials, in *Chemical and Biochemical Applications of Lasers*, Moore, C. B., Ed., Academic Press, New York, 1974, 29.
13. Spiro, T. G., Resonance Raman spectroscopy: a new structural probe for biological chromophores, *Acc. Chem. Res.*, 7, 339, 1974.
14. Spiro, T. G. and Loehr, T. M., Resonance Raman spectra of hemeproteins and other biological systems, in *Advances in Infrared and Raman Spectroscopy*, Vol. 1, Clark, R. J. H. and Hester, R. E., Eds., Heyden and Sons, London, 1975, chap. 3.
15. Lewis, A. and Spoonhower, J., Tunable laser Raman spectroscopy in biology, in *Neutron, X-Ray and Laser Spectroscopy*, Yip, S. and Chen, S., Eds., Academic Press, New York, 1975, chap. 3.
16. Wilson, E. B., Decius, J. C., and Cross, P. C., *Molecular Vibrations*, McGraw-Hill, New York, 1955, 43.
17. McClain, W. M., Excited state symmetry assignment through polarized two-photon absorption studies of fluids, *J. Chem. Phys.*, 55, 2789, 1971.
18a. Jahn, H. A. and Teller, E., Stability of polyatomic molecules in degenerate electronic states. I. Orbital degeneracy, *Proc. Roy. Soc.* (London), A 161, 220, 1937.
18b. Herzberg, G., *Molecular Spectra and Molecular Structure. III. Electronic Spectra and Electronic Structure of Polyatomic Molecules*, D. Van Nostrand, Princeton, N.J., 1967, 40.
19. Jones, W. J. and Stoicheff, B. P., Inverse Raman spectra: induced absorption at optical frequencies, *Phys. Rev. Lett.*, 13, 657, 1964.
20. Werncke, W., Lau, A., Pfeiffer, M., Weigmann, H. J., Hunsalz, G., and Lenz, K., Inverse resonance Raman scattering and resonance Raman amplification, *Opt. Commun.*, 16, 128, 1976.
21. Werncke, W., Klein, J., Lau, A., Lenz, K., and Hunsalz, G., Investigation of inverse Raman scattering using the method of intracavity spectroscopy, *Opt. Commun.*, 11, 159, 1974.
22. Maker, P. D. and Terhune, R. W., Study of optical effects due to an induced polarization. Third order in the electric field strength, *Phys. Rev. A*, 137, 801, 1965.
23. Begley, R. F., Harvey, A. B., Byer, R. L., and Hudson, B. S., Raman spectroscopy with intense, coherent, anti-Stokes beam, *J. Chem. Phys.*, 61, 2466, 1974.
24a. Chabay, I., Klauminzer, G. K., and Hudson, B. S., Coherent anti-Stokes Raman spectroscopy (CARS): improved experimental design and observation of a new higher-order process, *Appl. Phys. Lett.*, 28, 27, 1975.
24b. Hudson, B., Hetherington, W., Cramer, S., Chabay, I., and Klaumunzer, G. K., Resonance enhanced coherent anti-Stokes Raman scattering, *Proc. Natl. Acad. Sci. U.S.A.*, in press.
25a. Carriera, L. A., Goss, L., and Yu, N. T., unpublished results.
25b. Nester, J., Spiro, T. G., and Kaluminzer, G. K., Resonance CARS spectra of cytochrome C and vitamin B_{12} in dilute aqueous solution, *Proc. Natl. Acad. Sci. U.S.A.*, 1976, in press.
26. Adhav, R. S. and Orszag, M., Frequency doubling crystals – unscrambling the acronym, in *Electro-Optical Systems Design*, Kiver Publications, Chicago, 1974, 20.
27. Shelnutt, J. A., Resonance Raman Spectroscopy of Manganese(III) Etioporphyrin I: Theory and Experiment, Ph.D. thesis, Georgia Institute of Technology, 1975.
28. McClain, W. M., Excited state symmetry assignment through polarized two-photon absorption studies of fluids, *J. Chem. Phys.*, 55, 2789, 1971.
29. Albrecht, A. C., The theory of Raman intensities, *J. Chem. Phys.*, 34, 1476, 1961.
30. Mingardi, M. and Siebrand, W., Theory of resonance Raman scattering: An improved formulation of the vibronic expansion method, *J. Chem. Phys.*, 62, 1074, 1975.
31. Shelnutt, J. A., O'Shea, D. C., Yu, N. T., Cheung, L. D., and Felton, R. H., Resonance Raman spectroscopy of manganese(III) etioporphyrin I, *J. Chem. Phys.*, 64, 1156, 1976.
32. Hirakawa, A. Y. and Tsuboi, M., Molecular geometry in an excited electronic state and a preresonance Raman effect, *Science*, 188, 359, 1975.
33. Mathies, R., Oseroff, A. R., and Stryer, L., Rapid-flow resonance Raman spectroscopy of photolabile molecules: rhodopsin and isorhodopsin, *Proc. Natl. Acad. Sci. U.S.A.*, 73, 1, 1976.
34. Callender, R. H., Doukas, A., Crouch, R., and Nakanishi, K., Molecular flow resonance Raman effect from retinal and rhodopsin, *Biochemistry*, 15, 1621, 1976.

35. **Walrafen, G. E.,** New slitless optical fiber laser-Raman spectrometer, *Appl. Spectrosc.*, 29, 179, 1975.
36. **Thomas, G. J., Jr. and Barylski, J. R.,** Thermostating capillary cells for a laser Raman spectrometer, *Appl. Spectrosc.*, 24, 463, 1970.
37. **Yu, N. T., Jo, B. H., and Liu, C. S.,** A laser Raman spectroscopic study of the effect of solvation on the conformation of ribonuclease A, *J. Am. Chem. Soc.*, 94, 7572, 1972.
38. **Yu, N. T., Jo, B. Y., Chang, R. C. C., and Huber, J. D.,** Single-crystal Raman spectra of native insulin; Structures of insulin fibrils, glucagon fibrils and intact calf lens, *Arch. Biochem. Biophys.*, 160, 614, 1974.
39. **Kuck, J. F. R., Jr., East, E. J., and Yu, N. T.,** Prevalence of α-helical form in avian lens proteins, *Exp. Eye Res.*, 23, 9, 1976.
40. **Spaulding, L. D., Chang, R. C. C., Yu, N. T., and Felton, R. H.,** Resonance Raman spectra of metallooctaethylporphyrins. A structural probe of metal displacement, *J. Am. Chem. Soc.*, 97, 2517, 1975.
41. **Arguello, C. A., Mendes, G. F., and Leite, R. C. C.,** Simple technique to suppress spurious luminescence in Raman spectroscopy, *Appl. Opt.*, 13, 1731, 1974.
42. **Bell, M. I. and Tyte, R. N.,** Pulsed dye laser system for Raman and luminescence spectroscopy, *Appl. Opt.*, 13, 1610, 1974.
43. **Cantor, C. R. and Tao, T.,** Application of fluorescence techniques to the study of nucleic acids, in *Proc. Nucleic Acid Res.*, Vol. 2, Cantoni, G. L. and Davies, D. R., Eds., Harper and Row, New York, 1971, 31.
44. **Ambrose, E. J. and Elliott, A.,** Infrared spectroscopic studies of globular protein structure, *Proc. R. Soc. London Ser. A*, 208, 75, 1951.
45. **Miyazawa, T.,** Perturbation treatment of the characteristic vibrations of polypeptide chains in various configurations, *J. Chem. Phys.*, 32, 1647, 1960.
46. **Miyazawa, T. and Blout, E. R.,** The infrared spectra of polypeptides in various conformations: amide I and II bands, *J. Am. Chem. Soc.*, 83, 712, 1961.
47. **Krimm, S.,** Infrared spectra and chain conformation of proteins, *J. Mol. Biol.*, 4, 528, 1962.
48. **Krimm, S. and Abe, Y.,** Intermolecular interaction effects in the amide I vibrations of β polypeptides, *Proc. Natl. Acad. Sci. U.S.A.*, 69, 2788, 1972.
49. **Susi, H., Timasheff, S. N., and Stevens, L.,** Infrared spectra and protein conformations in aqueous solution. I. The amide I band in H_2O and D_2O solutions, *J. Biol. Chem.*, 242, 5460, 1967.
50. **Yu, N. T., Liu, C. S., and O'Shea, D. C.,** Laser Raman spectroscopy and the conformation of insulin and proinsulin, *J. Mol. Biol.*, 70, 117, 1972.
51. **Chen, M. C. and Lord, R. C.,** Laser-excited Raman spectroscopy of biomolecules. VI. Some polypeptides as conformational models, *J. Am. Chem. Soc.*, 96, 4750, 1974.
52. **Yu, T. J., Lippert, J. L., and Peticolas, W. L.,** Laser Raman studies of conformational variations of poly-L-lysine, *Biopolymers*, 12, 2161, 1973.
53. **Hsu, S. L., Moore, W. H., and Krimm, S.,** Vibrational spectrum of unordered polypeptide chain: a Raman study of feather keratin, *Biopolymers*, in press.
54. **Harada, I., Sygawara, Y., Matsurra, H., and Shimanouchi, T.,** Preresonance Raman spectra of simple amides using ultraviolet lasers, *J. Raman Spectrosc.*, 4, 91, 1975.
55a. **Richards, R. E. and Thompson, H. W.,** Spectroscopic studies of the amide linkage, *J. Chem. Soc.* (London), 1248, 1947.
55b. **Shimanouchi, T., Koyama, Y. and Itoh, K.,** Studies on the structure of polypeptides and protein molecules, in *Polymer Science of Japan*, Vol. 3, Otsu, T. and Takayanagi, M., Eds., 1974, 273.
56. **Small, E. W., Fanconi, B., and Peticolas, W. L.,** Raman spectra and the phonon dispersion of polyglycine, *J. Chem. Phys.*, 52, 4369, 1970.
57. **Moore, W. H. and Krimm, S.,** Transition dipole coupling in amide I modes of β-polypeptides, *Proc. Natl. Acad. Sci. U.S.A.*, 72, 4933, 1976.
58. **Miyazawa, T.,** Infrared spectra and helical conformations, in *Poly-α-Amino Acids*, Fasman, G. D., Ed., Marcel Dekker, 1967, 69.
59. **Itoh, K., Foxman, B., and Fasman, G. D.,** The two β-forms of poly-(L-glutamic acid), *Biopolymers*, 15, 419, 1976.
60. **Fasman, G. D., Liu, C. S., and Lord, R. C.,** unpublished results.
61. **Liu, C. S.,** Raman Spectroscopic Studies of Synthetic Polypeptides and Protein-peptide Complexes, Ph.D. thesis, Massachusetts Institute of Technology, Cambridge, 1975.
62. **Painter, P. C. and Koenig, J. L.,** Interpretation of hypochromic and hyperchromic intensity changes in the Raman spectra of polypeptides and polynucleotides undergoing transition, *Biopolymers*, 15, 241, 1976.
63. **Kuck, J. F. R., Jr., East, E. J., and Yu, N. T.,** Prevalence of α-helical form in avian lens protein, *Exp. Eye Res.*, 23, 9, 1976.
64. **Thomas, G. J., Jr. and Murphy, P.,** Structure of coat proteins in Pfl and fd virions by laser Raman spectroscopy, *Science*, 188, 1205, 1975.
65. **Davidson, B. and Fasman, G. D.,** The conformational transitions of uncharged poly-L-lysine. α Helix-random coil-β structure, *Biochemistry*, 6, 1616, 1967.
66. **Tiffany, M. L. and Krimm, S.,** Circular dichroism of the "random" polypeptide chain, *Biopolymers*, 8, 347, 1969.
67. **Yu, N. T. and Liu, C. S.,** Laser Raman spectra of crystalline and aqueous glucagon, *J. Am. Chem. Soc.*, 94, 5127, 1972.

68. Lord, R. C. and Yu, N. T., Laser-excited Raman spectroscopy of biomolecules. II. Native ribonuclease and α-chymotrypsin, *J. Mol. Biol.*, 51, 203, 1970.
69. Yu, N. T., Jo, B. H., and O'Shea, D. C., Laser Raman scattering of cobramine B, a basic protein from cobra venom, *Arch. Biochem. Biophys.*, 156, 71, 1973.
70. Yu, N. T. and Jo, B. H., Comparison of protein structure in crystals and in solution by laser Raman scattering. II. Ribonuclease A and carboxypeptidase A, *J. Am. Chem. Soc.*, 95, 5033, 1973.
71. Bellocq, A. M., Lord, R. C., and Mendelsohn, R., Laser-excited Raman spectroscopy of biomolecules. III. Native bovine serum albumin and β-lactoglobulin, *Biochim. Biophys. Acta*, 257, 280, 1972.
72. Siamwiza, M. N., Lord, R. C., Chen, M. C., Takamatsu, T., Harada, I., Matsuura, H., and Shimanouchi, T., Interpretation of the doublet at 850 and 830 cm^{-1} in the Raman spectra of tyrosyl residues in proteins and certain model compounds, *Biochemistry*, 14, 4870, 1975.
73. Bastian, E. J., Jr. and Martin, R. B., Disulfide vibrational spectra in the sulfur–sulfur and carbon–sulfur stretching region, *J. Phys. Chem.*, 77, 1129, 1973.
74. VanWart, H. E., Lewis, A., Scheraga, H. A., and Saeva, F. D., Disulfide bond dihedral angles from Raman spectroscopy, *Proc. Natl. Acad. Sci. U.S.A.*, 70, 2619, 1973.
75. Sugeta, H., Go, A., and Miyazawa, T., S–S and C–S stretching vibrations and molecular conformations of dialkyl disulfides and cystine, *Chem. Lett.*, p. 83, 1972.
76. Sugeta, H., Go, A., and Miyazawa, T., Vibrational spectra and molecular conformations of dialkyl disulfides, *Bull. Chem. Soc. Jpn.*, 46, 3407, 1973.
77. Nogami, N., Sugeta, H., and Miyazawa, T., C–S stretching vibrations and molecular conformations of isobutyl methyl sulfide and related alkyl sulfides, *Bull. Chem. Soc. Jpn.*, 48, 2417, 1975.
78. Miyazawa, T. and Sugeta, H., Raman Scattering of Protein Side-chains: cystine and methionine, Abstr. U.S.-Japan Joint Raman Seminar, Cleveland, Ohio, 1974, 7.
79. Chen, M. C. and Lord, R. C., Laser Raman spectroscopic studies of the thermal unfolding of ribonuclease A, *Biochemistry*, 15, 1889, 1976.
80. Nakanishi, M., Takesada, H., and Tsuboi, M., Conformation of the cystine linkages in bovine α-lactalbumin as revealed by its Raman effect, *J. Mol. Biol.*, 89, 241, 1974.
81. Yu, N. T., East, E. J., Chang, R. C. C., and Kuck, J. F. R., Jr., Raman spectra of bird and reptile lens proteins, *Exp. Eye Res.*, in press.
82. Yu, N. T. and Jo, B. H., Comparison of protein structure in crystals and in solution by laser Raman scattering. I. Lysozyme, *Arch. Biochem. Biophys.*, 156, 469, 1973.
83. Yu, N. T., Comparison of protein structure in crystals, in lyophilized state and in solution by laser Raman scattering. III. α-Lactalbumin, *J. Am. Chem. Soc.*, 96, 4664, 1974.
84. Yu, N. T. and East, E. J., Laser Raman spectroscopic studies of ocular lens and its isolated protein fractions, *J. Biol. Chem.*, 250, 2196, 1975.
85. Kuck, J. F. R., Jr., Cataract formation, in *Biochemistry of the Eye*, Graymore, C., Ed., Academic Press, New York, 1970, 319.
86. Chang, R. C. C., Resonance and Non-resonance Raman Studies of Biological Molecules, Ph.D. thesis, Georgia Institute of Technology, Atlanta, 1976.
87. Schachar, R. A. and Solin, S. A., The microscopic protein structure of the lens with a theory for cataract formation as determined by Raman spectroscopy of intact bovine lens, *Invest. Ophthalmol.*, 14, 380, 1975.
88. Hockwin, O., The presence of glycogen in lenses of different species, *Exp. Eye Res.*, 15, 235, 1973.
89. Waugh, D. F., The linkage of corpuscular protein molecules I. A fibrous modification of insulin, *J. Am. Chem. Soc.*, 66, 663, 1944.
90. Koltun, W. L., Waugh, D. F., and Bear, R. S., An X-ray diffraction investigation of selected types of insulin fibrils, *J. Am. Chem. Soc.*, 76, 413, 1954.
91. Beaven, G. H., Gratzer, W. B., and Davies, H. G., Formation and structure of gels and fibrils from glucagon, *Eur. J. Biochem.*, 11, 37, 1969.
92. Reithel, F. J., The dissociation and association of protein structures, *Adv. Protein Chem.*, 18, 159, 1963.
93. Burke, M. J. and Rougvie, M. A., Cross-β- protein structures. I. Insulin fibrils, *Biochemistry*, 11, 2435, 1972.
94. Burgess, A. W. and Scheraga, H. A., A hypothesis for the pathway of the thermally-induced unfolding of bovine pancreatic ribonuclease, *J. Theor. Biol.*, 53, 403, 1975.
95. Wilser, W. T. and Fitchen, D. B., Polarized Raman scattering from a helical biopolymer, *J. Chem. Phys.*, 62, 720, 1975.
96. Tsuboi, M., Infrared dichroism and molecular conformation of α- form poly-γ-benzyl-L-glutamate, *J. Poly. Sci.*, 59, 139, 1962.
97. Strekas, T. C. and Spiro, T. G., Hemoglobin: Resonance Raman spectra, *Biochim. Biophys. Acta*, 263, 830, 1972.
98. Spiro, T. G. and Burke, J. M., Protein control of porphyrin conformation: comparison of resonance Raman spectra of hemeproteins with mesoporphyrin (IX) analogues, *J. Am. Chem. Soc.*, 98, 5482, 1976.
99. Felton, R. H. and Yu, N. T., Resonance Raman scattering from metalloporphyrins and hemeproteins, in *The Porphyrin*, Dolphin, D., Ed., Academic Press, New York, in press.
100. Spaulding, L. D., Chang, R. C. C., Yu, N. T., and Felton, R. H., Resonance Raman spectra of metallooctaethylporphyrins. A structural probe of metal displacement, *J. Am. Chem. Soc.*, 97, 2517, 1975.

101. Shelnutt, J. A., O'Shea, D. C., Yu, N. T., Cheung, L. D., and Felton, R. H., Resonance Raman spectra of manganese(III)etioporphyrin I, *J. Chem. Phys.*, 64, 1156, 1976.
102. Yamamoto, T., Palmer, G., Gill, D., Salmeen, I. T., and Rimai, L., The valence and spin state of iron in oxyhemoglobin as inferred from resonance Raman spectroscopy, *J. Biol. Chem.*, 248, 5211, 1973.
103. Spiro, T. G. and Strekas, T. C., Resonance Raman spectra of heme proteins: effects of oxidation and spin state, *J. Am. Chem. Soc.*, 96, 338, 1974.
104. Loehr, T. M. and Loehr, J. S., Determination of oxidation and spin states of heme iron. Resonance Raman spectroscopy of cytochrome *c*, microperoxidase, and horseradish peroxidase, *Biochem. Biophys. Res. Commun.*, 55, 218, 1973.
105. Szabo, A. and Barron, L. D., Resonance Raman studies of nitric oxide hemoglobin, *J. Am. Chem. Soc.*, 97, 660, 1975.
106. Stein, P., Burke, J. M., and Spiro, T. G., Structural interpretation of heme protein resonance Raman frequencies: preliminary normal coordinate analysis results, *J. Am. Chem. Soc.*, 97, 2304, 1975.
107. Kitagawa, T., Abe, M., Kyogoku, Y., Ogoshi, H., Watanabe, E., and Yoshida, Z., Resonance Raman spectra of metallooctaethylporphyrins. Low frequency vibrations of porphyrin and iron-axial ligand stretching modes, *J. Phys. Chem.*, 80, 1181, 1976.
108. Abe, M., Kitagawa, T., and Kyogoku, Y., Vibrational assignments of resonance Raman lines of Ni(octaethylporphyrin) on the basis of a normal coordinate treatment, *Chem. Lett.*, p. 249, 1976.
109. Rimai, L., Resonance Raman Spectroscopy of Hemeproteins, presented to the 20th Biophysical Society Annu. Meet. (Abstr.), Seattle, Wash., 1976.
110. Ogoshi, H., Saito, Y., and Nakamoto, K., Infrared spectra and normal coordinate analysis of metalloporphyrins, *J. Chem. Phys.*, 57, 4194, 1972.
111. Perutz, M. F., Nature of heme-heme interaction, *Nature*, 237, 495, 1972.
112. Perutz, M. F. and Fermi, G., unpublished results, as cited in Reference 98.
113. Eicher, H., Bade, D., and Parak, F., Theoretical determination of the electronic structure and the spatial arrangement of ferrous iron in deoxygenated sperm whale myoglobin and human hemoglobin from Mossbauer experiments, *J. Chem. Phys.*, 64, 1446, 1976.
114. Felton, R. H., Romans, A. Y., Yu, N. T., and Schonbaum, G. R., Laser Raman spectra of oxidized hydroperoxidases, *Biochim. Biophys. Acta*, 434, 82, 1976.
115. Carey, P. R. and Schneider, H., Resonance Raman spectra of chymotrypsin acyl enzymes, *Biochem. Biophys. Res. Commun.*, 57, 831, 1974.
116. Carey, P. R. and Schneider, H., Evidence for a structural change in the substrate preceding hydrolysis of a chymotrypsin acyl enzyme: application of the resonance Raman labelling technique to a dynamic biochemical system, *J. Mol. Biol.*, 102, 679, 1976.
117. Carey, P. R., Carriere, R. G., Lynn, K. R., and Schneider, H., Resonance Raman evidence for substrate reorganization in the active site of papain, *Biochemistry*, 15, 2387, 1976.
118. Kumar, K., King, R. W., and Carey, P. R., Resonance Raman studies on some carbonic anhydrase-aromatic sulfonamide complexes, *Biochemistry*, 15, 2195, 1976.
119. Wald, G., The molecular basis of visual excitation, *Nature*, 219, 800, 1968.
120. Oesterkelt, D. and Stoeckenius, W., Functions of a new photoreceptor membrane, *Proc. Natl. Acad. Sci. U.S.A.*, 70, 2853, 1973.
121. Ebrey, T., Govindjee, R., Honig, B., Pollock, E., Chan, W., Crouch, R., Yudd, A., and Nakanishi, K., Properties of several sterically modified retinal analogs and their photosensitive pigments, *Biochemistry*, 14, 3933, 1975.
122. Oesterhelt, D., Meentzen, M. and Schuhmann, L., Reversible dissociation of the purple complex in bacteriorhodopsin and identification of 13-cis and all-trans-retinal as its chromophores, *Eur. J. Biochem.*, 40, 453, 1973.
123. Lewis, A., Fager, R. S., and Abrahamson, E. W., Tunable laser resonance Raman spectroscopy of the visual process. I. The spectrum of rhodopsin, *J. Raman Spectrosc.*, 1, 465, 1973.
124. Cookingham, R. E., Lewis, A., Collins, D. W., and Marcus, M. A., Preresonance Raman spectra of crystals of retinal isomers, *J. Am. Chem. Soc.*, in press.
125. Rimai, L., Kilponen, R. G., and Gill, D., Resonance-enhanced Raman spectra of visual pigments in intact bovine retinas at low temperatures, *Biochem. Biophys. Res. Commun.*, 41, 492, 1970.
126. Waleh, A. and Ingraham, L. L., A molecular orbital study of the protein-controlled bathochromic shift in a model of rhodopsin, *Arch. Biochem. Biophys.*, 156, 261, 1973.
127. Dartnall, H. J. A. and Lythgoe, J. N., Spectral clustering of visual pigments, *Vision Res.*, 5, 81, 1965.
128. Oseroff, A. R. and Callender, R. H., Resonance Raman spectroscopy of rhodopsin in retinal disk membranes, *Biochemistry*, 13, 4243, 1974.
129. Mendelsohn, R., Resonance Raman spectroscopy of the photoreceptor-like pigment of *Halobacterium halobium*, *Nature*, 243, 22, 1973.
130. Lewis, A., Spoonhower, J., Bogomolni, R. A., Lozier, R. H., and Stoeckenius, W., Tunable laser resonance Raman spectroscopy of bacteriorhodopsin, *Proc. Natl. Acad. Sci. U.S.A.*, 71, 4462, 1974.
131. Warshel, A. and Karplus, M., Calculation of $\pi\pi^*$ excited state conformations and vibronic structure of retinal and related molecules, *J. Am. Chem. Soc.*, 96, 5677, 1974.

132. Inagaki, F., Tasumi, M., and Miyazawa, T., Excitation profile of the resonance Raman effect of β-carotene, *J. Mol. Spectrosc.*, 50, 286, 1974.
133. Mendelsohn, R., Verma, A. L., Bernstein, H. J., and Kates, M., Structural studies of bacteriorhodopsin from *Halobacterium cutirubrum* by resonance Raman spectroscopy, *Can. J. Biochem.*, 52, 774, 1974.
134. Mendelsohn, R., Thermal denaturation and photochemistry of bacteriorhodopsin from *Halobacterium cutirubrum* as monitored by resonance Raman spectroscopy, *Biochim. Biophys. Acta*, 427, 295, 1976.
135. Inagaki, F., Tasumi, M., and Miyazawa, T., Vibrational analysis of polyene chains. Assignments of the resonance Raman lines of poly-(acetylene) and β-carotene, *J. Raman Spectrosc.*, 3, 335, 1975.
136. Rothschild, K. J., Andrew, J. R., DeGrip, W. J., and Stanley, H. E., Opsin structure probed by Raman spectroscopy of photoreceptor membranes, *Science*, 191, 1176, 1976.
137. Henderson, R. and Unwin, P. N. T., Three-dimensional model of purple membrane obtained by electron microscopy, *Nature*, 257, 28, 1975.
138. Erfurth, S. C., Kiser, E. J., and Peticolas, W. L., Determination of the backbone structure of nucleic acids and nucleic acid oligomers by laser Raman scattering, *Proc. Natl. Acad. Sci. U.S.A.*, 69, 938, 1972.
139. Yu, N. T., Infrared and Raman Spectra of Some Biopolymers and Related Molecules, Ph.D. thesis, Massachusetts Institute of Technology, 1969.
140. Shimanouchi, T., Tsuboi, M., and Kyogoku, Y., Infrared spectra of nucleic acids and related compounds, in *Advances in Chemical Physics*, Vol. 7, Duchesne, J., Ed., Interscience, London, 1964, 435.
141. Brown, E. B. and Peticolas, W. L., Conformational geometry and vibrational frequencies of nucleic acid chains, *Biopolymers*, 14, 1259, 1975.
142. Thomas, G. J., Jr., Raman spectroscopy of biopolymers, in *Vibrational Spectra and Structure*, Vol. 3, Durig, J. R., Ed., Marcel Dekker, New York, 1975, 239.
143. Thomas, G. J., Jr. and Hartman, K. A., Raman spectral studies of nucleic acids. VIII. Estimation of RNA secondary structure from Raman scattering by phosphate-group vibrations, *Biochim. Biophys. Acta*, 312, 311, 1973.
144. Tomlinson, B. and Peticolas, W. L., Conformational dependence of Raman scattering intensities in polyadenylic acid, *J. Chem. Phys.*, 52, 2154, 1970.
145. Pezolet, M., Yu, T. J., and Peticolas, W. L., Resonance and preresonance Raman spectra of nucleotides using ultraviolet lasers, *J. Raman Spectrosc.*, 3, 55, 1975.
146. Chen, M. C., Giege, R., Lord, R. C., and Rich, A., Raman spectra and structure of yeast phenylalanine transfer RNA in the crystalline state and in solution, *Biochemistry*, 14, 4385, 1975.
147. Hartman, K. A., Clayton, N. W., and Thomas, G. J., Jr., Studies of virus structure by Raman spectroscopy. I. R17 virus and R17 RNA, *Biochem. Biophys. Res. Commun.*, 50, 942, 1973.
148. Thomas, G. J., Jr. and Murphy, P., Structure of coat proteins in Pfl and fd virions by laser Raman spectroscopy, *Science*, 188, 1205, 1975.
149. Marvin, D. A. and Wachtel, E. J., Structure and assembly of filamentous bacterial viruses, *Nature*, 253, 19, 1975.
150. Chou, P. Y. and Fasman, G. D., Prediction of protein conformation, *Biochemistry*, 13, 222, 1974.
151. Day, L. A., Conformations of single-stranded DNA and coat protein in fd bacteriophage as revealed by ultraviolet absorption spectroscopy, *J. Mol. Biol.*, 39, 265, 1969.
152. Thomas, G. J., Jr., Prescott, B., McDonald-Ordzie, P. E., and Hartman, K. A., Studies of virus structure by laser Raman spectroscopy. II. MS 2 phage, MS 2 capsids, MS 2 RNA in aqueous solutions, *J. Mol. Biol.*, 102, 103, 1976.
153. Lippert, J. L. and Peticolas, W. L., Laser Raman investigations of the effect of cholesterol on conformational changes in dipalmatoyl lecithin multilayers, *Proc. Natl. Acad. Sci. U.S.A.*, 68, 1572, 1971.
154. Spiker, R. C., Jr. and Levin, I. W., Raman spectra and vibrational assignments for dipalmitoyl phosphatidylcholine and structurally related molecules, *Biochim. Biophys. Acta*, 388, 361, 1975.
155. Gaber, B. P. and Peticolas, W. L., On the quantitative interpretation of biomembrane structure by Raman spectroscopy, *Biochim. Biophys. Acta*, in press.
156. Larsson, K., Conformational-dependent features in the Raman spectra of simple lipids, *Chem. Phys. Lipids*, 10, 165, 1973.
157. Larsson, K. and Rand, R. P., Detection of changes in the environment of hydrocarbon chains by Raman spectroscopy and its application to lipid-protein systems, *Biochim. Biophys. Acta*, 326, 245, 1973.
158. Brown, K. G., Peticolas, W. L., and Brown, E., Raman studies of conformational changes in model membrane systems, *Biochem. Biophys. Res. Commun.*, 54, 358, 1973.
159. Schachtschneider, J. H. and Snyder, R. G., Vibrational analysis of the n-paraffins. II. Normal coordinate calculations, *Spectrochim. Acta*, 19, 117, 1963.
160. Bulkin, B. J., Raman spectroscopic study of human erythrocyte membranes, *Biochim. Biophys. Acta*, 274, 649, 1972.
161. Lippert, J. L., Gorczyca, L. E., and Meiklejohn, G., A laser Raman spectroscopic investigation of phospholipid and protein configurations in hemoglobin-free erythrocyte ghosts, *Biochim. Biophys. Acta*, 382, 51, 1975.
162. Wallach, D. F. H. and Verma, S. P., Raman and resonance-Raman scattering by erythrocyte ghosts, *Biochim. Biophys. Acta*, 382, 542, 1975.
163. Verma, S. P., Wallach, D. F. H., and Schmidt-Ullrich, R., The structure and thermotropism of thymocyte plasma membranes as revealed by laser Raman spectroscopy, *Biochim. Biophys. Acta*, 394, 633, 1975.
164. Milanovich, F. P., Yeh, Y., Baskin, N. J., and Harvey, R. C., Raman spectroscopic investigations of sarcoplasmic reticulum membranes, *Biochim. Biophys. Acta*, 419, 243, 1976.